AN EXPERIMENTAL INVESTIGATION OF COOLANT MIXING IN A WIRE WRAPPED LMFBR BLANKET SUBASSEMBLY

[pt.1]

Carl Henry Oosterman

[pt. 1]

AN EXPERIMENTAL INVESTIGATION OF COOLANT MIXING IN A WIRE WRAPPED LMFBR BLANKET SUBASSEMBLY

by

CARL HENRY OOSTERMAN

B.S., United States Naval Academy
1969

M.C.E., University of Delaware
1970

SUBMITTED IN PARTIAL FULFILLMENT
OF THE REQUIREMENTS FOR THE DEGREES OF
MASTER OF SCIENCE IN NUCLEAR ENGINEERING
AND NAVAL ENGINEER

at the

MASSACHUSETTS INSTITUTE OF
TECHNOLOGY

June, 1975

ABSTRACT

AN EXPERIMENTAL INVESTIGATION OF COOLANT MIXING IN AN LMFBR WIRE WRAPPED BLANKET SUBASSEMBLY

by

Carl Henry Oosterman

Lieutenant, United States Navy

Submitted to the Department of Ocean Engineering, Massachusetts Institute of Technology, in partial fulfillment of the requirements for the degrees of Master of Science in Nuclear Engineering and Naval Engineer.

The design and construction of a test section for the MIT mixing flow loop to collect LMFBR blanket subassembly mixing data for analysis by the ENERGY computer code and to collect pressure drop data to provide information on blanket subassembly flow characteristics is presented. Mixing data is collected using the salt injection technique. The test section consists of a hexagonal flow housing, 61 blanket fuel rods (3 of which are salt injection rods) and 126 conductivity cell probes. Six pressure taps are provided at 12 and 42 inches below the test section exit. Axial pressure data is collected using the injection rods.

The pressure drop data shows a periodic variation both axially and circumferentially. Test section friction factors are not well fit by existing correlations since the correlations are based on test sections with different geometrical parameters. A friction factor is proposed which fits the data well.

Mixing data collected also shows periodic variation with wire wrap lead length. Salt dispersion characteristics show that the wire wraps push the salt into adjacent subchannels. The errors shown in the fit of the calibration curves may require reanalysis of the data or a repetition of the experiment before ENERGY analysis is performed.

Thesis Supervisor: Neil E. Todreas
Title: Professor of Nuclear Engineering

TABLE OF CONTENTS

ACKNOWLEDGMENTS

The author would like to express his gratitude to Professor Neil E. Todreas for his assistance and advice throughout the course of this project. Professor Todreas has continually and freely given of his time and has provided encouragement as supervisor of this thesis. Gratitude is also extended to Professor Clark Graham, LCDR, USN for being thesis reader.

The financial support of the U.S. Navy for this thesis and for three years at MIT is gratefully acknowledged. The financial support of the experimental program by U.S. Atomic Energy Commission Contract AT(11-1)-2245, "Coolant Mixing in LMFBR Rod Bundles," is also gratefully acknowledged.

Conducting this project has required the soliciting of the technical advice and assistance of many persons. Appreciation for assistance is extended to the following: Mr. J.A. (Tiny) Caloggero of the Mechanical Engineering Department Engineering Project Laboratory, Mr. Alan S. Hanson and Mr. Tom E. Eaton of the Nuclear Engineering Department. The author is especially grateful to Mr. Brian Bosy of the Mechanical Engineering Department for his advice and assistance. A note of thanks goes to Mrs. Shirley Okun and Mrs. Virginia O'Keefe who typed the final manuscript.

A special, final acknowledgment must go to my wife, Margaret, who was patient and understanding beyond the call of duty during the course of this thesis.

NOMENCLATURE

A_{FT} = Total area for flow

A_T = Total area inside hexagonal flow duct

C = Swirl flow coefficient ($\bar{V}_g/\bar{V}$)

C_o = Injection salt concentration

C^* = C/C_o where C is salt concentration

De = Hydraulic diameter

D_f = Distance across flats of hexagonal flow duct

D_ℓ = Length of the face of hexagonal flow duct

D_p = Diameter of blanket fuel rod

D_s = Diameter of blanket wire wrap spacer

ε = Uniform, lateral, effective enhanced eddy diffusivity

ε^* = Effective eddy diffusivity ($\varepsilon/\bar{V}De$)

ε^*_D = Mass eddy diffusivity

ε^*_H = Thermal eddy diffusivity

$f(P_{abs})$ = Friction factor calculated from absolute pressure measurements

$f(P_{dif})$ = Friction factor calculated from differential pressure measurements

f(slope) = Friction factor calculated from slope of axial pressure measurements

f' = Rehme friction factor

f" = Adjusted Rehme friction factor

F = Rehme geometry factor

g = Width of gap between rods and walls

g_o = Constant, 32.17 lbm. ft./lbf.sec.^{2}

G = Flow rate in gpm

γ = Kinematic viscosity

h = Wire wrap lead length

L = Length over which pressure drop is measured

N* = Number of blanket fuel rods

N_1 = Number of interior subchannels

N_2 = Number of edge subchannels

N_3 = Number of corner subchannels

N_R = Number of rings of rods in subassembly

N = Novendstern geometry factor

P = Rod pitch

P_{abs} = Absolute pressure measurement $\equiv P_{TAPn}$

$\overline{P}_{abs}$ = Average of absolute pressure measurements

$$\equiv \frac{\sum_{n=1}^{N} P_{TAPn}}{N}$$

P_{dif} = Differential pressure measurement (ref. TAP #1)

$\equiv P_1 - P_{TAPn}$

$\overline{P}_{dif}$ = Average of differential pressure measurements

$$\equiv \frac{\sum_{n=1}^{N} (P_1 - P_{TAPn})}{N}$$

Pr = Prandtl number

P_T = Wetted perimeter

ΔP = Pressure difference

Re = Reynolds number

Re' = Rehme adjusted Reynolds number

ρ = Density

Sc = Schmidt number

$\overline{V} = V_T$ = Average axial bundle velocity

$\bar{V}_g$ = Average velocity in the gap between the rods and the wall

W = Flow rate in lbm/min

Z = Axial reference axis

Chapter 1

INTRODUCTION

1.1. ENERGY Subassembly Analysis Code

The need for a relatively simple approach to predicting, within engineering limits of accuracy, energy transfer in Liquid Metal Fast Breeder Reactor (LMFBR) wire wrapped blanket rod bundles has been fulfilled by the development of the ENERGY computer code by Khan at MIT [1]. The major effort in subchannel analysis code development has been in codes where axial momentum, energy, and continuity equations are written for each subchannel along with the cross-flow coupling terms. The temperature and flow fields are solved in these programs as either a boundary value problem (usually by iterative schemes) or an initial value problem (usually by marching procedures). Both the boundary and initial value subchannel analyses have the following characteristics[1]. First, each of the four empirical constants required [one each for turbulent exchange, diversion cross-flow and flow sweeping in central and wall channels (see Appendix 1 for mixing definitions)]cannot be separately and accurately determined. Second, errors in energy transport may be caused by the fact that the various modes of mixing are considered separately and added together.

The ENERGY code expresses the net interaction between flow sweeping, diversion and turbulent cross-flow in a bulk fashion by lumping them together in one parameter. In the central zone of a subassembly the mixing mechanisms, viewed over a sufficient fraction of a wire lead, are nondirectional and are modeled by an effective eddy diffusivity, $\varepsilon^* = (\varepsilon/\bar{V}De)$. ε is defined as a uniform, lateral, effective enhanced eddy diffusivity. Thus, in the central zone there is superimposed on a predominately axial flow a fluctuating transverse flow modeled by an effective eddy diffusivity. The outer fuel subassembly region is modeled as having an additional component of velocity, a swirl component. C is the empirical coefficient which represents the swirl flow in the wall region and is defined as the ratio of the velocity in the gap between the rods and the wall to the average axial bundle velocity ($C = \bar{V}_g/\bar{V}$). C is assumed to be constant and represents the average circumferential swirl velocity in the gap between the rod and wall. For simplicity, ε^* is generally assumed constant throughout the subassembly[1]. The axial velocity in the two subassembly regions is determined by dividing the flow to yield uniform axial pressure drops. Based on inspection of the energy balance equation and

consideration of the physical processes involved, ε^* and C can be shown to be dependent on the following parameters [2]:

$$\varepsilon^* = f(h/D_p,\ P/D_p,\ Re,\ Pr) \qquad (1\text{-}1)$$

$$C = f(h/D_p,\ P/D_p,\ Re,\ Pr) \qquad (1\text{-}2)$$

For example, ε^* has shown dependence on h/D_p and P/D_p as shown in figure 1-1. Both ε^* and C are found to be independent of Reynold's number (Re) for Re greater than 10,000 in LMFBR fuel subassemblies [2]. The Re dependence is expected to be similar in blanket subassemblies. Prandtl number (Pr) effects are generally neglected at high Re due to the predominance of wire wrap mixing [2]. However, at low flows the effects of natural convection are important.

This fact led to the development of a series of computer programs called ENERGY I, ENERGY II and ENERGY III. ENERGY I applies to subassemblies in the forced convection regime, while ENERGY II and ENERGY III apply to subassemblies in a regime of mixed forced and free convection. The formulation for ENERGY III is more complex than for ENERGY I because, for subassemblies operating in mixed convection, the axial momentum and

energy equations are coupled, and a simultaneous solution of continuity, momentum and energy equations is required [3]. The coupling effects are not present in forced convection. The ENERGY II computer program performs similar calculations to that of ENERGY III except that the convective terms in the momentum equations are neglected. The results of ENERGY II and ENERGY III show only small differences over a wide range of operating conditions [3]. ENERGY II and ENERGY III apply also for forced convection, but ENERGY I is more desirable for that regime because it is simpler and less costly to run on the computer.

With ε^* and C known, the ENERGY codes calculate energy transport by treating the rod assembly as a continuous porous media. Energy generation by the fuel rods is modeled by a continuous volumetric heat source distribution [3].

Various types of experiments can be used to determine the empirical constants ε^* and C. The three most common are heated rod, salt solution injection and hot water injection experiments. Heated rod experiments have given the best accuracy [2] but require sophisticated and high power electrical equipment which is not presently available at MIT. Hot water injection has a lower tracer-to-background ratio than salt injection (7:1 versus 300:1) and thus requires a higher injection flow

rate for comparable instrument readings. Therefore, the salt injection technique is used at MIT for mixing studies (see Chapter 2 for more detail).

Salt injection experiments yield a mixing coefficient which can be used directly in the ENERGY code. Since ε^* predominately represents the wire sweep flow mixing effect, the mixing coefficient, determined from the equation below, describing salt diffusion need not be modified for use in ENERGY [2].

$$\frac{DC^*}{Dz} = \frac{1}{Re}\left(\frac{\varepsilon^*_D}{\gamma} + \frac{1}{Sc}\right) \nabla^2 C^* \qquad (1\text{-}3)$$

when $z = 0$, $C^* = 1$

where $C^* = C/C_o$

C_o = inlet salt concentration

For all tracers $\varepsilon^*_D/\gamma >> 1/Sc$

and $\varepsilon^*_D = \varepsilon^*_H$

1.2. The Need for Blanket Data

Experiments are presently underway at MIT to generate mixing data needed for LMFBR fuel subassemblies. Mixing data is also needed for LMFBR blanket subassemblies because the results from the fuel tests do not necessarily apply to blanket subassemblies. As can be seen from

table 1-1, blanket design parameters differ markedly from fuel design parameters both in geometry and in flow conditions. There are large uncertainties in blanket coolant flow and heat removal characteristics especially at low Reynolds numbers. At low flows, heat removal by natural convection may exceed that by forced convection resulting in flow instabilities, local recirculation or preferential flow channeling. Flow and temperature information is needed to determine blanket duct and rod bowing, wire wrap looseness or compression due to differential swelling and rod and duct interactions. Accurate blanket subassembly temperature profiles are needed to better determine optimum subassembly flow rates, overall plant thermal efficiencies and to analyze core restraint schemes. Assembly temperatures also must be compatible with the thermal stress, strain and metallurgical limitations of the structural components. The differences, uncertainties and requirements listed above necessitate an analytical model with supporting experiments to describe blanket subassembly temperature profiles [7].

The ENERGY code, though not developed specifically for blanket subassemblies, is readily applicable to blanket subassembly analysis when utilized with proper values of ε^* and C[8]. The nonrelevance of fuel bundle

data can be seen from figure 1-1 which was generated from data analyzed with the ENERGY code [2]. Figure 1-1 shows ε^* as a function of $D_p/h \times 10$. Since h for blanket subassemblies can be from 2 to 6 inches [4], D_p/h can range from 0.83 to 2.5. As shown in figure 1-1 fuel subassembly data is limited to values of D_p/h less than 0.7. The values for pitch-to-diameter ratio (P/D_p) presented have only one point in the range of blanket geometries. Extrapolation of the one applicable point into the proper D_p/h range is not justifiable.

1.3. Objective

The objective of this thesis is to collect the required mixing data so that the ENERGY code can be applied to a blanket geometry. The salt solution tracer technique will be used to generate the data from which the constants ε^* and C may be resolved. Pressure drop data will also be taken to supply needed blanket subassembly flow data.

CHAPTER 2

Test Section and Tracer System Design

The purpose of a coolant mixing experiment is to observe the dispersion of fluid caused by various mixing mechanisms (discussed in Appendix 1) within the flow passages of a fuel assembly. This can be accomplished by injecting a tracer into the fluid flowing through the fuel subassembly of interest. Tracer dispersion is detected by instrumentation mounted downstream from the tracer injector. A coolant mixing test flow loop is available in EPL - EEL - 2 in the basement of Building 3 at MIT. Figure 2-1 is a diagram of the loop. Each 20 horsepower pump is rated at 300 gallons per minute at a 180 foot water head (78 psig.). The pumps can run individually, in series or in parallel. Electronics are also available to read and record voltages on up to 128 different channels (see section 2.3.3.3.). A test section for an LMFBR fuel subassembly has been built and experiments run on it using the MIT loop and electronics.

To accomplish a mixing experiment on an LMFBR blanket fuel subassembly, a test section flow housing, the associated fuel rods and a tracer system must be designed.

2.1 Flow Housing Design

The flow housing must provide two functions. One is

to provide the proper subassembly boundary. The other is to provide vertical positioning for the blanket fuel rods.

2.1.1. Test Section Geometry

2.1.1.1. Basic Requirements

The dimensions of the flow duct are determined by the rod and wire wrap spacer dimensions. A sample of 11 of the 1/2 inch diameter blanket fuel rods shows an average diameter of 0.501 inches with a standard deviation of 0.0005 inches. The theory of Significance Testing [6], using these statistics and assuming a Normal Distribution of rod diameters, determines that there is a 95% confidence level that all the rod diameters are 0.502 inches or less (commercial tolerances are 0.500 ± 0.002 inches). Similarly, 13 samples of the 1/32 inch diameter wire wrap showed an average diameter of 0.0315 inches with a standard deviation of 0.00018 inches. Using these statistics, there is a 95% confidence level that the wire wrap diameter is less than or equal to 0.032 inches. The above dimensions are conservative which means that a complement of rods and wire wrap, ordered to nominal dimensions, are ensured to fit into the flow housing.

2.1.1.2 Geometry Calculations [12]

The 61 rods in the blanket fuel subassembly are arranged in a triangular array. This gives 4 rings (N_R) of

rods, 96 interior subchannels (N_1), 24 edge subchannels (N_2) and 6 corner subchannels (N_3) (see figure 2-2.).

1) Total area inside hexagonal flow duct (A_T)

$$A_T = D_f D_\ell + 2(\tfrac{1}{2}) D_f D_\ell \text{ Sin } 30^\circ \qquad (2\text{-}1)$$

where $$D_\ell = \frac{D}{2}f \frac{1}{\text{Cos } 30^\circ} = \frac{D}{\sqrt{3}}f \qquad (2\text{-}2)$$

$$A_T = \frac{\sqrt{3}}{2} D_f^2 \qquad (2\text{-}3)$$

where $$D_f = 2\left[\frac{\sqrt{3}}{2} N_R P + \frac{D}{2}p + D_s\right] \qquad (2\text{-}4)$$

N_R = 4

P = 0.534

D_p = 0.502

D_s = 0.032

D_f = 4.266 in

D_ℓ = 2.463 in

A_T = 15.761 in^2

2) Total cross-sectional area for Flow (A_{FT})

$$A_{FT} = A_T - N\frac{\pi}{4}(D_p^2 + D_s^2) \qquad (2\text{-}5)$$

N = 61

A_{FT} = 3.638 in^2

3) Total wetted perimeter (P_T)

$$P_T = 6D_\ell + N\pi(D_p + D_s) \qquad (2\text{-}6)$$

$$P_T = 117.16 \text{ in}$$

4) Equivalent diameter (De)

$$De = \frac{4A_{FT}}{P_T} \qquad (2\text{-}7)$$

$$De = 0.124 \text{ in}$$

5) Unit subdivision dimensions

a) Interior

(1) Area for flow

$$\frac{\sqrt{3}}{4} P^2 - \frac{\pi D_p^2}{8} - \frac{\pi}{8} D_s^2 = 0.0246 \text{ in}^2 \qquad (2\text{-}8)$$

(2) Wetted perimeter

$$\frac{1}{2}\pi D_p + \frac{1}{2}\pi D_s = 0.840 \text{ in} \qquad (2\text{-}9)$$

b) Edge

(1) Area for flow

$$P(\frac{D_p}{2} + g) - \frac{\pi D_p^2}{8} - \frac{\pi}{8} D_s^2 = 0.052 \text{ in}^2 \qquad (2\text{-}10)$$

$$g = 0.032 \text{ in}$$

(2) Wetted perimeter

$$\frac{1}{2}\pi D_p + P + \frac{1}{2}\pi D_s = 1.374 \text{ in} \qquad (2\text{-}11)$$

c) Corner

(1) Area for flow

$$2\left[\frac{1}{2}\left(\frac{D_p}{2} + g\right)\left(\frac{D_\ell - P(N_R)}{2}\right) - \frac{\pi D_p^2}{48}\right] - \frac{\pi D_s^2}{24} = 0.013 \text{ in}^2 \qquad (2\text{-}12)$$

(2) Wetted perimeter

$$\frac{\pi}{6}D_p + D_\ell - PN_R + \frac{\pi}{6}D_s = 0.571 \qquad (2\text{-}13)$$

A summary of the results is shown in table 2-1.

2.1.2. Flow Housing Construction

A flow housing of aluminum and plexiglass to model LMFBR fuel subassemblies is constructed as shown in figure 2-3. For the blanket fuel subassembly flow housing, aluminum is eliminated as a material because stainless steel fuel rods are used. An aluminum housing with stainless steel rods results in corrosion problems as experienced in the fuel flow housing. Brass or stainless steel can be used in the above design, but the resulting weight of the flow housing is 250 pounds. The total blanket rod bundle weight is then 460 pounds. Brass or stainless steel stock the required size is not a standard

stock item and, therefore, requires a long lead time and extra expense to procure. The design shown in cross-section in figure 2-4 reduces the weight of the flow housing and eliminates the material procurement problems. This design has a flow housing weight of 125 pounds and a total test section weight of 335 pounds. Considerably less machining time and complication is involved, and standard $\frac{1}{2}$ inch aluminum plate is used. Stainless steel is chosen over brass due to its superior strength. Type 303 has good machineability. The cap screws holding the plexiglass to the metal sides are spaced every 2 inches. The outer row on one side is spaced every 6 inches. All other screws are spaced every 4 inches.

A static pressure tap is placed in each face of the hexagonal flow housing at the 1 foot and 3-1/2 foot levels below the top of the 5 foot long flow housing as shown in figure 2-5. These pressure taps are to monitor both axial and circumferential pressure drops. The levels are chosen to minimize any entrance or exit effects. Flow is assumed to be fully developed after one wire wrap lead length[7].

Time and expense are saved by following the proper sequence in constructing a flow housing such as this one.

First, the plexiglass sides are machined and holes are drilled in them. The metal pieces are machined, but the holes to connect the plexiglass to the metal sides are not drilled. Two hexagonal jigs are machined to the inner dimensions of the flow housing. All the pieces are assembled around the jigs using the jigs to ensure that proper positioning of the pieces is maintained. The cap screw holes in the metal sides to hold on the plexiglass sides are marked with a center-punch, since all parts are properly aligned. Before disassembly, dowel pin holes are drilled through the plexiglass into the metal sides to ensure proper alignment each time the housing is assembled. The flow housing is disassembled, and the holes for the cap screws for the plexiglass are drilled.

In constructing any future flow housing, it is advantageous to cut the o-ring slot in the metal side rather than in the plexiglass. Plexiglass has very poor dimensional tolerances, and a proper slot depth cannot be maintained unless the face of the plexiglass is machined.

Vertical rod positioning is provided by 2 sets of 9 rows of horizontal rods as shown in figure 2-6. The first set of 1/4 inch rods is 1.5 inches above the bottom of the flow housing. The second set is 2.5 inches above the bottom. The rods must be drilled accordingly (see sec. 2.2.2.). Upper rod support is described in section 2.3.3.2.

The two flow housing end plates are shown in figure 2-7. Two dowel pins are placed in each end of the flow housing in the metal sides to match the holes in the end plates. These provide alignment of the flow housing with the end plates. The end plates mate with the flow loop.

2.2 Blanket Fuel Rods

2.2.1. Wire Wrap Apparatus

Under the direction of the author, a mechanical device to wrap the helical wire spacer on test section fuel rods was designed and constructed by Mechanical Engineering Graduate Student Brian J. Bosy. The wire wrap apparatus consists of a gearbox and leadscrew arrangement which rotates the rod as a shuttle is translated. The shuttle lays the wire on the rod in a helix. The gearbox consists of a basic mechanism (figure 2-8) to which various gears can be added to achieve up to a 6 inch lead (figure 2-9). At present, a gearbox for a 4 inch lead (figure 2-10) is installed.

The apparatus may be adapted for 1/4 inch diameter rods by fitting sleeves into parts A (rod sleeve), B (bearing) and C (gear). The rod end support (part D) and the shuttle must also be changed to accept 1/4 inch rods. Only 60 inch long rods fit in the apparatus.

2.2.2. Wire Wrap Procedure

Step 1. Rod holes

All rods are trimmed to 60 inches in length and

holes drilled as shown in figure 2-11. A drill jig can be constructed to aid in this work. The wire wrap start hole is 6 inches from the end of the rod so that laser anemometer measurements can be taken on unwrapped portions of the test section.

Step 2. Set up

The shuttle (part E) is turned to the far end of the apparatus so that it fits over part D. Part A is slipped over the bottom end of a rod, and the rod is slipped through parts B and C (figure 2-8). The upper rod support hole is placed over part D (figure 2-12). A dowel pin is placed through part A and through the hole at 2.5 inches in the rod. The shuttle is brought back to within 6 inches of the wire wrap start hole.

A piece of wire is fed backwards through the shuttle and through the hole in the top of part D. The wire is inserted into the start hole and bent over with a hammer. Move the shuttle so the edge closest to the gears is halfway over the wire wrap start hole. The start hole is facing vertically, and part A is snug against part B. Part C is placed snugly against the other side of part B and secured to the rod by a set screw. The end of the wire through part D is bent in a loop, and an approximately 4 pound weight attached to put tension on the wire. This ensures that the wire is tightly wrapped. Do not use more

than a 5 pound weight since the wire will have too much strain for a low temperature solder to hold.

Step 3. Wrap wire

Turn the handle on the large gear clockwise for a clockwise wire wrap. After the wire makes 2 revolutions around the rod, stop wrapping and solder the end of the wire into the start hole. A low temperature stainless steel solder is recommended. (See Appendix 2, Equipment List). Brazing is stronger but is much more difficult to do. Continue wire wrapping until the shuttle passes approximately 1/4 inch beyond the end of the rod. Carefully solder the wire at the end of the rod and about 4 inches back from the end. All parts must be thoroughly cleaned for a good joint. The rod can be cooled with a wet rag, and the wire cut at the end of the rod with a fine file.

Step 4. Rod removal

Remove the wrapped rod by loosening the set screw in part C, sliding the rod off part D and pulling the rod slightly to one side and out of part B. Remove part A from the rod and file the excess wire and solder off the rod. Let the rod set for several days and then check for cracks in the solder. A crack is a sign that the parts were not properly cleaned before joining or that too

heavy a weight was used. Rewrap all rods with cracked joints.

2.3 Tracer System Design

A tracer injection experiment is designed by choosing a tracer, an injection scheme and a detection system. Key factors in tracer selection are accuracy, influence on subchannel flow characteristics, and the influence on detection system design. Key factors in the design of the injector system are location and mobility. Key factors in the design of the detection system are the type and the design of the measuring instruments and instrument location relative to the experimental array (inside or outside). Injection and detection of tracer must not significantly interfere with the mixing phenomena being observed.

2.3.1. Tracer selection

Salt solution tracer is selected as the best tracer for the experiments at hand. Visual tracers are not accurate enough and radioactive tracers create a handling problem. The remaining options are heated rods, hot water and salt solution tracers.

Heat addition by heated rods is the optimum tracer injection technique. Heated rod experiment energy balances have been within 3-5% while mass and energy

balances for salt and hot water injection experiments have been only within 13-35% (2). The heated pin method includes buoyant effects, and there is no injector to disturb subchannel flow. Heated rod experiments, however, require high (100 kw) power sources and specially designed heated rods. Also, thermistors should be used as sensors. Since equipment costs would, therefore, be high and involve a lead time of several months, this precluded heated pin experiments for this project (see Chapter 6, Future Work).

Hot water injection requires very sensitive instrumentation since tracer-to-background ratios are low and diffusivity relatively high. For water at atmospheric pressure and 60°F, the enthalpy is 28 Btu/lbm. The practical limit of tracer enthalpy (212°F) is 180 Btu/lbm which gives a tracer-to-background ratio of 7:1.

Salt solution tracers have low mass diffusivity yet high tracer-to-background ratios. The equivalent conductivity of tap water at 140°F is about 150 ppm of NaCl. Tracers can be injected at concentrations of 50,000 ppm giving a tracer-to-background ratio of 300:1. This shows that a much higher flow rate must be injected for a hot water tracer than for a salt solution tracer causing more disturbance in the subchannel. Therefore, salt solution

is judged superior to hot water injection and is chosen for this experiment.

2.3.2. Injector design

The purpose of the injection system is to insert a tracer into the main flow of the test section with a minimum disturbance to the subchannel flow. The level of subchannel flow perturbation is a function of injector design and injection flow rate. Injector design should present a minimum interference with the subchannel flow. The injection flow rate required is determined by the tracer used, in this case salt solution. Experiments [1,4] have shown that injecting at a velocity equal to the subchannel flow velocity minimizes the disturbance to the subchannel flow.

Injectors can be stationary with injectors at several levels, or they can be axially mobile. Multiple stationary injectors give less flexibility than axially mobile injectors. Axial resolution can be obtained with fixed injectors by moving the detection devices. However, it is much more difficult to move the detection system, with its numerous instruments inside the test section than it is to move a single or several injectors inside the test section. The small subchannels of the blanket fuel subassembly further complicate the movable detector problem. Therefore, an axially movable, rod mounted,

injector device with fixed detection instrumentation is chosen as the best option.

The salt solution injector design developed consists of an outer injector rod with an inner sliding injector mechanism. The injector rod has 77 holes of 0.031 inches diameter. The holes are spaced, beginning at the top of the rod, in the following intervals.

Hole Spacing	Distance from top of rod (inches)
every 1/4 inch	1 - 12
every 1/2 inch	12 - 24
every 1 inch	24 - 30
every 6 inches	30 - 42

These intervals reflect the fact that as the distance from the end of the test section increases, mixing becomes more thorough and small distances between injections will not give noticeable differences in instrumentation readings. Therefore, hole spacing is increased with distance from the top of the injection rod. Adequate injection flow rates in past experiments using the equal velocity injection criteria have been experienced with approximately 0.031 inch injector holes [18].

The smaller the angle of the holes with the rod axis, the less the subchannel flow velocity is disturbed. Thirty degrees is chosen because it is a reasonable angle to drill and causes a negligible effect on the subchannel flow,

due to the relatively small salt solution flow rate compared to the subchannel flow rate (3.2% at 200 gpm total flow for an interior subchannel).

As shown in cross-section in figure 2-13, inside the injector rod is a sliding injector mechanism. The mechanism lines up with the rod holes to inject salt solution through the holes into a subchannel. Leakage is prevented by two pairs of o-rings which seal the gap between the mechanism and the injector rod. Recirculation of salt water into the injector rod above the injector mechanism is prevented by enclosing the inner rod in neoprene tubing which serves to seal the injector rod above the injector.

An injector design option considered but rejected is that presently used at MIT in salt tracer experiments for LMFBR fuel assemblies. It consists of a slotted tube with an inner sliding tube which has a single injection hole or needle. This scheme has the advantage of continuous axial injection. Machining the required 1/16 inch wide slot in thin-walled, 1/2 inch stainless steel tubing can cause serious bowing of the rod. This is difficult to correct due to the strength of the 1/2 inch tubing compared to the 1/4 inch tubing used in the fuel experiments. Also, a follower rod is required to block

the slot below the injector hole to minimize subchannel flow disturbance. This limits injection to the upper half of the injection rod.

In order to avoid disassembling the test section to put the injection rod in different radial positions, three injection rods are built. One is placed in a central interior subchannel, one in a peripheral interior subchannel and one in an edge subchannel. The central and edge injections are used to measure the two distinct mixing coefficients ε^* and C[2]. The peripheral injection is used to detect interchange between edge and interior subchannels. Salt solution is supplied from a pressurized tank as shown in figure 2-14.

2.3.3. Detection System Design

2.3.3.1. Measuring Electrolytic Conductance

2.3.3.1.1. Conductivity cell

The instrument used to measure the conductivity of an electrolyte is the conductivity cell. [Only alternating current (AC) conductivity cells are discussed, since the data acquisition system will accept only AC cells (see sec. 2.3.3.1.2. and 2.3.3.3.)]. The solution acts as an electrical conductor between the cell's exposed electrodes. The resistance measured by the cell is a function of the cell's design and the solution used.

The electrical network equivalent of a typical AC conductivity cell is shown in figure 2-15a [13]. Resistance R_1 is the resistance of the solution between the cell's electrodes. Capacitance C_o resluts from the dialectric action of the solution between the cell electrodes and of the capacitance effects of the lead wires connecting the cell to the measurement equipment, R_s, W_s and C_s are electrode surface effects due to electrolysis, and are discussed in detail in Robinson and Stokes [13].

The electrolysis effects, referred to as polarization, can essentially be eliminated by coating the electrodes with finely divided black platinum [14]. The network equivalent of a platinized conductivity cell is shown in figure 2-15b. The effect of C_o has been shown by experimentation to be negligible [4]. Therefore, the resistance of a platinized conductivity cell is read directly.

2.3.3.1.2. Conductance measurement networks

A preliminary consideration in selecting measuring equipment is the option of using either direct current (DC) or alternation current (AC) circuitry. AC equipment is generally used [13]. Polarization problems can be easily overcome with AC networks, while complicated probe designs are required to overcome polarization in DC networks. Also, AC equipment is readily available while

DC equipment, although simple, is difficult to obtain and is plagued by thermoelectric effects.

The common AC measuring device is the Wheatstone bridge. The balanced Wheatstone bridge schematic is shown in figure 2-16. A voltage is applied at points 1 and 3. The unknown resistance, R_u, is connected across points 1 and 2. The variable resistance is varied until the potentiometer reads zero. The bridge is considered balanced and $R_v = R_u$. The unbalanced Wheatstone bridge technique keeps R_v constant and correlates the voltage measured to the unknown resistance according to a calibration technique. The unbalanced Wheatstone bridge is more adaptable to an automatic data acquisition system than the balanced bridge technique as the unbalanced bridge requires no manual adjustments.

A simpler approach than the unbalanced bridge is to use a voltage or current divider circuit (figure 2-17). Resistance R_2 is the unknown resistance. A constant voltage or current is applied. Voltage V_2 in the voltage divider or $V_{2,3}$ in the current divider is measured and correlated to the unknown resistance R_2, or to the solution concentration, again, according to a calibration technique. The calibration technique is explained in Chapter 3, Experimental Procedure.

2.3.3.2. Conductivity Cell Probes

2.3.3.2.1. Probe design and construction

The conductivity cell probe design shown in figure 2-18 is the design developed for the blanket fuel subassembly mixing experiments. Ideally, to minimize exit effects, probes are inserted a short distance into each subchannel. To fit into the small (0.113 in. equivalent diameter) blanket interior subchannels and to allow for vibration and positioning errors, probes with a diameter close to 0.05 inches are required. Probes of that size are difficult to manufacture and are fragile. The smaller probes are, the more difficult they are to seal against water leakage. An option to the small probes which allows the use of larger, sturdier probes is to place the probes at the exit plane of the subchannels. Exit effects can exist but are considered unimportant as long as the probes are within one hydraulic diameter of the exit plane. Little flow redistribution is expected to occur within one hydraulic diameter of the exit plane[19]. The option of the probes placed at the exit plane is selected over the option of probes inserted into the subchannels primarily for manufacturing considerations. Because there is more space to work with in a larger probe, manufacturing is easier and quality control is,

therefore, much better. The option of placing the probes at the exit plane gives more reliable probes than those which are made to fit into the subchannels. Probes for the LMFBR fuel assembly salt injection experiment at MIT are 0.09 inches in diameter and are beset by failure problems due to leakage. The probe tube diameter chosen for the blanket experiment is 0.125 inches to facilitate probe assembly. This size is considered small enough to not excessively disturb subchannel flow distributions. Special precautions are taken in the design to minimize probe failures due to leakage past the epoxy seals at the ends of the probes. The soldered joint is covered with heat shrinkable insulation, and the probe tube is backfilled with polyurethane. Platinum is chosen for the probe electrodes because of its chemical inertness and high electrical conductivity. Probes are assembled as described below (figure 2-18).

One-half inch pieces of platinum wire are soldered to two insulated, copper lead wires. A minimum of 1/4 inch of the platinum wire extends beyond the soldered connection. The wires are fed through the stainless steel tube. The soldered connections are coated with epoxy glue, and about a half-inch long piece of polyolefin insulation is slipped over each connection. The polyolefin

is heat shrunk over a candle flame. The leads are pushed into the tubing until the platinum wire extends about 1/4 inch beyond the tubing. That end of the tubing is sealed with epoxy.

Once the epoxy dries the tube is backfilled with polyurethane plastic. A large hypodermic syringe is useful in this step. Several applications are necessary to ensure the tube is full of plastic. After the last application dries the top end of the probe tube is sealed with epoxy. All excess epoxy is removed after it has dried.

The length of the lead wires required is judged by the experimenter. Ample length must be provided to connect the probes to the data acquisition system. In this case five feet is adequate. The lead wires are connected to 16 conductor ribbon wire with plugs to plug into the data acquisition system. There are 8 probes connected to each ribbon wire. As a result, the probes are divided into 15 groups of 8 and one group of 6.

After at least 2 days drying time probes are leak tested. Immerse the probes in water for 2 to 3 days. Connect the probes to the data acquisition system and read each probe while it is still immersed in water. Ensure probe lead wires are suspended in the water and not touching anything. Probes with a reading significantly lower than the rest of the probes or which give

successively lower readings are suspect of leaking. Remove these probes from the water and dry the lead wires. These probes are read again by the data acquisition system. If the probes read open circuit voltage they are not leaking. Any reading below open circuit is an indication of leakage. Leaking probes are repaired or replaced.

2.3.3.2.2. Platinization

Platinization is the process of electroplating finely divided black platinum on the electrodes of the conductivity cell probes. The probe electrodes are first cleaned by dipping them in a solution of isopropyl alcohol, ethyl ether and hydrochloric acid (see Appendix 2, Equipment List). The electrodes are electroplated in a solution of 0.025N hydrochloric acid containing 0.3% plantinic chloride and 0.025% lead acetate. The platinizing current is 10mA per square centimeter of exposed electrode surface area. The polarity is reversed every 10 seconds until both electrodes are covered [13]. For the probe shown in figure 2-18, the platinizing current is 1.62mA.

The effectiveness of platinization is assessed by making conductance measurements at several frequencies. Deviation of the resistance readings with frequency is limited to within 2% if platinization is effective [14].

To prevent gas absorption by the platinization on the probe electrodes, probes are stored in water. Gas absorption causes polarization errors. If a probe is allowed to dry for several days it is cleaned and replatinized.

2.3.3.2.3. Probe support scheme

The purpose of the probes is to monitor the conductivity of each subchannel of the blanket fuel subassembly. The subchannels and the desired probe positions are shown in figure 2-19. The numbering scheme shown in figure 2-19 is for reference purposes only. The numbers denote the geometric position of subchannels and not probe numbers. The centroid of each subchannel is the most logical position for each probe. To achieve the exact positioning required, the positioning scheme shown in figure 2-20 is utilized. The blanket fuel rods are held in place by 6 inch long, 1/4 inch diameter upper support rods. Each upper support rod fits one inch into each fuel rod and fits through a countersunk hole in support plate 3. Four of the corner rod support rods are extended 1-1/2 inches and are threaded to position the support plates.

The holes for the upper support and injection rods are shown in figure 2-21 and listed in table 2-2. The

holes for the probes are shown in figure 2-22 and listed in table 2-3. Support plate 3 has holes for support rods, injector rods and probes. Support plates 1 and 2 have holes for the probes, injector rods and the four extended corner support rods (holes 1, 27, 35 and 61 in table 2-2).

The rubber gland is included to ensure probe position does not change due to vibration of the test section. Once all the probes are in place the top 4 nuts are tightened down expanding the rubber gland and securing the probes.

2.3.3.3. Data Acquisition System

The data acquisition system shown in block diagram form in figure 2-23 was designed and built under the direction of Alan S. Hanson, a Graduate Student in the Nuclear Engineering Department. Up to 128 channels can be monitored using a current divider circuit to measure the unknown resistance. The use of the current divider allows the system to normalize voltage output in a zero to unity range. The channels are numbered using a three digit octal scale beginning with 000 for channel number one and ending with 177 for channel number 128.

Once the data collection process is started a different probe is read every 2 seconds. As each probe is energized, its voltage is filtered and amplified by the

signal conditioning circuits. The analog signal from the probes is converted to a digital signal in the analog-to-digital converter (ADC). The digital data output from the ADC is in the form of a parallel signal which is not compatible with a Teletype machine. Thus a parallel-to-serial converter or serial transmitter is required to interface the ADC to the Teletype. This component takes a three-digit octal channel address and a three-digit voltage data signal, converts them to serial ASCII code and transmits them to the Teletype one digit at a time. Output from the Teletype is a listing of the data as well as a punched paper tape record of the data. The paper tape is read into the IBM 360/168 computer via a Teletype Model 38 through a time sharing option at the MIT Information Processing Center. This means the paper tape is read directly into secondary computer disc storage without having to punch the data onto computer cards.

Operation of the data acquisition system requires the use of three commands on the Teletype. An exclamation point(!) tells the system to start at the beginning, channel 000. An asterisk (*) tells the system to proceed while a dollar sign($) is a signal to stop. Printing must be stopped before an asterisk or exclamation point are used. Ensure the system has warmed up at least one-half

hour before use. A good operating frequency for the oscillator is around 1150 Hertz, although any frequency from about 500 to 5000 Hertz should give good results [16].

Chapter 3

Experimental Procedure

The major objective of this work is to gather both mixing and pressure drop data. The first step in any experiment is to ensure that all systems are properly assembled and line up. The initial experiment is the taking of the pressure drop data, and the final is the collection of the mixing data. This order is chosen because the pressure drop experiment serves to test the blanket bundle without the probes in place, thus minimizing any chance of damage to the probes.

Data is collected over the Reynolds number range of 0 to 12000 (see pages 52 and 58 and table 3-2). Using water as the experimental fluid is justifiable for high Reynolds numbers because buoyant effects are unimportant [2]. The validity of water based data for low flows is not established due to possible flow instabilities caused by natural convection effects at low sodium flow rates. Since the flow conditions at which data collected from water based experiments becomes invalid is not known, data for the low flow rate is included. Twenty-five gallons per minute (Re = 1540) is the lowest flow used because it is the lowest flow rate for which the appropriate salt solution flow rate can be measured with any confidence.

3.1 Test Section Assembly

Proper assembly and disassembly procedures are followed to ensure that all components are in their correct position for an experiment and to ensure that no components are damaged by improper handling. The assembly procedure consists of the fitting together of the blanket rod bundle, its placement in the flow loop, and the placement of the probes in their proper position.

3.1.1. Assembly Procedure

Step 1. Attach the bottom end plate to the lower plenum. Attach a lifting plate to each metal side of the flow housing. Attach the two plexiglass sides to one metal side using three cap screws on each side. The dowel pins in the plexiglass on the open side are knocked flush with the inside faces. Place the attached plexiglass and metal sides vertically on blocks next to the lower plenum where the chainfall can reach from the padeye in the overhead. Ensure the pieces are supported so they cannot fall over.

Step 2. Put all the bottom support rods in their holes in the metal side. Put all the blanket rods and injector rods in place with orientation as shown in figure 2-19. Injector rods are placed in rod positions 31, 55 and 59 (figure 2-21). If the wire wrap orientation is reversed, the holes in the edge injector rod are not in an edge subchannel.

Step 3. Put the second metal side in place and knock the dowel pins into their holes in the second metal side. Put at least three cap screws in both sides of each metal side.

Step 4. Loosen one plexiglass side and shim it about $\frac{1}{16}$ inch away from the metal sides. Feed the o-ring seal down each slot. Ensure the o-ring extends about $\frac{1}{16}$ inch beyond each end of the flow housing for a proper seal. Remove the shims and secure the plexiglass in place using all the cap screws for that side.

Step 5. Repeat step 4 for the other plexiglass side.

Step 6. Gaskets are cut beforehand by placing gasket material on each end plate and cutting out the holes for the dowel pins and the flow housing. Place a gasket on the bottom end plate and put the assembled bundle in place by putting the dowel pins which are on the flow housing in the dowel pin holes in the end plate. Put a gasket on top of the bundle and put the top end plate in position. Install the four tierods.

Step 7. Place the upper support rods in the rods and assemble the upper rod support structure (figure 2-20).

Step 8. Platinize the conductivity cell probes according to section 2.3.3.2. Probes may be platinized several days in advance of installation and stored in water. Probes are checked for leakage, again, after platinization.

Step 9. Install the probes according to the numbering scheme in figure 3-1. Probes in each subchannel type (interior, edge and corner) are numbered sequentially to conform to input requirements set by the data reduction computer code. The numbering sequence is designed to give minimum interference from adjacent probes during installation and to give maximum flexibility in data collection. Data collection is more rapid by not reading unnecessary probes.

Probe installation proceeds by gently pushing each probe through the 3 support plates and the rubber gland until the probe electrodes are $\frac{1}{32}$ inch above the bundle exit plane (figure 2-20). This ensures that vibration cannot cause any of the probes to touch any rods and give an incorrect reading. The $\frac{1}{32}(0.031)$ inch distance of the probe electrodes above the exit plane is considered close enough to the exit plane to yield a result representative of subchannel conditions since this distance is about $\frac{1}{3}$ the smallest hydraulic diameter (0.091 in., corner subchannel) of any of the subchannels.

Probes are installed in groups of 8. After each group is in place, it is temporarily plugged into the data acquisition system and is checked for short circuits. Shorts can occur from probe leakage or from probe electrodes

touching the stainless steel rods. After all probes are installed and checked, disconnect them from the data acquisition sytem.

Step 10. The upper plenum is installed by suspending it about 12 inches above the top end plate. This prevents the heavy upper plenum from damaging any probes or probe wires. The probe wires are passed into the bottom and out of the top of the upper plenum. The upper plenum is lowered in place and secured to the top end plate and the drain line. Plug the probes into the data acquisition system.

Step 11. Install the injector inner rods by passing them down through the large holes provided in the support plates and into the injector rods. Be careful not to damage any probes or probe wires.

Step 12. Connect about 15 feet of $\frac{1}{4}$ inch plastic tubing to each injector rod.. Connect about 10 feet of $\frac{1}{2}$ inch tubing to each pressure tap on the flow housing. For the mixing experiments, the pressure taps may be plugged.

Since pressure gauges for each pressure line are not available, the pressure lines are connected to a manifold which is connected to the low pressure end of a differential pressure gauge (figure 3-2). One of the 12 pressure taps in the flow housing is selected as the reference pressure tap and is connected to the high

pressure side of the differential gauge and to an absolute pressure gauge. The differential pressure gauge has a high pressure side and low pressure side. If the pressure in the high line to the gauge is lower than the low line, the gauge does not give a reading. To avoid reversing pressure lines on the gauge, a line which is higher, or lower, than the rest can be chosen as the reference line. Assuming circumferential pressure differences exist, the pressure at tap 1 (figure 2-5) in the lower set of pressure taps may be the highest because subchannel velocity may be the lowest among the subchannels monitored. The subchannel conditions at tap 1 at the lower level of taps may be considered analogous to an expansion in a pipe since it is the furthest from any wire wrap which may serve to constrict the flow in the subchannel. Since the velocity is likely to be low relative to the other edge subchannels at that level, the pressure should be relatively high. The lower level of taps also has the highest average pressure.

The possibility exists that the pressure at the lower injector rod position is higher than at the pressure taps. However, since the inner rods have their position changed, they are not a constant reference pressure. If the injector rod pressures are higher, the pressure lines to the differential gauge are reversed for those readings.

3.2. Pressure Drop Experiments

3.2.1. System Assembly and Line Up

The directions in sections 3.1. are followed, with the exception of steps 8, 9 and 13. To commence the pressure drop experiment, the flow loop is lined up as in figure 3-3 and table 3-1.

3.2.2. Pressure Drop Experimental Procedure

There are to be two series of pressure drop tests. The first series is to determine the circumferential and axial pressure drops according to sections located 1 foot and 3.5 feet down from the exit plane of the test section. The circumferential pressure data will show if pressure differences exist around the bundle. This is valuable in determining bundle flow patterns. The axial pressure drop is useful for determining pumping power requirements.

The second series of pressure drop tests are detailed axial pressure drop measurements using the injector rods as pressure taps. This also gives information on flow patterns. A record of axial pressure variation is also valuable for rod vibration and support analysis.

Although referred to as a two series experiment, the data for both pressure series is taken almost concurrently.

Once a flow rate is set, the pressure taps at both levels are measured. All three injector rods are used to measure axial pressure traverses according to the following intervals.

Distance from exit plane (in.)	Interval
42-30	every 6 in.
30-12	every 1 in.

These intervals are expanded if results show larger intervals are adequate, or they are shortened if smaller intervals are required. Injector rod readings at the 42 and 12 inch levels complement the flow housing pressure tap readings.

Flow rates are varied from zero to the maximum attainable, 200 gpm. This spans the Reynolds number range from 0 to 12,000. All subchannels are fully turbulent at 157 gpm. Readings are taken at the following flow rate intervals.

GPM	Interval
0-50	every 5 gpm
50-100	every 10 gpm
100-200	every 25 gpm

The 5 and 10 gpm intervals are close to the mimimum which can be read on the flow meters in those flow ranges. The intervals are expanded above 100 gpm because any hydraulic flow instabilities and fluctuations are expected to exist only at the low flow rates.

The results of these experiments are compared to theoretical pressure drop predictions. Also, from the pressure drop data, overall bundle friction factors are determined.

3.3. Mixing Experiment

3.3.1. System Assembly and Line Up

The directions in section 3.1. are followed, with the exception of step 12. To commence the mixing experiments, the flow loop is lined up as in figure 3-3 and table 3-1. If there is a temporary rescission of the mixing experiment, it is necessary to ensure that the probe electrodes remain covered with water. This is accomplished by closing valve 5 after the upper plenum is filled with water. Monitor the water level to ensure that it stays above the probe electrodes.

3.3.2. Mixing Experimental Procedure

The approach to the mixing tests is to inject salt solution over the total possible axial range at bundle Reynolds numbers of 1540 (25 gpm) and 11400 (185 gpm). As noted earlier, all subchannels are turbulent (Re = 2300) at a flow rate of 157 gpm. Next, one injector position, depending on the results of the previous two tests, is chosen. Injection at this position is accomplished for the full range of flow conditions (laminar, transition, turbulent) to show variations between the other two flow

rates. The first step in a mixing experiment is the calibration of the conductivity cell probes. Once this is accomplished, the mixing data can be collected.

3.3.2.1. Calibration

A calibration curve for each probe must be generated since each probe has slightly different response characteristics. To generate the required calibration curves, the probes are subjected to various concentrations of salt water. Curves are formulated from the data using a least squares fitting criterion to Chebyschev polynomials (see Appendix 3, Data Reduction). A better fit is obtained using these polynomials than with ordinary monomials and in a manner that is economical in use of computer times. The salt solutions used in the calibration curves must bracket the expected concentrations the probes experience in a mixing test.

The lower value for the concentration curve is the background reading. The upper value is determined by trial and error. A typical resistance versus concentration curve is shown in figure 3-4 [13]. The strong solution concentration dependence exhibited in figure 3-4 results from the effect that solution concentration has on the ionic dissociation of the salt. As concentration increases, interionic interactions increase and the percent of ionic dissociation decreases. Ion mobility also decreases due to interactions between oppositely charged

ions. At low concentrations there is more complete ionic dissociation and freer ion movement, since there are fewer interionic interactions. For accurate determination of salt concentrations, resistance readings ideally are kept to the left of the flat portion of the curve in figure 3-4. The further the readings are to the right on the curve, an error in resistance translates to a greater error in concentration. Therefore, a salt solution must be found which places the maximum reading to the left of the flat portion of the response curve for the probes. In addition, adequate solution concentration is required to give good probe response for injection deep in the test section.

The appropriate solutions are found by injecting a wide range of solution strengths deep in the bundle and near the top of the bundle for the two flow rates of interest for both central and edge injectors. A plot of the response of several probes will show where the response flattens out. The injection concentration is limited to no greater than that point. Injection of the same solutions deep in the bundle shows if they are of adequate strength to give good probe readings for deep injection. If not, a stronger concentration may have to be used for the lower injection points. For the low flow

case (25 gpm), and the high flow case (185 gpm), strengths of 10, 15 and 20 gm./lb. can be tried,

Once the upper limit of injection concentration has been set, the upper limit on the salt concentration which the probes actually experience is found. Probe response to injection of the maximum solution concentration close to the probes is determined first. For the mixing experiment, using the equal velocity injection criterion, the injection flow rate is 3.8% of the interior subchannel flow rate and 1.5% of the edge subchannel flow rate. Therefore, the salt solution may be expected to be diluted at least $\frac{1}{25}$ of its original value by the time it reaches the probes when injected 1 inch away. Starting with a solution $\frac{1}{25}$ of the maximum injection solution, the whole test section is filled with solution of this strength. Depending on the probe readings, the test section is refilled with a stronger or weaker solution until the maximum injection concentration readings are just exceeded. The solution strength which gives probe readings which just exceed those for the maximum injection solution is the maximum calibration solution. Assume the maximum calibration solution is X gm/lb. The remainder of the calibration solutions are $\frac{3}{4}$ X, $\frac{1}{2}$ X, $\frac{3}{8}$ X, $\frac{1}{4}$ X, $\frac{1}{8}$ X, $\frac{1}{16}$ X and 0 or background. A total of 8 calibration points are chosen to ensure the whole solution concentration

range is adequately covered. A closer interval between the lower concentrations is chosen due to the higher sensitivity of the instrumentation at changes at low concentrations.

The actual calibration data is now taken and recorded on paper tape. The required format is described in Appendix 3, Data Reduction. It is very important to take all readings at the same water temperature because conductivity changes about 2% per ^{o}C.

After all the calibration data has been collected, it is fed into secondary disc storage and edited using the time sharing option available at the MIT Information Processing Center. Calibration curves are generated with the calibration curve computer program (see Appendix 3, Data Reduction).

3.3.2.2. Mixing Data

In the previous section, Calibration, the solution strengths to be used are determined for the laminar and turbulent experiments. The injection rods are located so that injection can be accomplished into an edge, a peripheral and a central subchannel (positions 31, 55 and 59). There is no set order for which injection rod is used first. Approximately 30 pounds of water are required to fill the salt solution tank (figure 2-14) to the salt injection line outlet. For the 185 gpm injection

case, about 22 pounds of solution is used per hour, and a complete injection run for one injector will take about 5 hours. Therefore, a minimum of 140 pounds of solution is made up for each complete injection run for the 185 gpm experiment. Only about 3 lb/hr of solution is used for the 25 gpm injection runs, so that a total of 50 pounds of solution is adequate for each of those runs.

Each injection run consists of 48 injection points at the following intervals.

Distance from bundle exit	Interval (in.)	Number of points
1-6	1/4	21
6 1/2-12	1/2	12
13-24	1	12
30-42	6	3
		48

The increasing intervals reflect the fact that as the distance from the exit of the test section increases, mixing becomes more thorough and small distances between injections will not give noticeable differences in instrument readings. These intervals may be adjusted within the limits of the injector rod hole patterns as the data demands. For high flow rates, the greater mixing possible may require closer intervals near the top. At low flow rates, the intervals may be expanded.

Before starting an injection run, all systems, including the flow loop and injection system, are thoroughly flushed with water to wash out any salt or

debris. The salt solution is mixed, put into the salt injection tank and the injection tank charged with 60 psi of air. Sixty psi is considered adequate for the bundle pressure drops anticipated. It may be increased to 110 psi if needed. The flow loop is lined up according to figure 3-3 and table 3-1.

Once the loop flow rate has been set at the desired rate, the injection flow rate is set. Using the equal velocity injection criterion, which says the injection velocity equals the subchannel velocity, the injection flow rates are set according to table 3-2. The flow rate has to be set for each position of the inner rod because of the pressure drop in the test section.

After the experiments at 25 gpm and 185 gpm are complete, readings from several probes in different positions in the bundle are plotted for each flow rate. From these plots an injector position for flows spanning the range between the two flows is chosen. A position is chosen which shows the effects of mixing in both flow regimes. After the injector position has been chosen the final experiment is run at the loop and injection flow rates shown in table 3-3.

Salt solution injection is accomplished by first opening the valves between the injection tank, and the injection rod which is lined up to the tank. The sliding inner rod

is then lined up with the bottom hole in the injection rod. This is accomplished by pushing the inner rod as far as it will go into the injector and then pulling it up $\frac{1}{16}$ to $\frac{1}{8}$ inch, at which time it lines up with the bottom hole. Solution only flows through the injector when the inner rod is lined up with a hole in the injector rod. There are two ways to determine the position of the inner rod and both are used. One is to count the holes passed by the inner rod, and the other is to record the travel of the inner rod on a rule securely attached to the overhead.

The readings for the 3 mixing tests are analyzed by a computer program developed by Alan S. Hanson (see Appendix 3, Data Reduction). Outputs of the program are printouts and plots of concentration against axial injection distance for each probe and mass balances for each injection run.

Chapter 4

EXPERIMENTAL RESULTS

4.1. Pressure Drop Results

The readings for the various pressure drop experiments are listed in Appendix 4 in Tables A4-1 through A4-4. Tap 1 of the pressure taps 42 inches below the bundle exit (Fig. 2-5b) is the reference for all the differential pressure measurements. In this discussion, only the readings from the differential pressure gauges are used except when the readings are beyond the gauge range of 400 inches of water. Using the differential pressure gauges means that the reading from only one gauge is used at one time. Using the absolute gauge readings to determine a differential pressure means that readings from two gauges are used to determine a pressure difference, thus compounding any gauge errors.

4.1.1. Circumferential Pressure Results

With the exception of Fig. 4-2, the results of the circumferential pressure tap readings (Figs. 4-1 through 4-4) show a consistent variation around the rod bundle. Reference to Fig. 2-5 shows that tap 4 of the upper set and tap 1 of the lower set of pressure taps have the same wire wrap orientation. The behavior in Fig. 4-2 cannot be explained physically, except, possibly, by a flow blockage. The other three figures show that the minimum pressure

occurs at the tap location where the wire has passed from the edge subchannel into the gap between the rods. Since the taps which are right at the wire (5 and 6) are at a higher pressure, the low pressure can be caused by a low pressure region or wake behind the wire. The maximum pressure occurs when the wire wrap is in the gap between the rods and the wire is entering the edge subchannel. This can be due to the fact that this position is far enough upstream and downstream from the wire wrap to avoid its effects.

The axial wire wrap variation is analogous to the circumferential variation. This can be seen by comparing Figs. 2-5 and 4-5. Therefore, Fig. 4-6, which is a plot of axial pressure minus average axial pressure in the edge subchannel over 1-1/2 wire wrap lead lengths, varifies the pressure variations in Figs. 4-1, 4-3 and 4-4. In Fig. 4-6 the average axial pressure represents that pressure at location z obtained from passing a straight line through the average bundle pressure at the 12 and 42 inch axial measurement planes.

4.1.2 Axial Pressure Results

Figures 4-7 through 4-14 show the pressure variations for a central and an edge subchannel for various flow rates. Figure 4-7 is an overall view of the relationship between the pressure gradients for the central subchannel. The remaining seven figures are more detailed results over

several lead lengths. Figure 4-7 is a plot of the actual readings taken, which are the differences in pressure from pressure tap 1 at 42 inch level. This means that the higher the reading the lower the pressure. The remaining figures are plotted with an inverse differential pressure scale in order to present the true physical picture of the axial pressure variations.

The figures show that the axial pressure drop is non-uniform and is somewhat periodic. For the edge subchannel, minimum values occur where the wire wrap is entering from the edge subchannel into the gap between the rods (20, 24, 28 inch positions). The maximum values occur where the wire wrap is leaving the gap and entering the edge subchannel (22, 26, 30 inch positions). The pressure in the edge subchannel is, in general, lower than in the central subchannel. A major difference between the two subchannels types is the presence of swirl flow in the edge subchannel. Swirl flow may cause the velocities in the edge subchannel to be higher than in the central subchannel, thus giving a lower pressure in the edge subchannels.

The central subchannel has a smaller magnitude pressure variation than the edge subchannel. The high pressures for both subchannels are close together while the low pressure points are widely separated. As noted above, the lower edge subchannel pressures are probably caused by swirl flow effects.

However, since the high pressure points for both subchannel types nearly coincide in many cases, swirl flow can be considered to be absent at those points. This means that swirl flow is periodic in nature and is superimposed on the overall bundle flow sweeping pattern.

At some points the plots cross because the central subchannel pressure drops off sharper after a peak than the edge subchannel pressure. This can be due to the additional wire wrap present in a central subchannel which is absent in an edge subchannel. The additional wire means that there are shorter undisturbed lengths of rod in a central subchannel than in an edge subchannel. Therefore, the high pressure is present over a shorter distance in the central than the edge subchannel.

4.1.3 Friction Factor Results

The average pressure at both pressure tap locations was calculated by adding the readings and dividing by six. The difference between the average pressure at each location is the pressure drop over 30 inches of the bundle. The pressure drop is compared to Novendstern's correlation [15] in Fig. 4-15. Figure 4-16 is a plot of friction factors calculated according to Appendix 4. As in Fig. 4-15, Novendstern's correlation is high. Blasius and Rehme [22] give results which are low.

The difference in Novendstern's results and the experimental results is explained by comparing the applicable range

of conditions for Novendstern's correlation with the experimental conditions (Table 4-1). Since a correlation favors the center of the range of data used, a difference in results can be expected since the experiment is outside the applicable range of rod diameter and is at the limits for pitch to diameter and lead to diameter ratios.

Rehme's friction factor does not give a close correlation because it was determined for pitch to diameter ratios of 1.125 to 1.417. Blasius' friction factor is low because it applies to smooth pipes, and wire wrap can be considered to be a surface roughness.

Rehme's friction factor curve appears to fit the shape of the experimental friction factors the best of the three calculated curves. By trial and error, the constants in Rehme's friction factor equation (see Appendix 4) are varied until a good fit with the data is obtained. The form of Rehme's friction factor shown below is suggested.

$$f'' = \frac{80}{Re'} + \frac{0.114}{Re'^{0.133}} \qquad (4\text{-}1)$$

A comparison of the adjusted friction (f") with the experimental results in Fig. 4-17 shows f" fits the data well.

4.1.4 Pressure Drop Error Analysis

Only relatively minor errors are expected for the pressure drop experiment. The absolute pressure gauges are

rated at ± 0.15 psi. The differential pressure gauges were not rated for error, but a ± 1% error is estimated. This estimate is based on the recommendations of laboratory personnel. The error in bundle flow rate is estimated at ± 2% [19]. When several readings are used for calculations, the total error is estimated by a root mean square error. A root mean square error involves squaring each error estimate, adding all the squared errors and taking the square root of the sum.

4.2 Mixing Results

The results of the mixing experiments in the form of salt concentrations (gm salt/lb water) are listed in Appendix 5. Plots of the calibration curves for various probes are shown in Figs. 4-18 to 4-33. Results of five experiments are shown in Figs. 4-34 to 4-88. Salt concentration curves for the injection subchannel and other selected subchannels, a salt mass balance curve and cross-sectional or planar plots of salt concentrations at various axial levels are presented for each experiment. Although seven mixing experiments were conducted only four and part of the fifth are presented. The data for two and part of the third has been garbled by the computer. When the data for these experiments was being read into secondary storage, half of the total storage space available in the computer was not available due to a system malfunction. According to computer operators in the

Information Processing Center, the Time Sharing Option (TSO), which is utilized to read in paper tape inputs, could not respond to the rapid input of data from the tape because of the lost memory space. At this time there was a high user demand on the system and the TSO, in trying to meet all user demands, could not keep up with the paper tape being read in. The result in the computer was garbled data. The computer finally went off the line before the last set of data was completely read in. When the computer was put back in full service, the teletype which is used to read in the paper tape had lost power. In the past teletype repair has been very prompt. However, this time it was delayed for several days. When the teletype was finally repaired, the time available was too short to read in, edit and analyze the remaining data. As a result, the experiments presented are:

Central Injection 25 and 185 gpm flow rates

Edge Injection 25 and part of 185 gpm flow rates

Peripheral Injection 25 gpm flow rate.

4.2.1. Calibration Results

Following the procedures in Chapter 3, 25 gm of salt/lb of water was judged to be a good injection concentration. The salt concentration which covered the lower limit of probe response for 25 gm/lb injection was 0.25 gm/lb. The calibration curves were generated using salt concentrations of 0.25, 0.18, 0.12, 0.09, 0.06, 0.03, 0.15 gm/lb and background.

Sketches of the response of several probes showed the curves to be within the guidelines specified in Chapter 3.

Figures 4-18 to 4-23 show the curves for probes 1 and 2 using 4, 5 and 6 coefficients to fit curves to the data. These are two sets of lines in each figure. One line is point to point while the other is the fitted curve. The four coefficient curves are judged to have too much error over the whole range of the data. The five coefficient curves tend to be much too low at the beginning of the curves. The six coefficient curves give the best fit although some are high at the beginning as seen in Fig. 4-23. However, in comparing several probes calibration curves, the six coefficient curve fits are judged best and are used throughout. However, Figs. 4-25 through 4-33 show that the fit for many probes is still not good at the beginning of the curve.

This poor fit may have been due to the fact that the calibration curves had too much curvature to give a good fit. That is, too strong an injection concentration was used which means high concentrations were used to calibrate the probes. This high concentration led to curvature at the high end of the calibration curves which made it more difficult to curve fit data (see Sections 5.1 and 5.2 for possible corrective procedures).

4.2.2 Central Injection Results (25 gpm, Re = 1542)

The central injection results are shown in Figs. 4-32 to 4-43. (Refer to Fig. 3-1 for probe and injector positions.) The salt concentrations (Figs. 4-34 to 4-38) are generally periodic every wire wrap lead length with smaller perturbations every half lead length. These are the points where the wire is in the gap between the rods and are the same position that the high and low pressure points are found (Sec. 4.1.2).

The mass balance plot (Fig. 4-39) also shows variation every lead length and half-lead length. The mass balance drops off sharply two lead lengths from the exit. This shows the salt is not dispersed well in the subchannels for at least two lead lengths after injection.

The planar salt distributions (Figs. 4-40 to 4-43) show the cross-sectional salt concentrations at various axial levels. These figures show the salt dispersion is centered below the injection subchannel (underlined in the figures). This shows that, since the wire wrap direction is counterclockwise looking downstream (see Fig. 4-5), the salt is pushed by the wire wrap [21].

4.2.3 Central Injection Results (185 gpm, Re = 11, 410)

The probes plotted for the high flow central injection (Figs. 4-44 to 4-48) show responses very similar to the low flow responses. The mass balance (Fig. 4-49) is not as good for deep injection, and it also drops off two lead lengths

from the exit. The planar salt dispersions (Figs. 4-50 to 4-57) are also similar to the flow dispersions. The high flow planar dispersions are slightly wider and are centered more to the left than for the low flow case. Even though there is less time for mixing in the high flow case, there seems to be greater rate of radial dispersion. The centering of the salt dispersion down and to the left of the injection subchannel further confirms that the salt is pushed by the wire wraps.

4.2.4 Edge Injection Results (25 gpm, Re = 1542)

Figures 4-58 to 4-61 show that the salt concentrations for the edge subchannel at low flow are periodic with lead length but have very erratic magnitudes. The erratic magnitudes may be caused by swirl flow effects. Since the major peaks in the plots occur at different positions for different probes, swirl flow is apparently transferring the majority of the salt from one subchannel to another.

The spike shown in the mass balance plot (Fig. 4-62) occurs at one half lead below the exit. There is no wire wrap above that level in the injector subchannel. This spike, coupled with the increasing mass balance with distance, leads to the conclusion that the salt is being channeled along the wires in the edge subchannels. This is further supported by the peaks in the mass balance curve occurring at the half-lead points. These are the positions where the

wire is entering the gap between the rods from the edge subchannels and are the high pressure points (see Sect. 4.1.2).

The planar salt distributions (Figs. 4-63 to 4-67) show that the salt is carried in the direction of the wire wrap but is not dispersed as much as for the central subchannels. This, again, can be due to the salt being channeled along the wires in the edge subchannels.

4.2.5 Edge Injection Results (185 gpm, Re = 11,410)

This experiment is complete only for the 23 to 42 inch levels due to the computer problems mentioned above. The salt concentration and mass balance curves (Figs. 4-68 to 4-72) give little information. The planar salt dispersions (Figs. 4-73 and 4-74) show a greater dispersion into and around the bundle than for the low flow case.

4.2.6 Peripheral Injection Results (25 gpm, Re = 1542)

The peripheral data has several bad data points between the two lead length level and the exit, which give too high readings. However, since poor mass balance occur in this area, this region is of little value. The salt concentration data (Figs. 4-75 to 4-79) show periodicity with lead length, but show little consistency from one subchannel to the next. The peripheral region, therefore, appears to be a region of confused flow compared to the rest of the bundle. This can be due to the fact that it is a transition region between the predominant swirl flow in the edge subchannels and the flow

sweeping patterns in the interior subchannels.

The mass balance plot scale is distorted due to the bad data points, but shows a better mass balance than the other subchannel types. Therefore, this peripheral area in the bundle may have better mixing due to its more confused flow patterns.

The planar dispersions (Figs. 4-81 and 4-82) show that salt is carried into the interior and the edge subchannels. The majority of the salt stays in the peripheral region.

4.2.6 Mixing Error Analysis

The errors in the mixing experiments are combined into the salt mass balance error. Salt mass balance is affected by flow meter error, injection and main flow variations, error in preparation of salt solutions, background variations, foreign matter in the water, probe positioning, calibration curve data fit, and instrumentation error.

Instrumentation shop personnel estimate that flow meter errors are $\pm$ 2%. However, injection flow variations of various magnitudes were occasionally experienced due to foreign matter fouling the flow meter float. These variations lasted until detected by the operator. Most lasted only 5-10 seconds. Main flow variations were no more than $\pm$ 2%. Salt solutions were carefully prepared so that at most an error of $\pm$ 1% in solution concentration is expected. Overall background variations are negligible. However, at times pieces of metal and

rust were observed passing through the bundle. These pieces probably caused error in some probe readings. The fact that probes are positioned at the exit to the subchannel instead of inside it may cause some salt to pass undetected. At most, 5% may go undetected [19].

Calibration curve error is concentrated in the beginning of the curve where the low salt concentrations occur. Large errors for small readings may occur. Since many probes may have readings in this area the overall effect may be as high as an overall error of 10% in salt mass balance. Instrumentation error is determined by data acquisition system error. The data acquisition error is made up of voltage variations and system sensitivity. Voltage variations are approximately $\pm$ 1%. System sensitivity is a function of the background readings. Above readings of 0.6 millivolts system sensitivity may be poor. This applies to the present experiment because background readings were 0.65-0.7. The actual sensitivity is not known.

The root mean square error of the above errors, neglecting system sensitivity, is as follows:

$$\sqrt{(.02)^2 + (.02)^2 + (.05)^2 + (.1)^2} = 12\%$$

Examination of the mass balance plot shows that the 25 gpm central and peripheral and part of the 185 gpm central experiments are close to this error.

This means that the sensitivity error may be not much more than 10% which yields a root mean square error of 15%. Examination of the various error types gives the conclusion the RMS error cannot be reduced much below 10%. This can be achieved by eliminating the sensitivity error (see Sect. 5.2) by taking great care in positioning the probes and preparing salt solutions, and by reducing the calibration curve error (see Sect. 5.2).

Chapter 5

FUTURE WORK

This chapter is divided into four sections. The first section discusses a step which may improve the mass balances, and therefore, the reliability, of the mixing data already collected. Since the LMFBR blanket wire wrap design has been changed to shaved wires for the edge rods [21], the blanket mixing experiment is likely to be repeated for the new design geometry. The second section of this chapter discusses recommendations to follow for future blanket mixing experiments. The third section discusses possible future experiments utilizing the blanket test section. The fourth section discusses analytical work which may be performed on the data.

5.1 Improvement on Present Work

Section 4.2 points out that the calibration curves do not fit the data well at low salt concentrations. A possible improvement is to separate the calibration curve into two separate curves each with six calibration points. One curve is calculated using the first six points and the second using the latter six points. The new curves should fit the calibration data better because the six data points have less curvature than all eight points. The data reduction program should be altered so that it determined which curve is appropriate for each probe reading. The appropriate curve is used to assign

a salt concentration to the probe reading, which for low concentrations, should be more accurate than before.

The above procedure can be accomplished by minor changes to the CALIB and the data reduction programs (see Appendix 4). The CALIB program should be used for each set of six calibration points. For the first set of six, it can be used in its present form with NPTS = 6. For the second set of six points use NPTS = 8, but all indices in the program after line 312 which involve NPTS should be changed from reading 1, NPTS to 3,NPTS. This means that only the latter six calibration points are curve fitted. Some variables should be renamed so that the computer does not call up the values for the first curve. Table 5-1 is a list of the changes in CALIB for the second curve.

The changes to the data reduction program listed in Table 5-2 enable it to read in both calibration curves and choose the appropriate curve for each probe reading. The changes apply only when the calibration curves are read in from secondary storage and not when the calibration curves are calculated as part of the data reduction program. Note that a job control language (JCL) card must be present in the program for each data set read in from secondary storage. Printouts of the program provided to Professor Todreas show the format and positions in the program of these JCL cards. This comment applies to CALIB, also.

The data in storage is listed with its data set name in Table 5-3. This data will be stored until 30 June 1975 or until funds in the account are depleted. The User Accounts Office at the Information Processing Center can be consulted for the procedure to continue storage of the data after 30 June. Since different user accounts probably will be used, a special procedure for using data under different accounts is required. See IPC publication OS-31. Paper tapes and printouts of the data are in Professor Todreas' custody. The steps to input data from a paper tape is described in IPC publication OS-41. Experience with inputting large amounts of data using paper tape has shown there are several things to watch for when using paper tape. The tape reader must be kept clean at all times. The paper tape leaves a deposit which fouls the tape reader after several hours of use. Cleaning the reader about once an hour with a small stiff brush prevents this accumulation. Using smooth, shiny paper tape instead of rough surfaced tape also minimizes the deposits from the paper tape. Experience has also shown that if the computer goes down during the time when paper tape is being read in, it is best to start the data set over. The computer will save the data that was put in before the failure, but attempts to edit such data have been unsuccessful. Specifically, inputs of corrected data are placed at the end of the data set instead of where directed, and when the command to go down a

certain number of lines is given, it may be followed or the computer goes to the end of the data set. In essence, if there is any problem with the time sharing option, make sure it has been completely cleared up for several hours before inputting data from paper tape.

5.2 Future Mixing Experiments

One discrepancy to be corrected in future experiments is the improper curve fit to the calibration curves experienced in the present experiment. This can be accomplished by using a lower injection concentration. Twenty instead of 25 gm/lb salt concentration is recommended. The procedure outlined in Chapter 3 to determine the calibration concentrations should be followed. After the new calibration concentrations are found, the probes should be calibrated. The calibration curves can therefore, be assured and the steep slope in the curve avoided before the experiment is conducted. Such a steep slope in the calibration curve leads to inaccuracies because a small error in the data translates a large error in salt concentration. If the calibration curves are unsatisfactory a lower salt injection concentration is chosen until a good curve fit is achieved. The procedure for an experiment is take the calibration data, analyze the calibration data using CALIB, repeat calibration until it is satisfactory, conduct the mixing tests and analyze the mixing data.

Chapter 4 pointed out that some of the error in mass balance may be due to the high value of the background measurements. Background readings typically were 0.65 to 0.7 millivolts. Readings of 0.55 to 0.6 are considered to give better accuracy [16]. This may be achieved by using warmer water which decreases background resistance, although care must be taken to utilize water at the same or nearly the same temperatures for both the calibration and the test because of the high sensitivity of conductivity to solution temperature. During the whole period over which the tests were run fresh water was constantly run into the water channel to flush out oil which had been spilled. This kept the temperature of the channel water low. During the summer the water temperature may be high enough to reduce the background to a good level. If not, the circuitry in the data acquisition system will have to be altered to reduce the background readings. The validity of the insensitivity of the instrumentation at the high background levels requires confirmation by reanalysis of the data according to section 5.1 before changes are made to the data acquisition system.

When taking data during an experiment, ensure that a smooth shiny paper tape is used. The rough surfaced tape tends to leave deposits which cause the tape punch to mispunch and jam the tape. Cleaning the tape punch about once an hour is helpful in preventing the tape from jamming. Be thoroughly familiar with the format for the data required for the data

reduction programs. Punching the data on the tape in the proper format saves much computer editing time.

5.3 Future Experiments

5.3.1 New Blanket Design

It is recommended that the mixing and pressure drop experiments be repeated for the most recent LMFBR wire wrap design utilizing wire shaved to 1/2 diameter where they touch the flow housing. In other words, the gap between the rods and flow duct is reduced to 1/2 the wire wrap diameter. Table 5-4 is a comparison of blanket bundle characteristics with and without shaved wires.

To accomplish an experiment with the new design, the 30 edge rod wire wraps are shaved to 1/2 their diameter where they touch the flow housing. The flow housing is machined to the new bundle dimensions and new plexiglass sides are made.

5.3.2 Heated Rod Experiments

Reference 2 recommends the use of a heated rod experiment to conduct mixing experiments. Heated rod tests have the advantage of giving more reliable results than salt or hot water injection experiments (see sect. 2.3.1). Such an experiment can be carried out using the blanket test section. For instrumentation, shielded thermistors are recommended over thermocouples for their superior sensitivity and response (see The Omega Temperature Measurement Handbook provided to Professor Todreas). Heated rods may be procured from WATLOW Electric

Manufacturing Company. A request for an estimate sent to WATLOW is enclosed in Appendix 6. This request gives the specifications for heated rods suggested by E.U. Khan [8]. The letter was not answered due to its low priority with the company. Information regarding solid-state AC power controllers for the heated rods may be obtained from Mr. Hugh Braus at Honeywell at 603-623-7294. AC transformer controller information may be obtained from Mr. Arthur C. Farnham at Superior Electric at 617-237-0750. Solid state controllers are less expensive than transformer controllers.

5.3.3 Outlet Velocity Profiles

The velocity profiles across the outlet of the blanket bundle can be calculated using a piezotube setup attached to a differential pressure gauge. The velocity at a point is calculated from the following equation.

$$V = (2g_o \Delta P)^{1/2}$$

With the arrangement available at Tom Eaton's test position in the flow loop, velocity profiles can be made halfway across the bundle at directions 90° to one another. This enables all types of subchannels to be traversed as shown in Fig. 5-1.

5.3.4 Pressure Drop

All recommendations for future pressure drop experiments involve incorporating more detail in the measurements. More taps can be drilled in the faces of the flow housing to achieve

finer detail for circumferential pressure drops. Relative to axial measurements using the injection rod, although the 1/2 inch spacing gave good results, the 1/4 inch hole spacing can be used to get finer axial pressure drop data. An additional injector rod can be positioned halfway in between the center and edge injector positions. The upper rod support plates can have another hole drilled to accommodate this injector rod in position number 47 (Fig. 2-21). This gives the ability to measure pressure profiles between the edge and center of the bundle for various axial positions.

It is recommended that circumferential pressure taps be placed at the 10 inch axial level. This will give 8 wire wrap lead lengths between the pressure taps instead of 7-1/2. The wire wrap orientation at the half lead length positions is a mirror image of that at the lead length positions. However, there may be unknown perturbations between lead lengths, so that it is better to measure pressure drop across distances that are a number of lead lengths apart.

Finally, the data shown in Fig. 4-2 for circumferential pressure variation must be proved or disproved. The pressure taps are set up according to Fig. 2-15b and connected to the valve manifold. The manifold is connected to the low side of a differential pressure gauge and tap 1 is connected to the high side. Readings are taken every 5 gpm for 0 to 50 gpm.

5.4 Future Analysis

5.4.1 Mixing Data

The purpose of this thesis has been to collect mixing data for analysis by the ENERGY code. The data presented in its present form, or after reanalysis according to section 5.2, should be analyzed by ENERGY [3].

5.4.2 Pressure Drop Data

Section 4.1.2 proposed that swirl flow be considered as being a periodic velocity which is superimposed in the edge subchannels on a general bundle flow sweeping pattern. This approach can be used in developing a hydraulic model which describes the detailed subchannel velocity and pressure variations.

Chapter 6
CONCLUSION

The design of a test section for the MIT mixing flow loop to collect LMFBR blanket mixing data for analysis by the ENERGY code and to collect pressure drop data to provide information on blanket subassembly flow characteristics is presented. The test section consists of a flow housing, 61 wire wrapped blanket fuel rods (three of which are salt solution injector rods), and 126 conductivity cell probes. Six pressure taps each are provided at 12 and 42 inches below the flow housing exit. Axial pressure data is also collected using the injector rods.

The pressure drop data collected shows a periodic variation in both axial and circumferential directions. The pressure is generally lower in the edge subchannel than the central subchannel due to swirl flow effects. Bundle friction factors are not well fit by existing correlations, because the correlations are based on different geometrical parameters. A friction factor which fits the data well is proposed.

Mixing data collected also shows periodic variations with wire wrap lead length. The dispersion characteristics of the salt shows that the wire wrap pushes the salt into the adjacent subchannels instead of pulling the salt along with the wire. Peripheral subchannels appear to be areas of flow which is more confused than the rest of the bundle and mixing appears to be

more thorough. The edge subchannel, at low flow, appears to have the salt channeled along the wires. This effect can be caused by swirl flow. The errors shown by the mass balances may require reanalysis of the data or a repetition of the experiment before ENERGY analysis is performed.

TABLES

Table 1-1. Comparison of LMFBR Core and Radial Blanket Design Parameters [5]

Number of Assemblies	198	120 to 180
Total Power Fraction	0.96 to 0.90	0.03 to 0.08
Fraction of Total Coolant Flow	0.89 to 0.82	0.05 to 0.12
Number of Fuel Rods/Assembly	217	61
Fuel Rod Diameter, in.	0.230	0.52
Wire Wrap Diameter	0.056	0.037
Rod Pitch to Diameter Ratio	1.252	1.078
Residence Time - Full Power Years	∿2	3 to 6
Type of Fuel	Enriched $(Pu,U)O_2$	Depleted UO_2
Peak Burnup, a/o	∿8	2 to 3
Pellet Density, % Theoretical	90	92 to 95
Fuel Volume Fraction	∿0.33	∿0.60
Bond Volume Fraction	∿0.02	∿0.01
Coolant Volume Fraction	∿0.40	∿0.24
Structure Volume Fraction	∿0.25	∿0.15
Radial Power Peaking	1.2 to 1.5	1.9 to 2.2
Axial Power Peaking	1.1 to 1.3	1.3 to 1.6
Peak Heat Flux 10^3Btu/hr. ft^2	500 to 700	400 to 600
Specific Power, watts/gram	100 to 300	4 to 60
Max. Allowable Linear Power, kW/ft (Melting Limit)	15 to 17	17 to 20
Maximum Velocity in Rod Bundle, ft/sec.	20 to 30	0.2 to 12
Maximum Free Stream Reynolds No. x 10^{-3}	100	20 to 30
Maximum Rod Plenum Pressure, psia	700 to 1000	200 to 300

Table 2-1

Blanket Subassembly

Geometry Summary

$P = 0.534$ in.

$D_p = 0.502$ in.

$D_s = 0.032$ in.

$D_f = 4.266$ in.

$D_\ell = 2.463$ in.

$A_T = 15.761$ in.^{2}

$A_{FT} = 3.638$ in.^{2}

$P_T = 117.160$ in.

$De_T = 0.124$ in.

Subchannel Geometry

Subchannel Type	Flow Area (in. sq.)	Wetted Perimeter (in.)	Hydraulic Dia. (in.)
interior	0.0246	0.084	0.117
edge	0.052	1.374	0.151
corner	0.013	0.571	0.023

Table 2-2

Upper Support Rod Hole Coordinates

X = 0 Y = 0 at plate center (figure 2-21)

Rod Number		Y Coordinate (in.)	X Coordinate (in.)
	27	0.0	-2.137
	28	0.0	-1.603
	29	0.0	-1.069
	30	0.0	-0.534
	31*	0.0	0.0
	32	0.0	0.534
	33	0.0	1.069
	34	0.0	1.603
	35	0.0	2.137
19	36	0.463, -0.463	-1.87
20	37	0.463, -0.463	-1.334
21	38	0.463, -0.463	-0.801
22	39	0.463, -0.463	-0.267
23	40	0.463, -0.463	0.267
24	41	0.463, -0.463	0.801
25	42	0.463, -0.463	1.334
26	43	0.463, -0.463	1.87
12	44	0.926, -0.926	-1.603
13	45	0.926, -0.926	-1.069
14	46	0.926, -0.926	-0.534
15	47	0.926, -0.926	0.0
16	48	0.926, -0.926	0.534
17	49	0.926, -0.926	1.069
18	50	0.926, -0.926	1.603
6	51	1.389, -1.389	-1.334
7	52	1.389, -1.389	-0.801
8	53	1.389, -1.389	-0.267
9	54	1.389, -1.389	0.267
10	55*	1.389, -1.389	0.801
11	56	1.389, -1.389	1.334
1	57	1.852, -1.852	-1.069
2	58	1.852, -1.852	-0.534
3	59*	1.852, -1.852	0.0
4	60	1.852, -1.852	0.534
5	61	1.852, -1.852	1.609

* $\frac{15}{32}$ dia. All other holes $\frac{1}{4}$-inch dia.

Table 2-3

Probe Support Hole Coordinates

X = 0 Y = 0 at plate center (figure 2-22)

Probe Number		Y Coordinate	X Coordinate
39	72	0.154, -0.154	-1.87
37	70	0.154, -0.154	-1.334
35	68	0.154, -0.154	-0.801
33	66	0.154, -0.154	-0.267
2	97	0.154, -0.154	0.267
4	99	0.154, -0.154	0.801
6	101	0.154, -0.154	1.334
8	103	0.154, -0.154	1.87
38	71	0.309, -0.309	-1.603
36	69	0.309, -0.309	-1.069
34	67	0.309, -0.309	-0.534
1	65	0.309, -0.309	0.0
3	98	0.309, -0.309	0.534
5	100	0.309, -0.309	1.069
7	102	0.309, -0.309	1.603
63	89	0.325, -0.325	-2.168
31	126	0.325, -0.325	2.168
45	79	0.617, -0.617	-1.603
43	77	0.617, -0.617	-1.069
41	75	0.617, -0.617	-0.534
9	73	0.617, -0.617	0.0
11	105	0.617, -0.617	0.534
13	107	0.617, -0.617	1.069
15	109	0.617, -0.617	1.603
44	78	0.772, -0.772	-1.334
42	76	0.772, -0.772	-0.801
40	74	0.772, -0.772	-0.267
10	104	0.772, -0.772	0.267
12	106	0.772, -0.772	0.801
14	108	0.772, -0.772	1.334
62	90	0.788, -0.788	-1.901
30	125	0.788, -0.788	1.901
51	84	1.080, -1.080	-1.334
49	82	1.080, -1.080	-0.801
47	80	1.080, -1.080	-0.267
16	111	1.080, -1.080	0.267
18	113	1.080, -1.080	0.801
20	115	1.080, -1.080	1.334

(continued)

Table 2-3 (concluded)

Probe Number		Y Coordinate	X Coordinate
50	83	1.235, -1.235	-1.069
48	81	1.235, -1.235	-0.534
46	110	1.235, -1.235	0.0
17	112	1.235, -1.235	0.534
19	114	1.235, -1.235	1.069
61	91	1.251, -1.251	-1.634
29	124	1.251, -1.251	1.634
56	88	1.543, -1.543	-1.069
54	86	1.543, -1.543	-0.534
52	116	1.543, -1.543	0.0
22	118	1.543, -1.543	0.534
24	120	1.543, -1.543	1.069
55	87	1.698, -1.698	-0.801
53	85	1.698, -1.698	-0.267
21	117	1.698, -1.698	0.267
23	119	1.698, -1.698	0.801
60	92	1.714, -1.714	-1.367
28	123	1.714, -1.714	1.367
58	94	2.041, -2.041	-0.801
57	95	2.041, -2.041	-0.267
25	96	2.041, -2.041	0.267
26	121	2.041, -2.041	0.801
59	27	2.110, -2.110	-1.218
93	122	2.110, -2.110	1.218

All holes 0.128 in. dia.

Table 3-1

Valve Lineup Table

Table 3-1a. Low Flow (≤ 50 gpm)

Valve	Pump on Line 1	2
1	closed	open
2	closed	closed
3	open	closed
4	open	open
5	closed	closed
6*	open	open

Table 3-1b. Medium to High Flow (≥ 50 gpm)

Valve	Pump on Line 1	2	1&2 parallel	1&2 series
1	closed	open	open	closed
2	closed	closed	closed	open
3	open	closed	open	closed
4	closed	closed	closed	closed
5	open	open	open	open
6*	open	open	open	open

* Flow through the test section is controlled by valve 6. There is no flow through the test section when valve 6 is open. Closing valve 6 will increase the flow through the test section.

Table 3-2

Injection Flow Rates

25 gpm loop flow rate

Subchannel	Injection Flow Rate
Interior	0.041 lb/min
Edge	0.049 lb/min

185 gpm loop flow rate

Subchannel	Injection Flow Rate
Interior	0.31 lb/min
Edge	0.36 lb/min

Table 3-3

Single Point Injection Flow Rates

Loop Flow Rate (gpm)	Injection Flow Rate (lb/min)	
	Interior	Edge
50	0.082	0.1
75	0.12	0.15
100	0.16	0.2
125	0.2	0.25
150	0.25	0.29
175	0.29	0.34

Table 5-1

CHANGES TO CALIB FOR SECOND CALIBRATION CURVE

Change:	To:
DO 320 I=1,NPTS	DO 320 I=3,NPTS
CALL APCH(DATI,NPTS,NCOEFF,XD,XO,WORK,IER)	INPTS = NPTS-2 (CALL APCH(DATI,INPTS,NCOEFF,XD,XO,WORK,IER)
DO 340 L=1,NPTS	DO 340 L=3,NPTS
WRITE(6,3)(X(I,J),I=1,NPTS)	WRITE(6,3)(X(I,J),I=3,NPTS)
WRITE(6,4)(X(I,J),I=1,NPTS)	WRITE(6,4)(X(I,J),I=3,NPTS)
WRITE(6,5)(X(I,J),I=1,NPTS)	WRITE(6,5)(X(I,J),I=3,NPTS
WRITE(6,6)(X(I,J),J=1,NPTS)	WRITE(6,6)(X(I,J),I=3,NPTS
NX=(NPTS-1)*NPERPT+1	NX=(NPTS-3)*NPERPT+1
DELTAX=(XI(NPTS)-XI(1)/(NX-1)	INPTS = NPTS-2 DELTAX=(XI(JNPTS)-XI(1))/(NX-1)
DO 371 I=1,NPTS	DO 371 I=3,NPTS

Before STOP and after CALL ENDPLT insert

```
      DO 400 J=1,NCURVES
      XPJ(J) = XOJ(J)
      XDJ(J) = XEJ(J)
      KREZ(J) = IREZ(J)
      KRES = KREZ(J)
      DO 400 I=1,KRES
      XCOEF(I,J) = CCOEF(I,J)
  400 CONTINUE
```

Table 5-2

CHANGES TO DATA REDUCTION PROGRAM

Change:

```
READ(5,2) NPTS,NCOEFF,NCURVS,IN,IPLOT,JPLOT,NPERPT,ICALB
```

To:

```
READ(5,2)  NPTS,NCOEFF,NCURVS,IN,IPLOT,JPLOT,NPERPT,ICALB,IM
       (IN refers to input source for first set of
        calibration curves, IM for the second)

      Insert before  77 CONTINUE:

      READ(IM,71) J,KREZ(J),BAKCAK(J),XEJ(J),XPJ(J)
      KRES = KREZ(J)
      READ(IM,72) (XCOEF(I,J),I=1,KRES)

      Insert after WRITE(6,73) IN

      WRITE(6,73) IM

      Insert after IF(IFLAG(J).GT.0) GO TO 342

      IF (SIGNAL(J,L).GE.0.3) GO TO 343

      Insert after line 342

      GO TO 345
  343 DD=SIGNAL(J,L)*XEJ(J)+XPJ(J)
      KRES=KREZ(J)
      DO 344 I=1,KRES
  344 XOEFF=XCOEF(I,J)
      CALL CNPS(EE,DD,XOEFF,KRES)
      SALT(J,L)=EE
```

Table 5-3

DATASETS SAVED IN SECONDARY STORAGE

Datasets Name	Dataset
CALA2. DATA	Calibration Data
CALCURV. DATA	Calibration Curves
CTL25. DATA	Central Injection Data (25 gpm)
CDL185. DATA	Central Injection Data (185 gpm)
ED25. DATA	Edge Injection Data (25 gpm)
PER25. DATA	Peripheral Injection Data (25 gpm)

Table 5-4

BLANKET BUNDLE CHARACTERISTICS WITH AND WITHOUT SHAVED WIRES

	Without Shaved Wires	With Shaved Wires
D_f	4.266 in	4.234 in
D_ℓ	2.463 in	2.445 in
A_T	15.761 in^2	15.525 in^2
A_{FT}	3.638 in^2	3.447 in^2
D_e	0.124 in	0.118 in

SUBCHANNEL GEOMETRY $\begin{pmatrix}\text{without shaving}\\ \text{with shaving}\end{pmatrix}$

Subchannel Type	Flow Area in^2	Wetted Perimeter in.	Hydraulic Dia. in.
Interior	0.0246	0.84	0.117
	0.0246	0.84	0.117
Edge	0.052	1.374	0.151
	0.043	1.371	0.126
Corner	0.013	0.571	0.023
	0.0081	0.5697	0.014

(see Appendix 7)

FIGURES

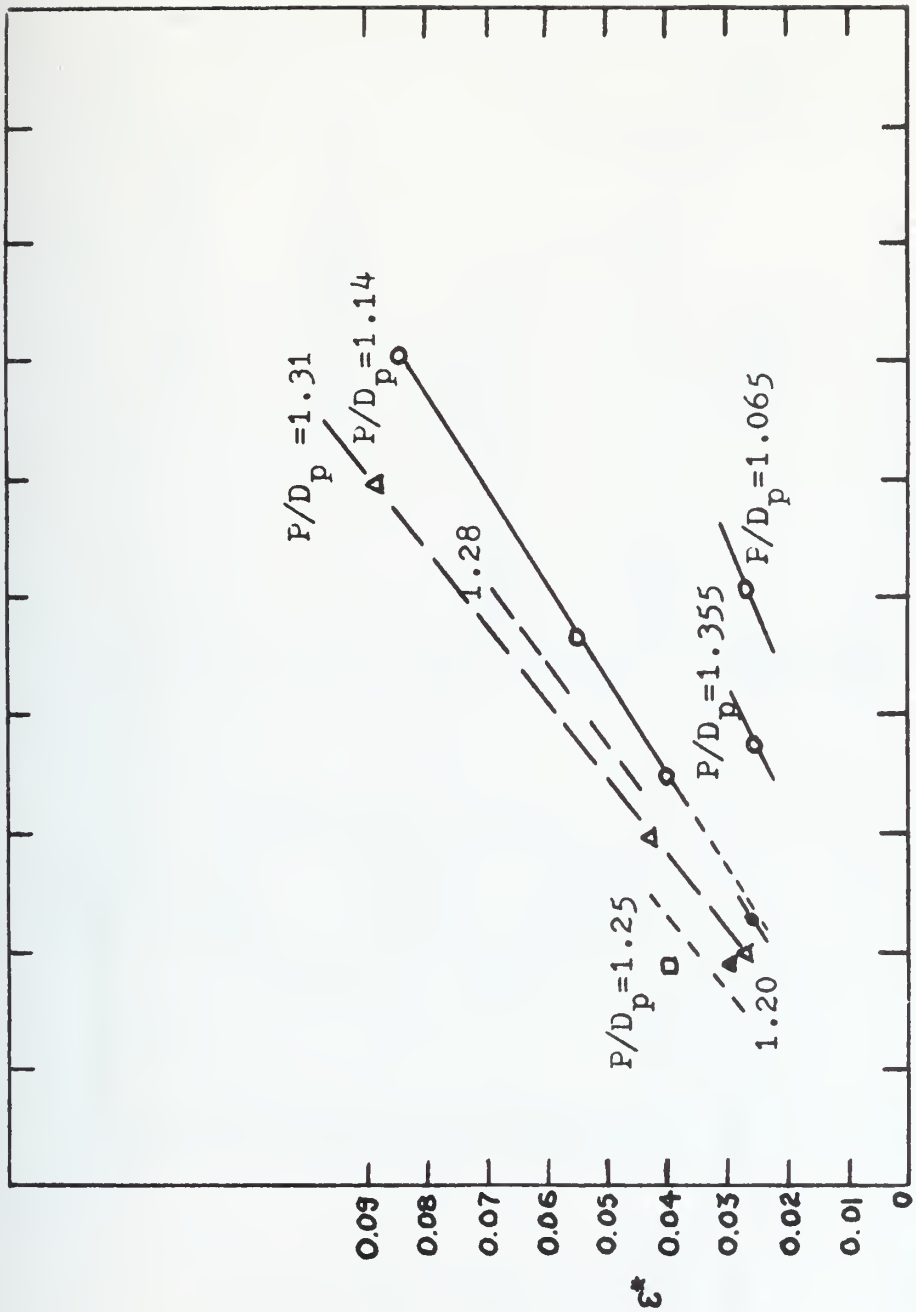

Figure 1-1 (Ref. 2)

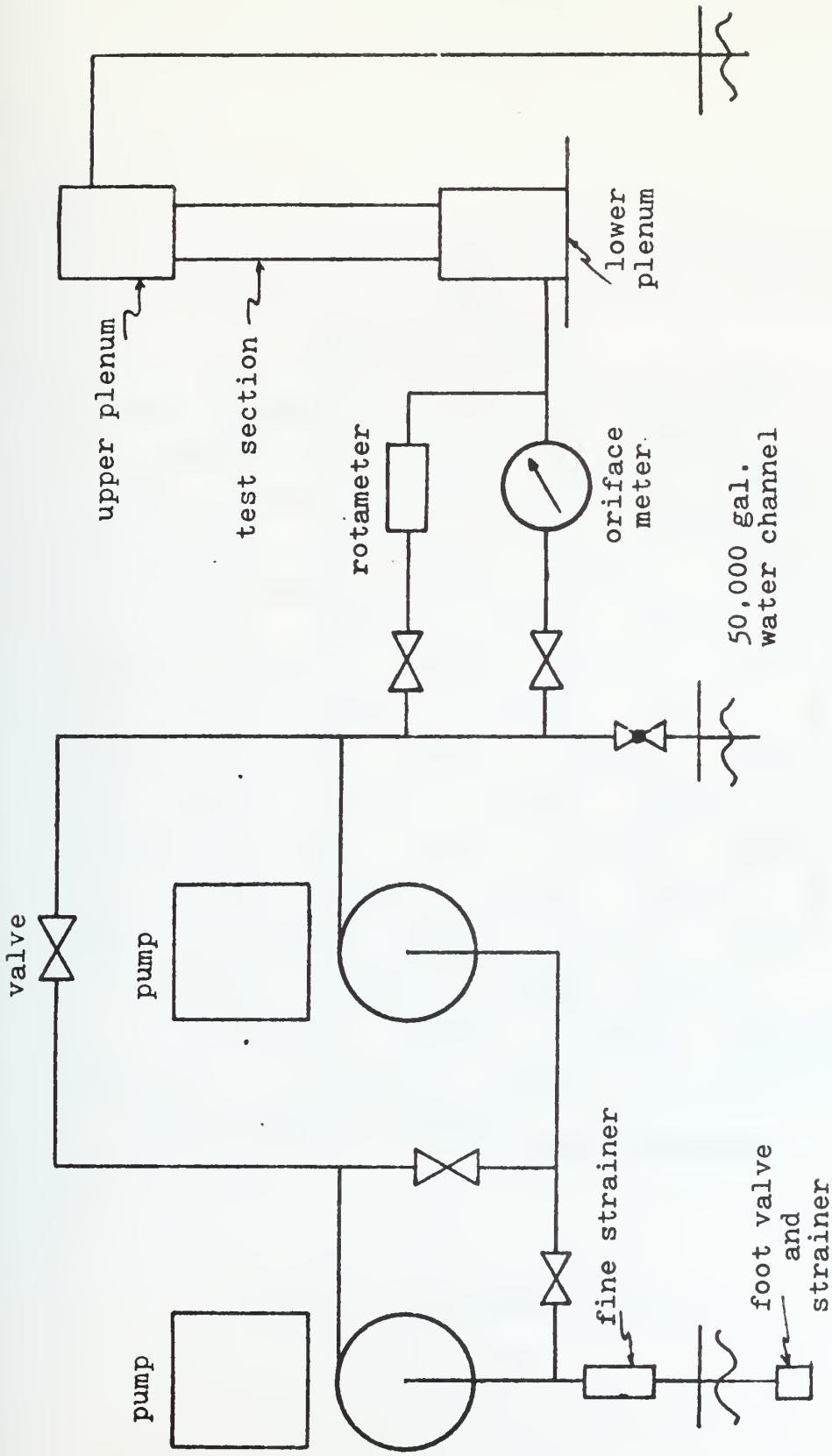

Diagram of MIT Flow Loop

Figure 2-1

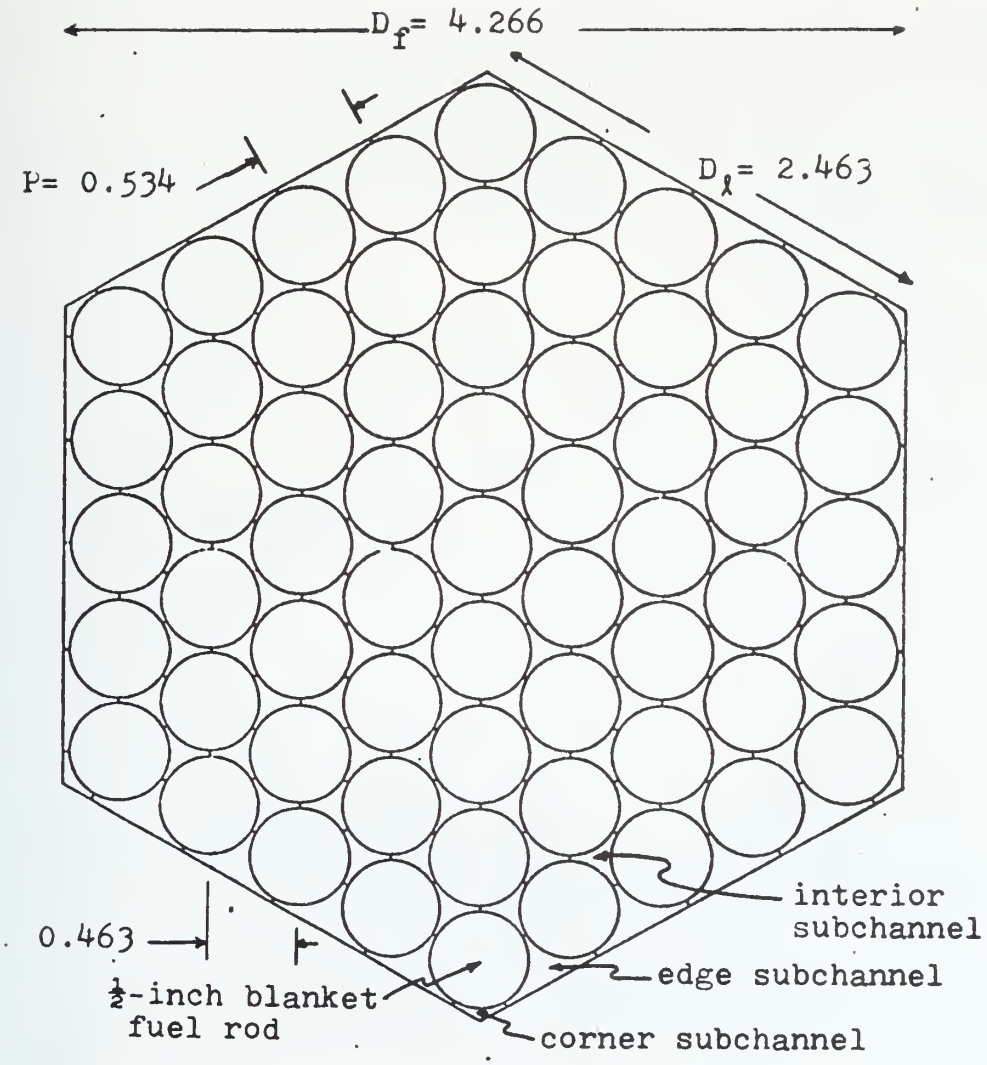

Blanket Subassembly Geometry

Figure 2-2

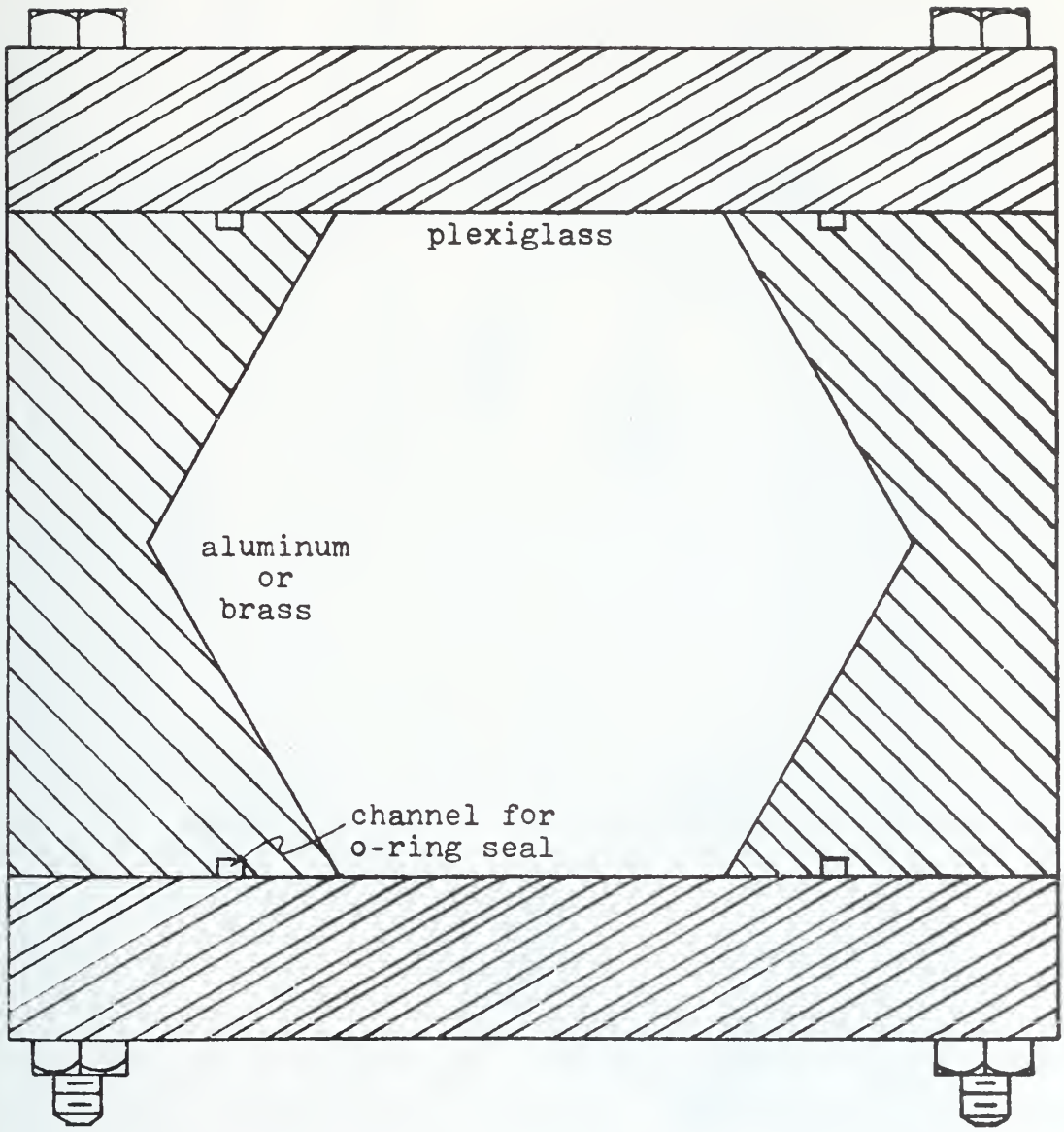

Flow Housing Design Option

Figure 2-3

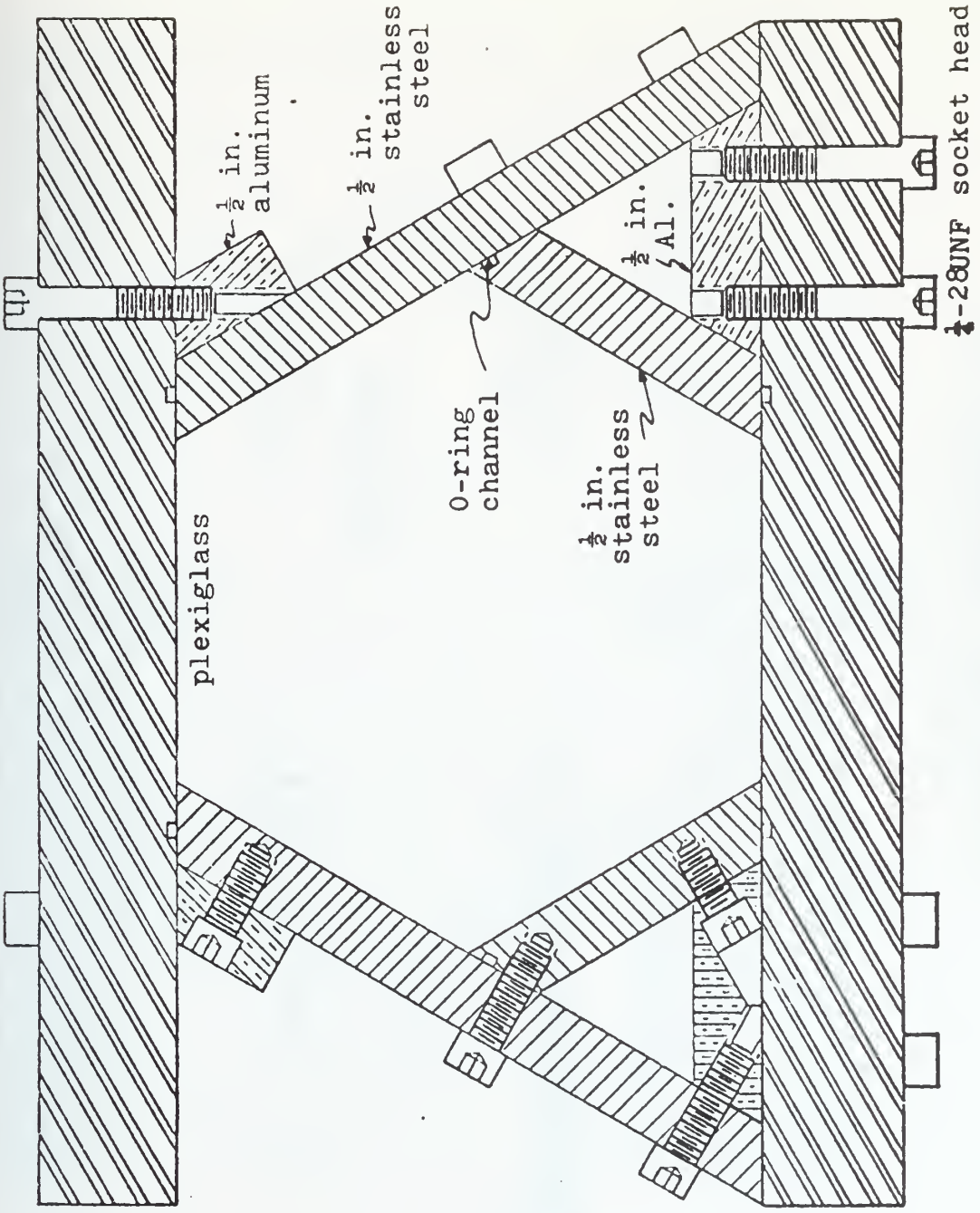

Flow Housing Design

Figure 2-4

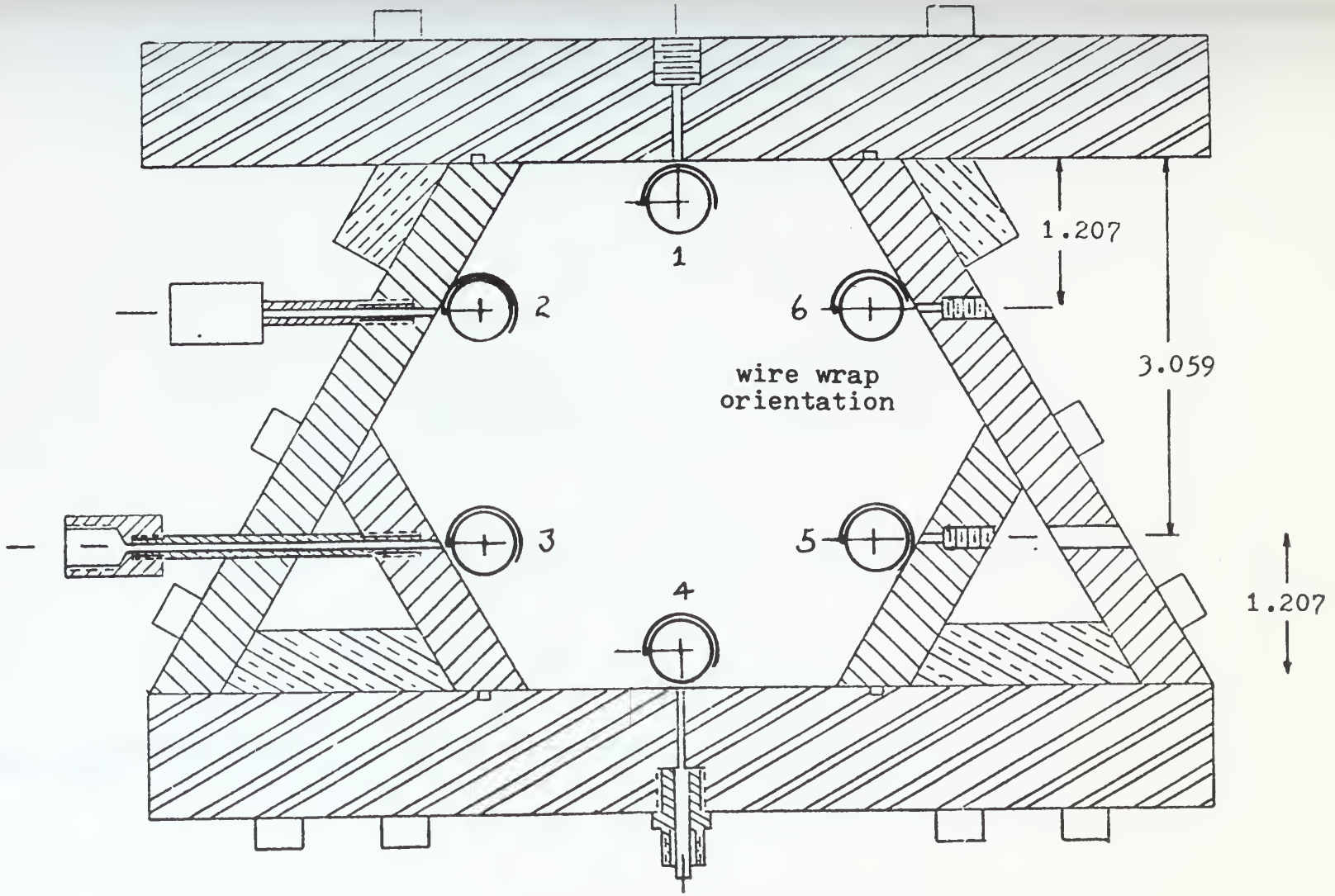

Pressure Tap Locations
12 Inches Below Flow Housing Exit

Figure 2-5a

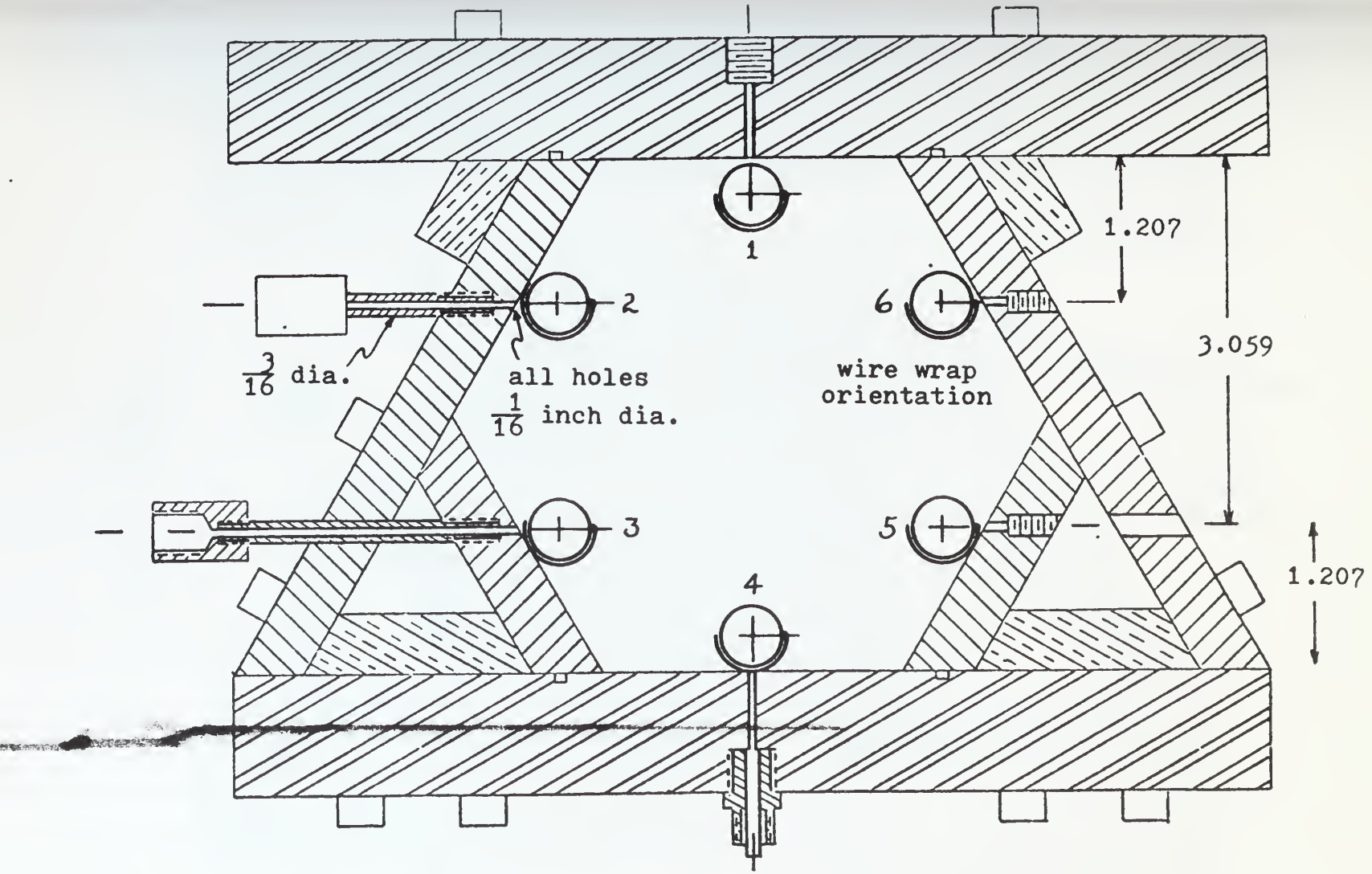

Pressure Tap Locations
42 Inches Below Flow Housing Exit

Figure 2-5b

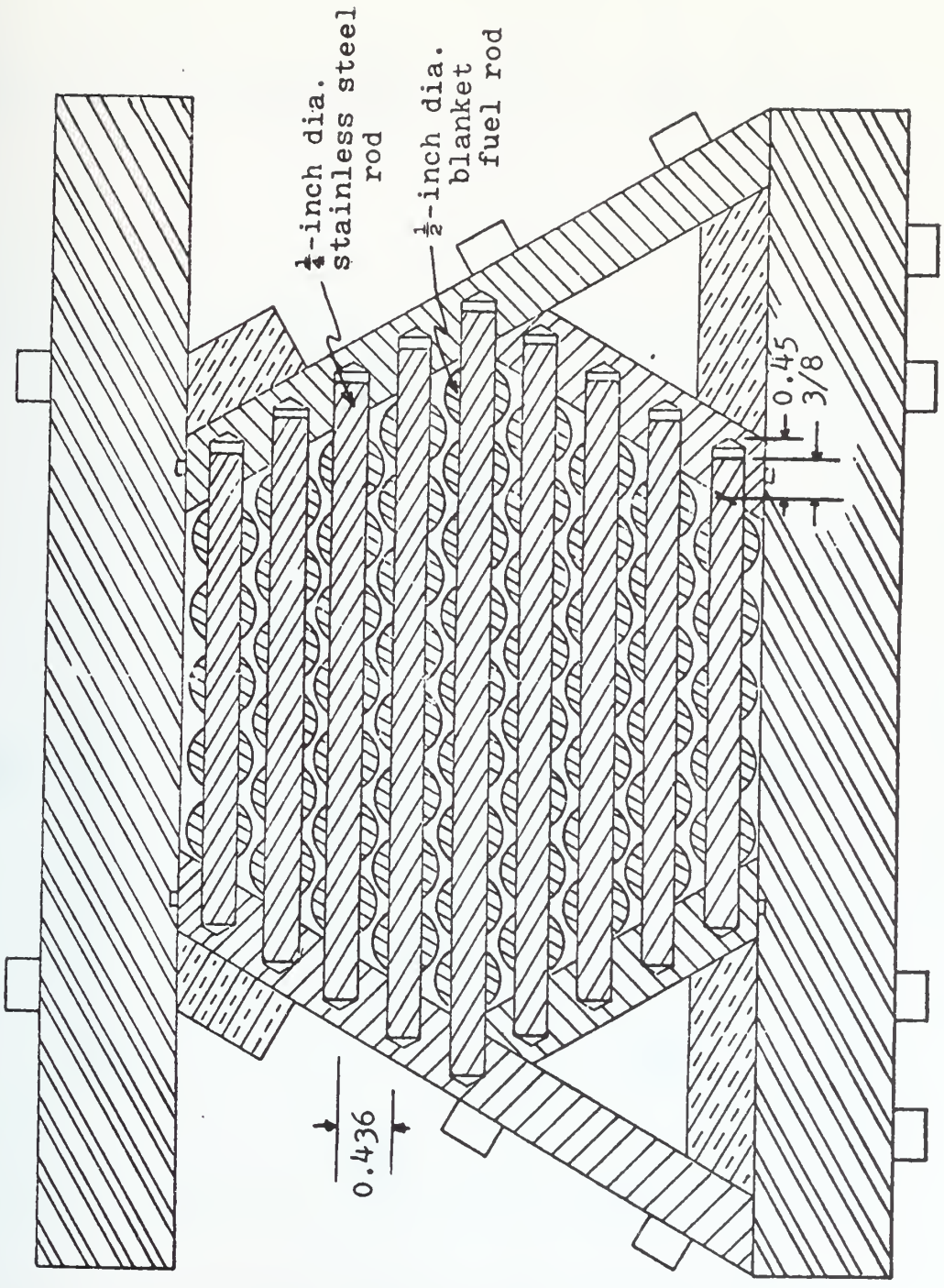

Rod Support Scheme
Figure 2-6

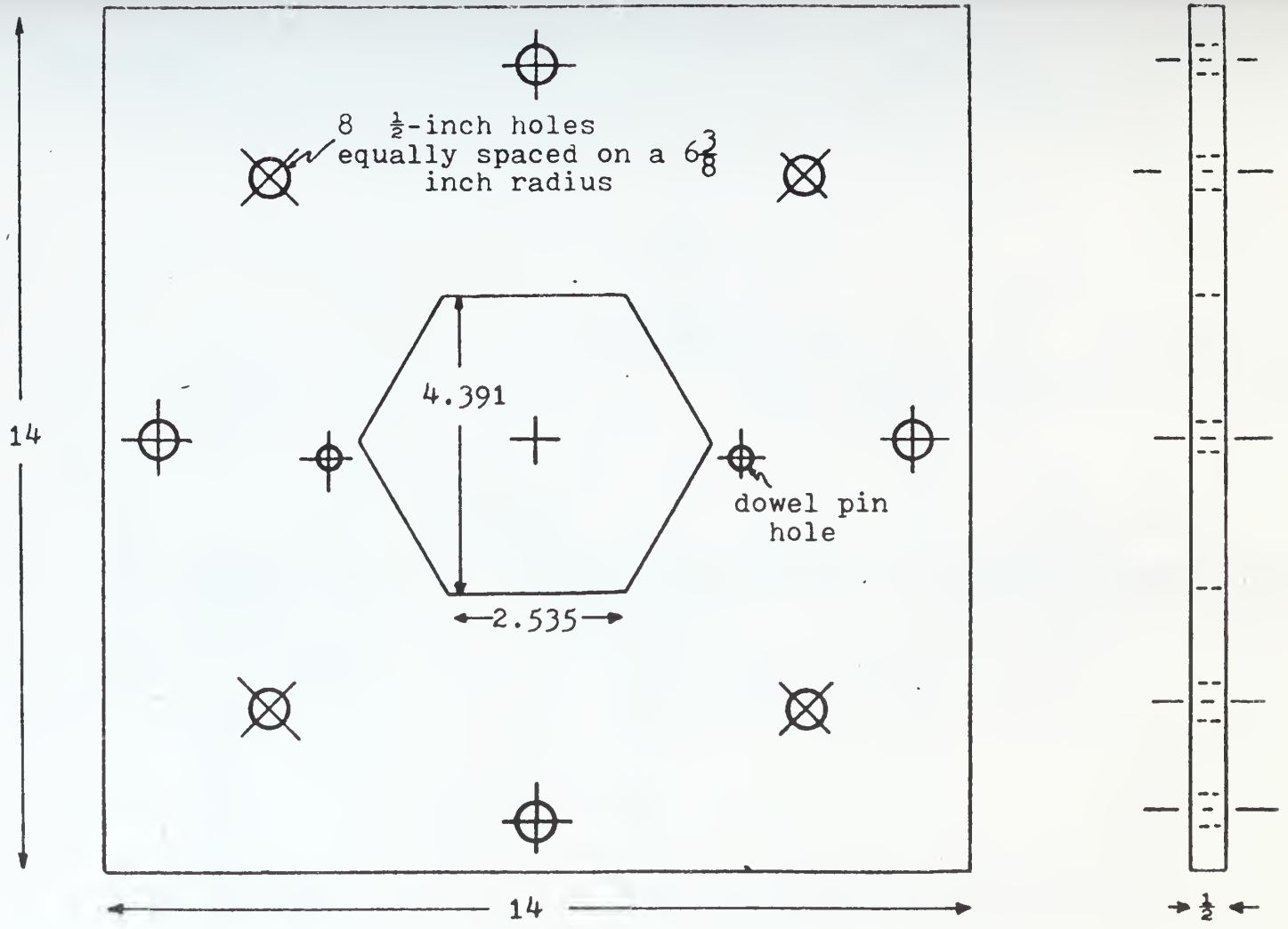

Flow Housing End Plate

Figure 2-7

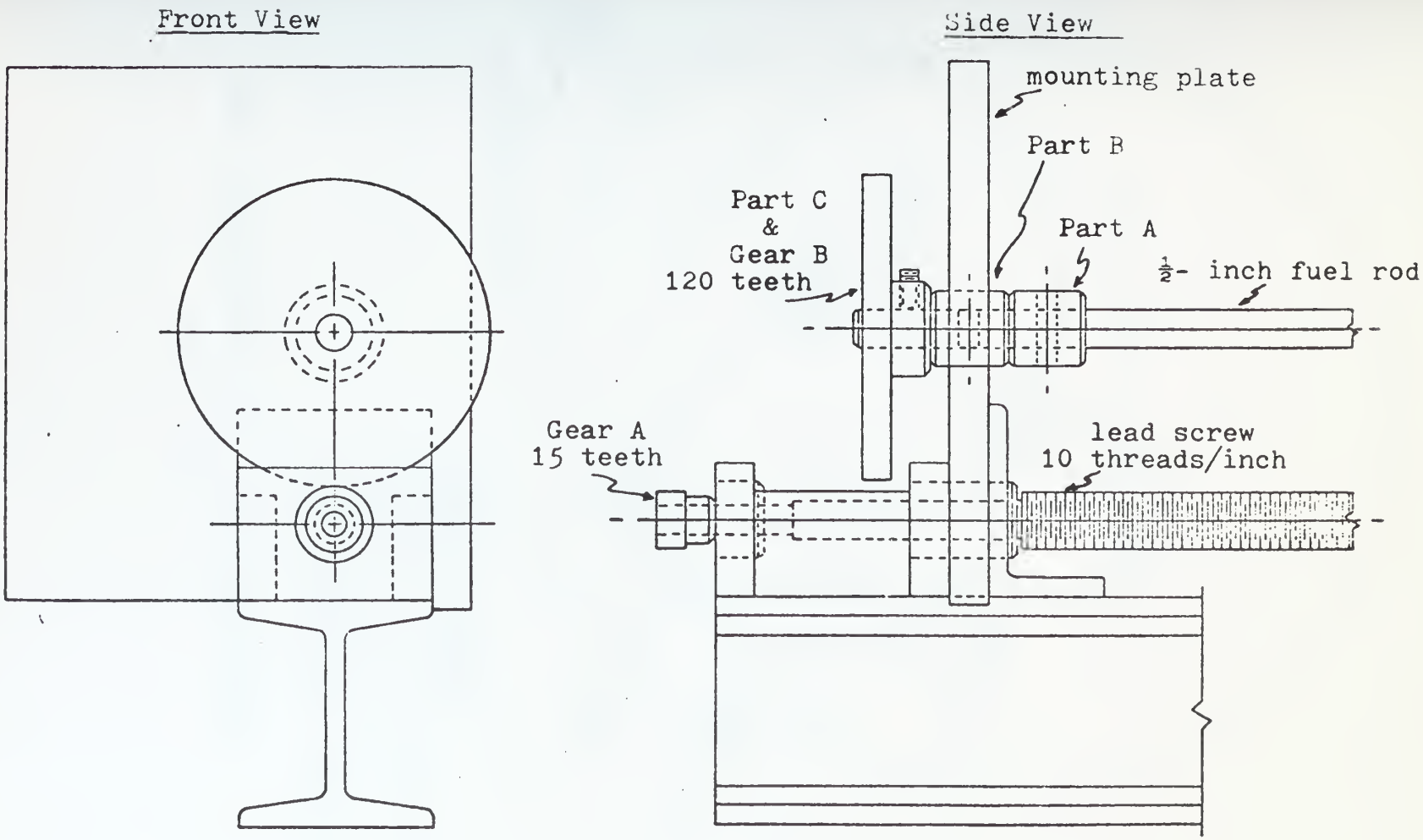

Basic Mechanism For Wire Wrap Apparatus

Figure 2-8

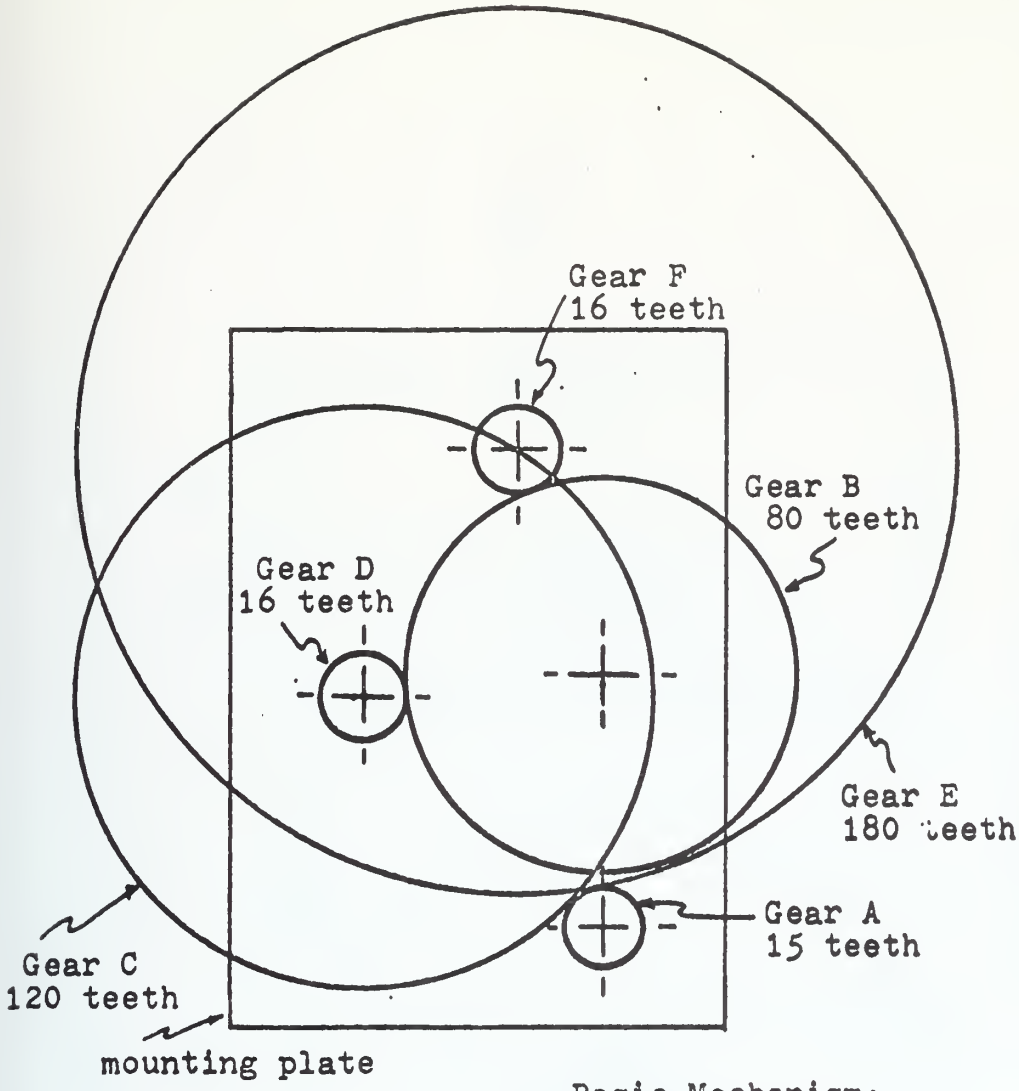

Basic Mechanism:
Gears A and B

4-inch lead; 40:1 gear ratio:
Gears A, B, C, D

6-inch lead; 60:1 gear ratio:
Gears A,B,E,F

Gear Combinations For 4 and 6 Inch Leads

Figure 2-9

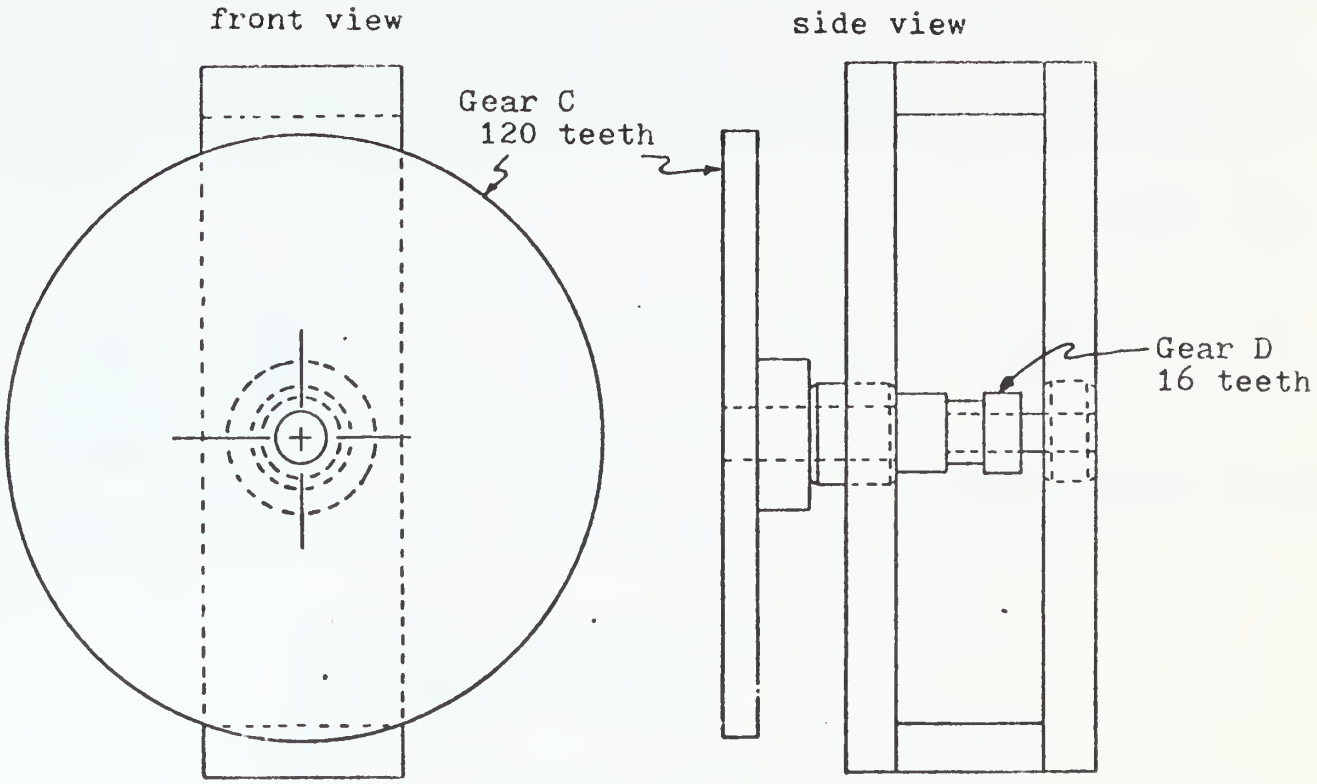

Gear Box For 4-Inch Lead

Figure 2-10

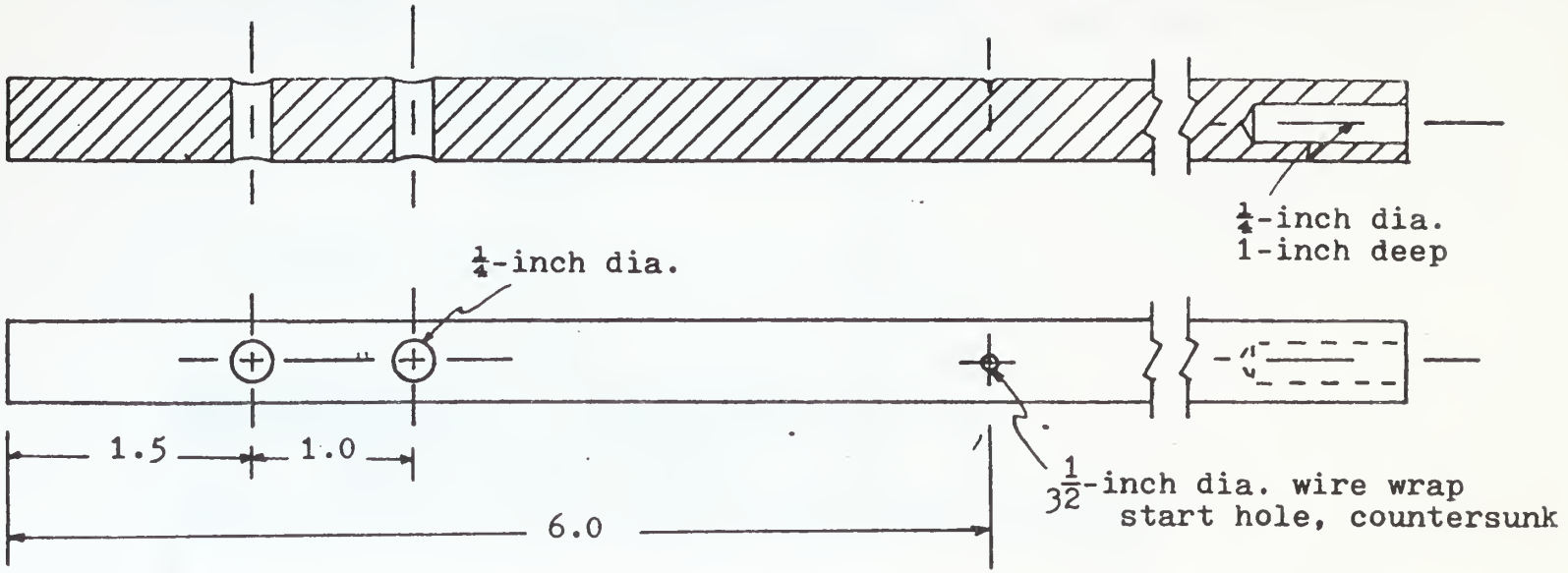

type 304 stainless steel
rod diameter = ½-inch
rod length = 60 inches

Rod Support Holes

Figure 2-11

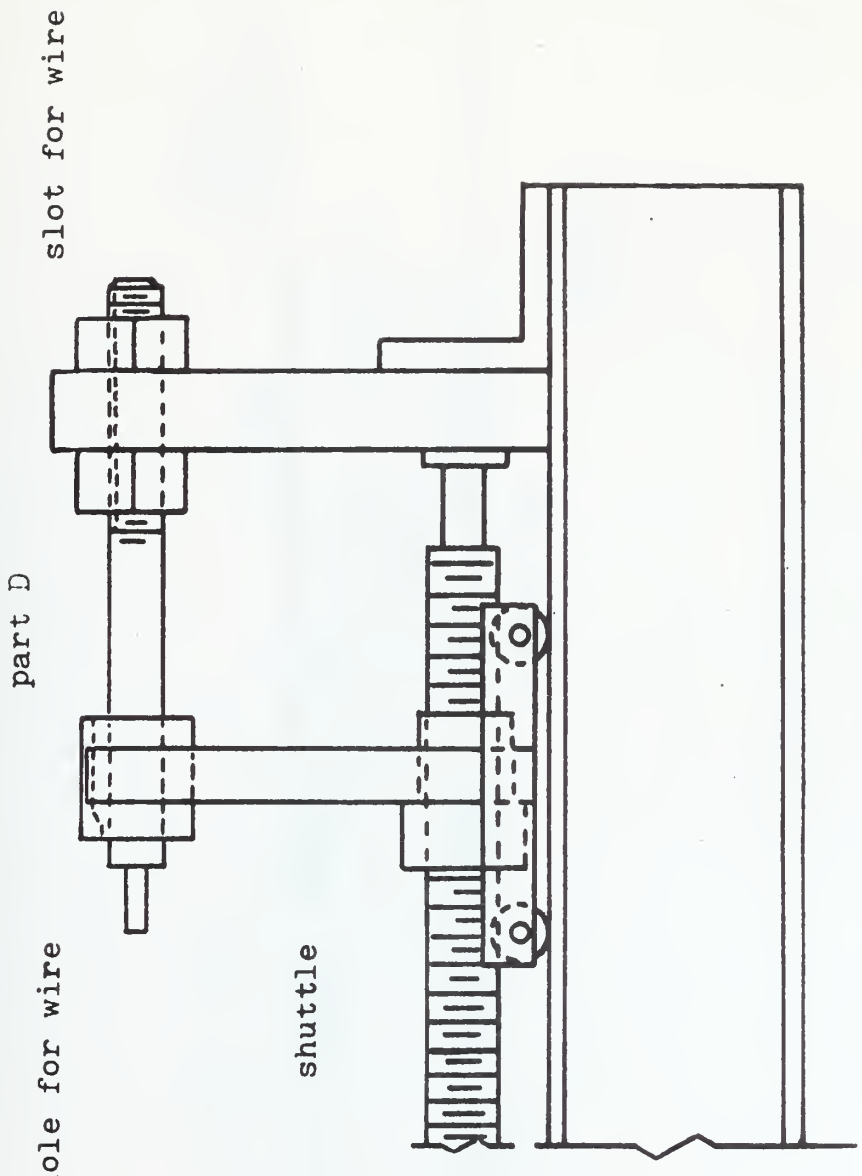

Wire Wrap Apparatus
Rod End Support and Shuttle

Figure 2-12

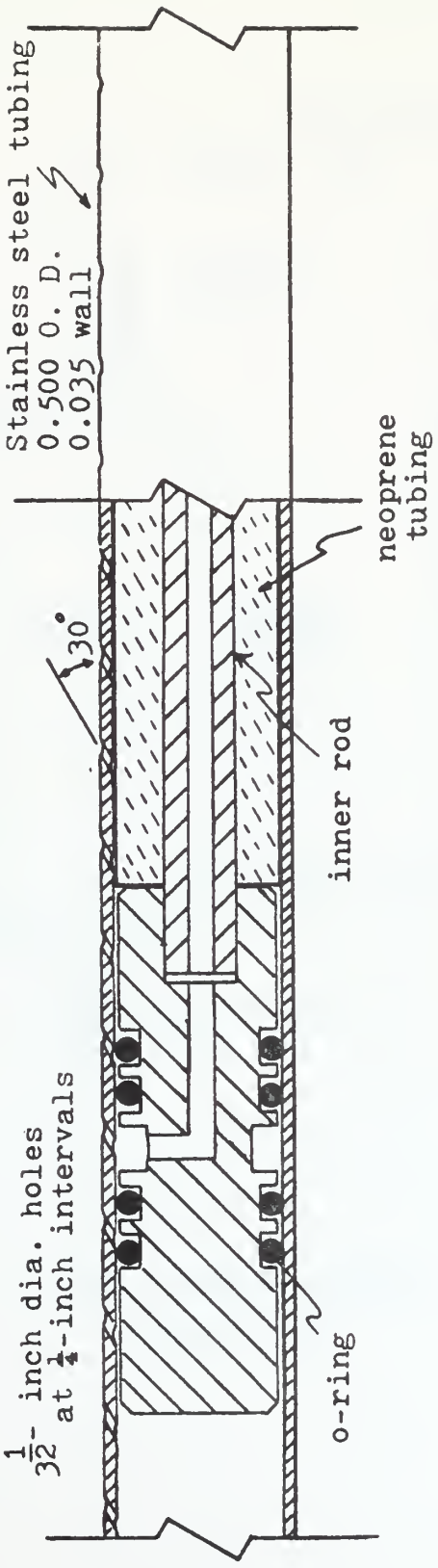

Injector Rod Mechanism

Figure 2-13

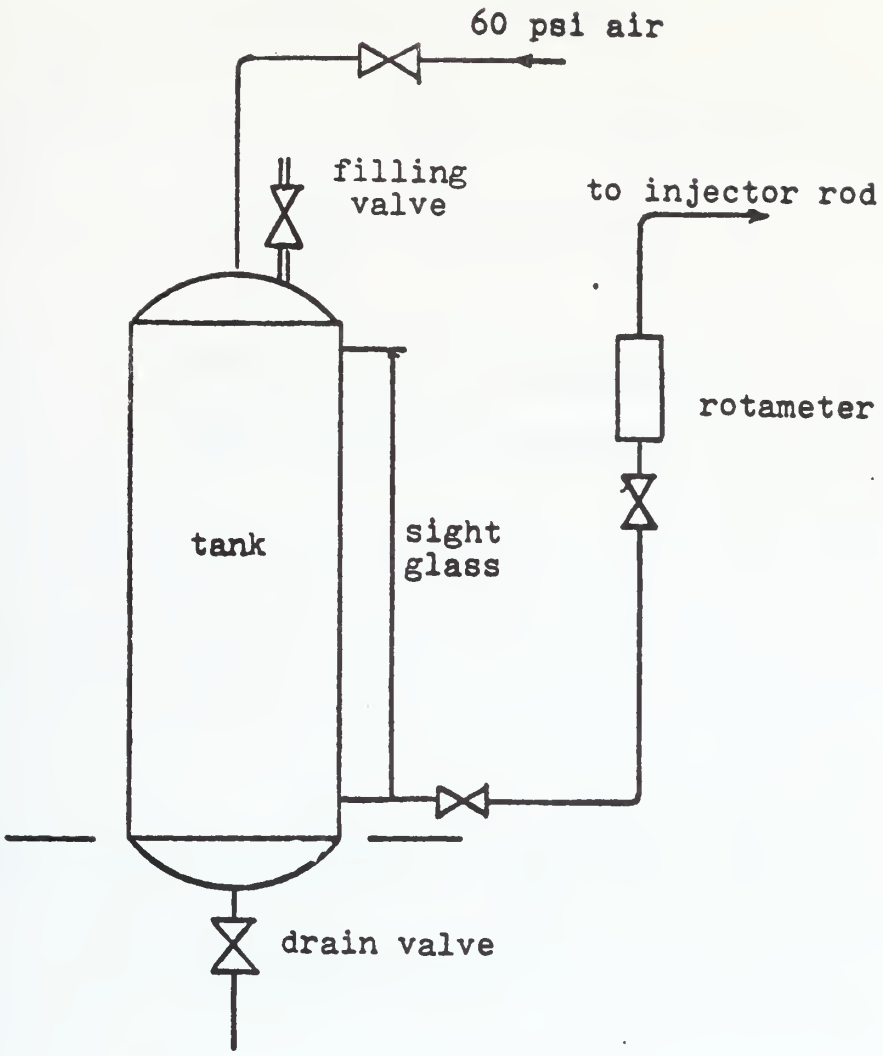

Salt Injection Tank

Figure 2-14

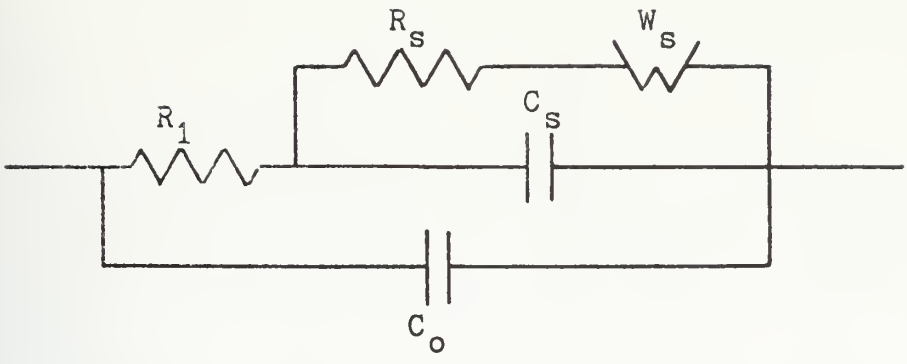

Conductivity Cell Schematic

Bright Platinum Electrodes

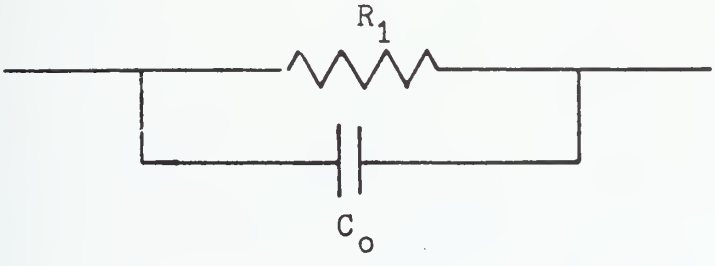

Conductivity Cell Schematic

Platinized Electrodes

Figure 2-15b

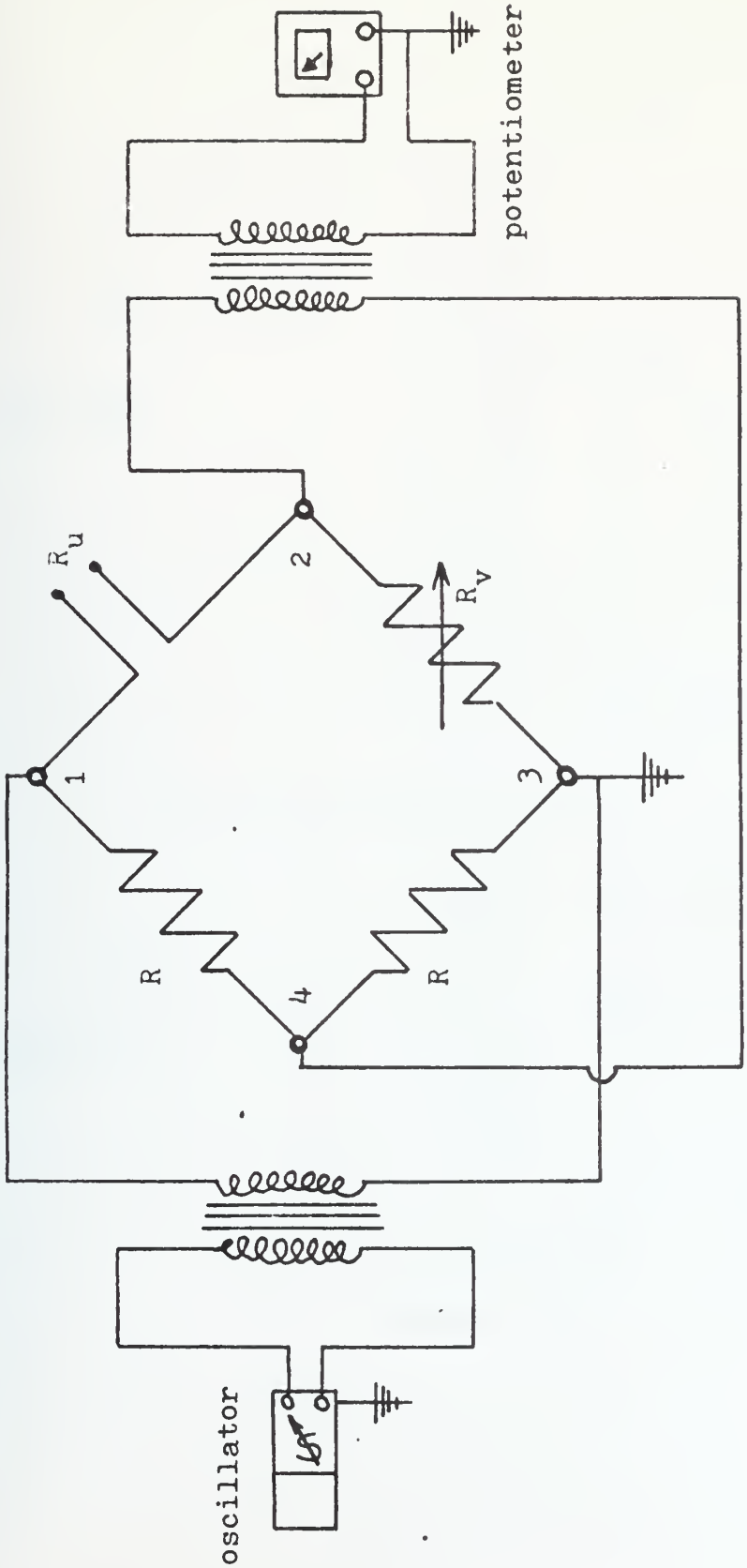

Wheatstone Bridge

Figure 2-16

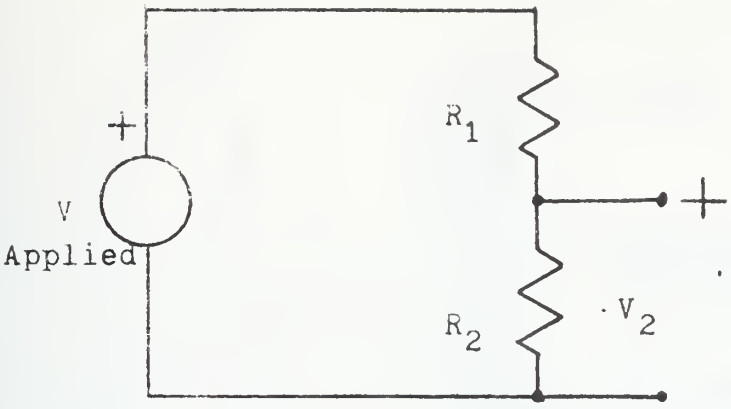

Voltage Divider

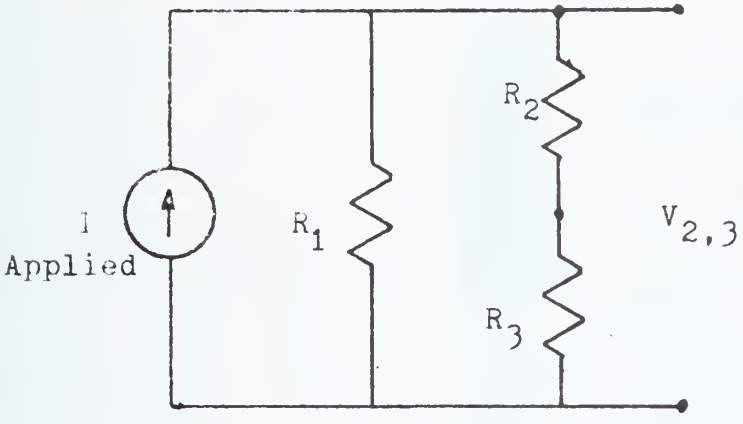

Current Divider

Figure 2-17

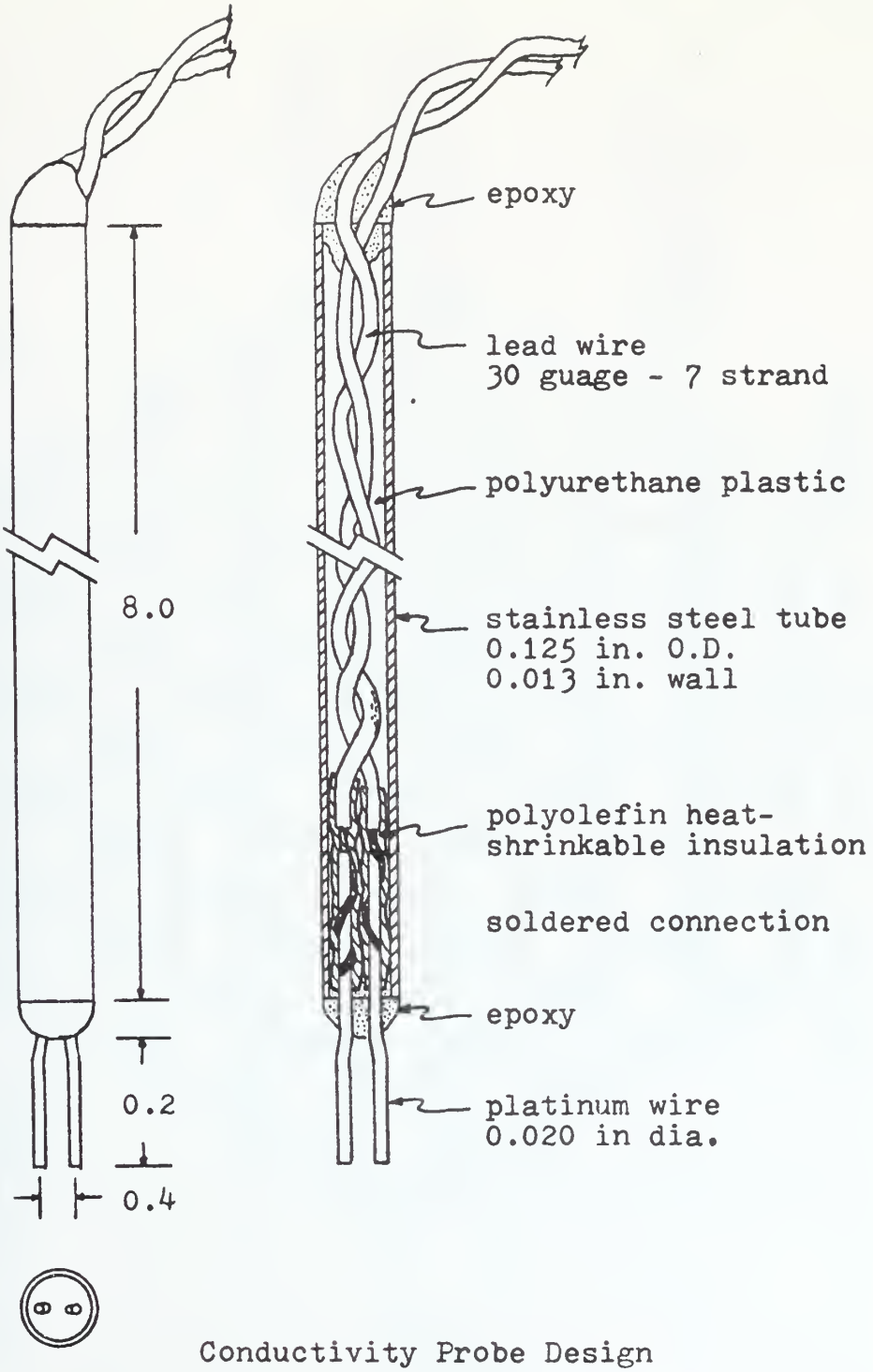

Conductivity Probe Design

Figure 2-18

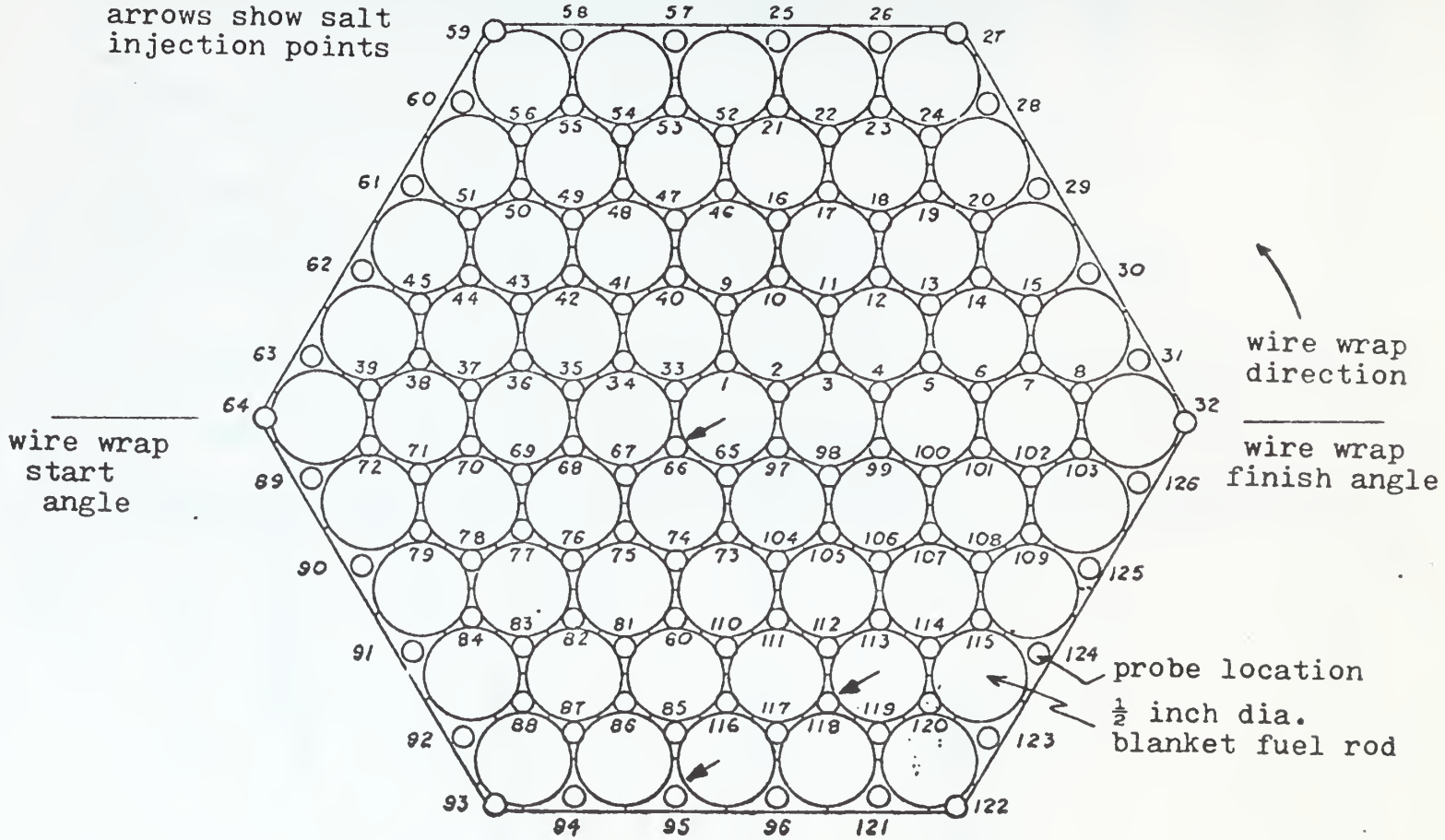

Subchannel Numbers and Probe Locations

Figure 2-19

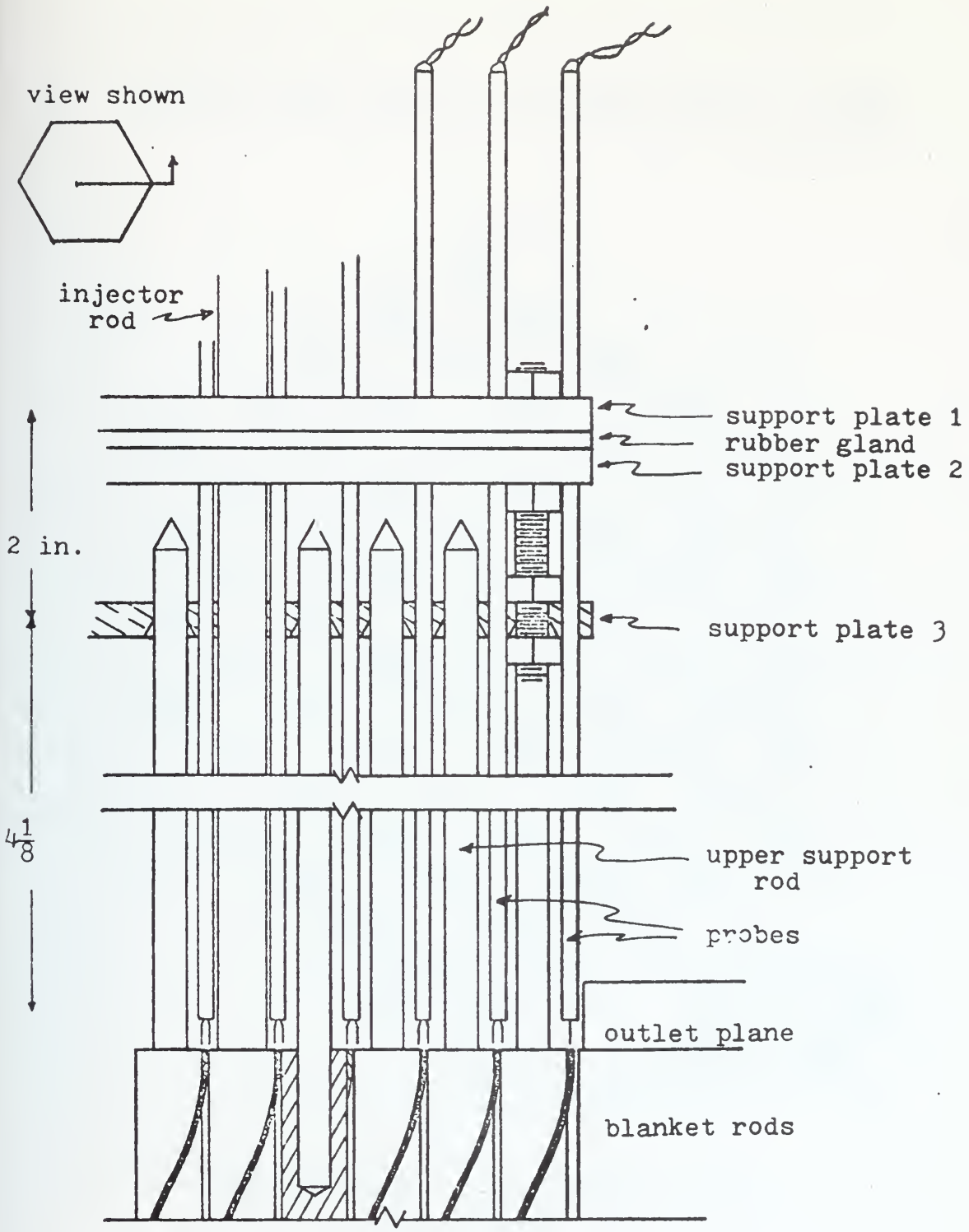

Probe and Rod Support Scheme

Figure 2-20

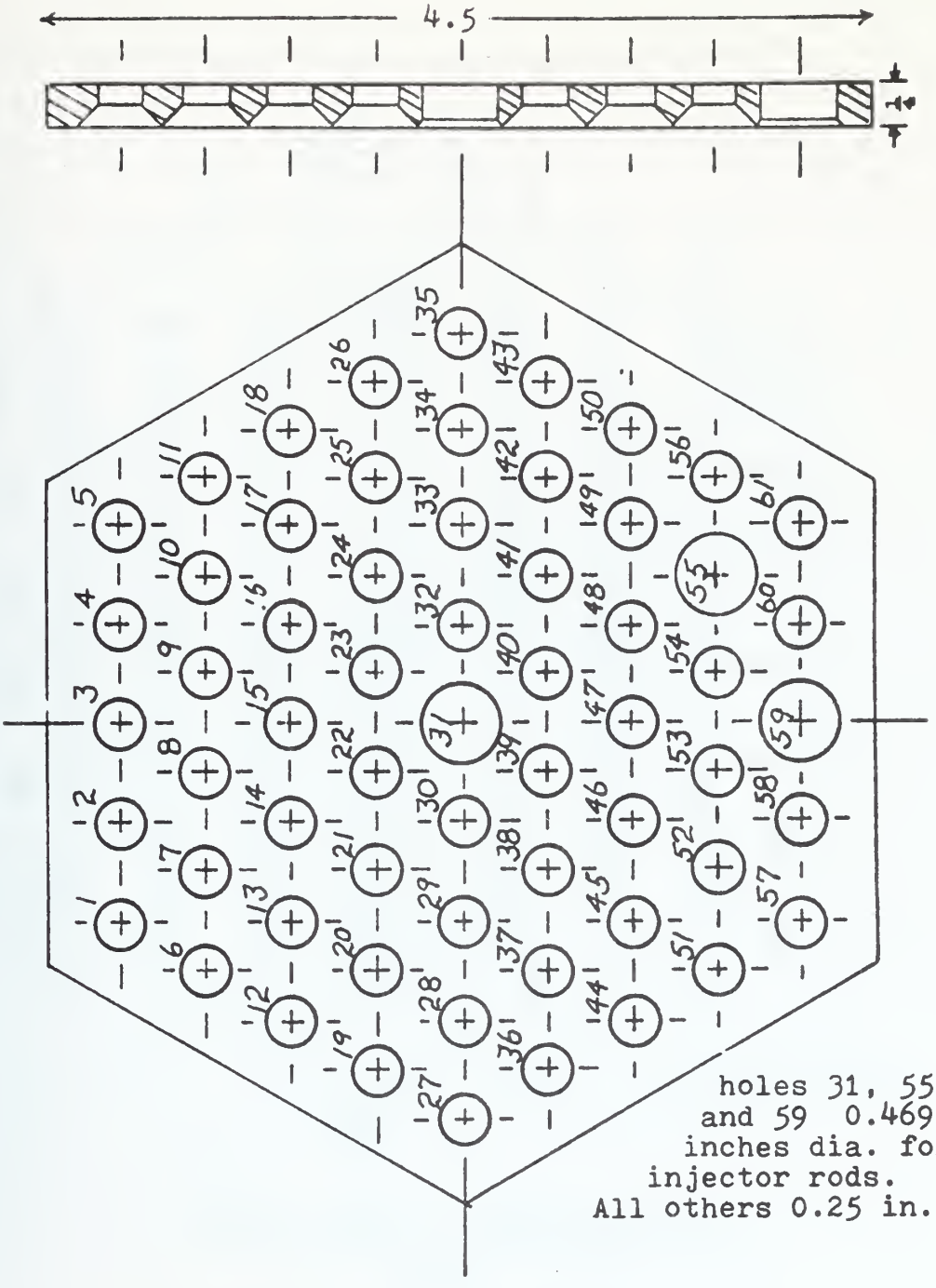

Hole Matrix For Upper Support Rods
Plate Three

Figure 2-21

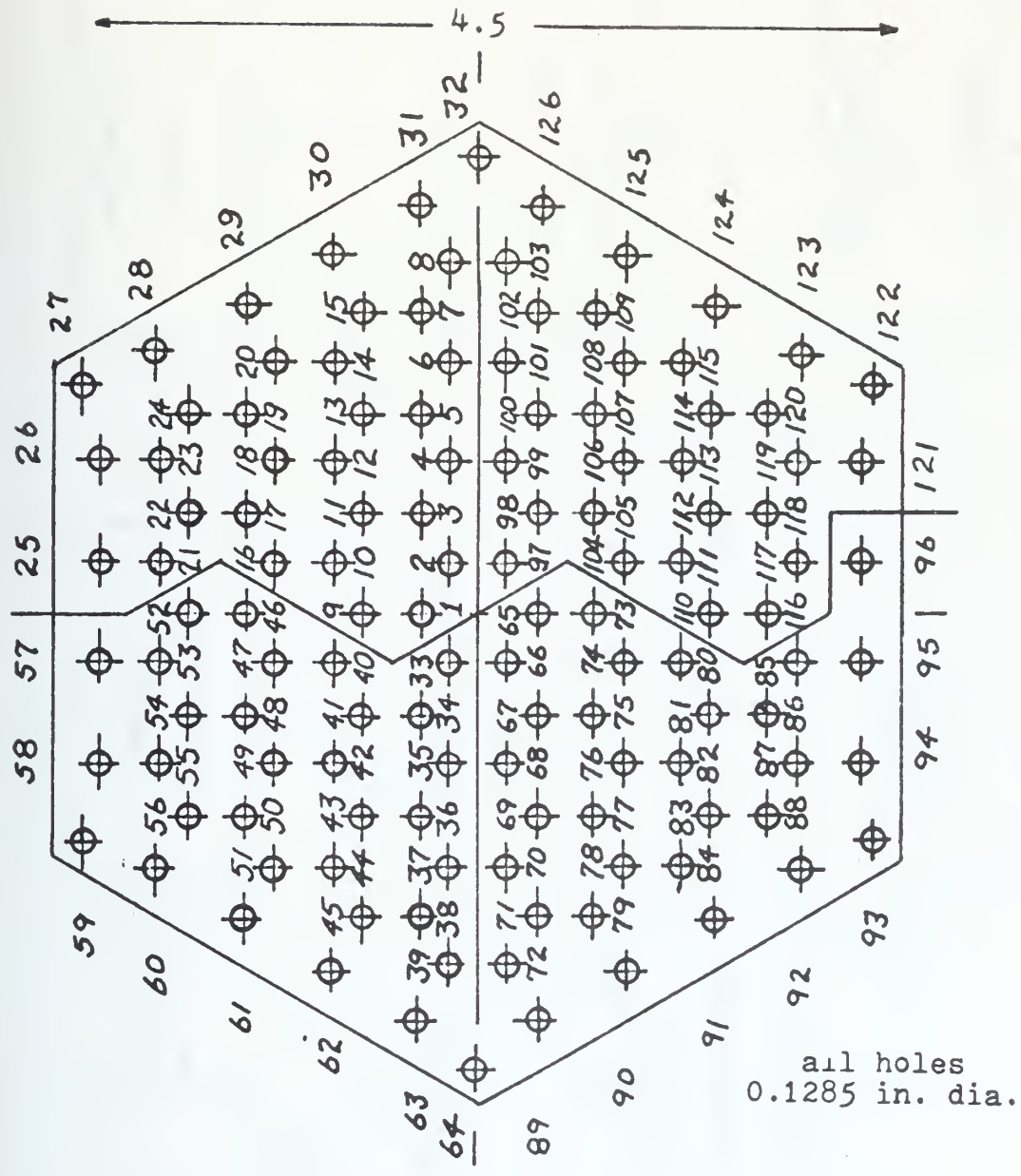

Support Plate Probe Hole Matrix
Plates One, Two And
Three

Figure 2-22

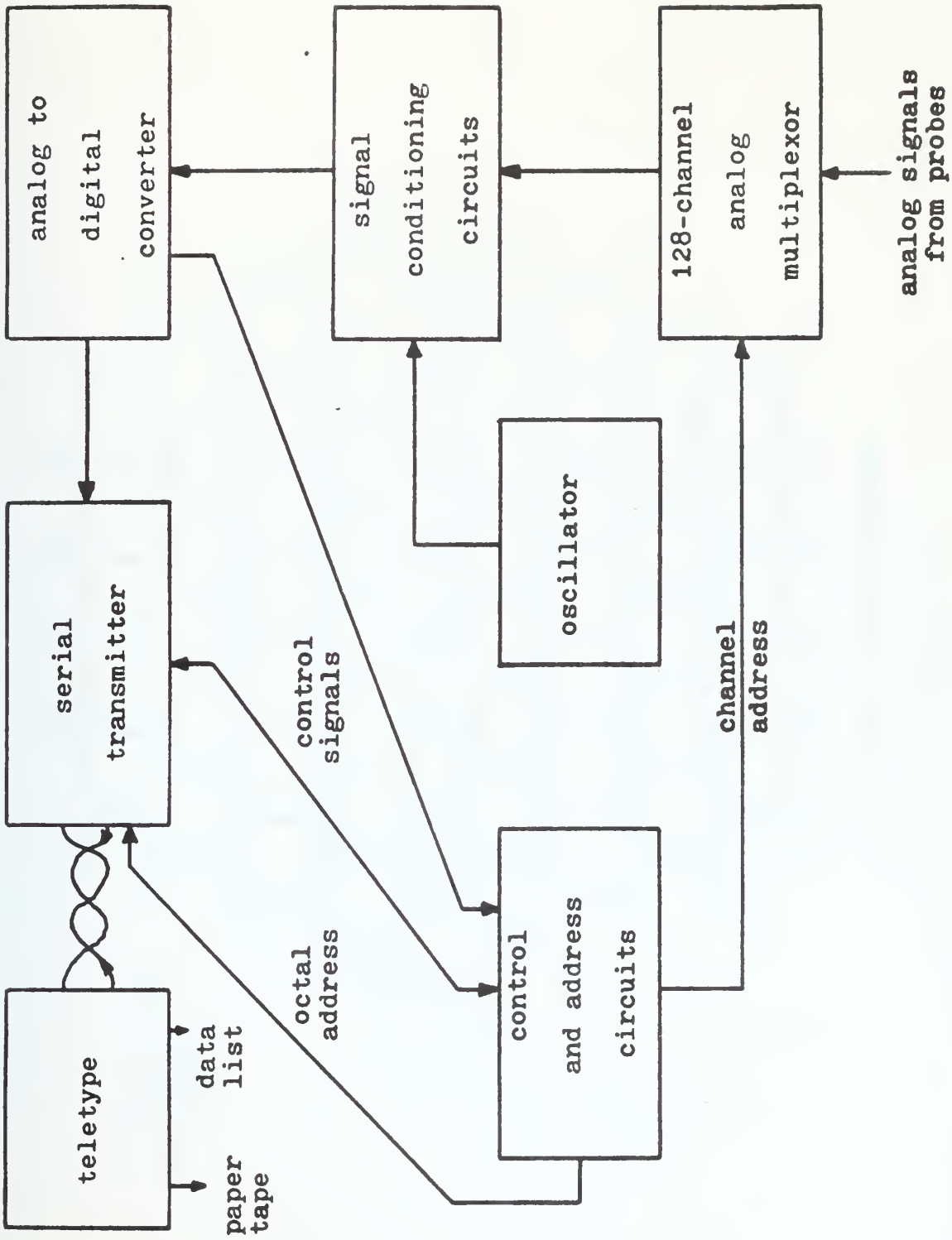

Block Diagram of Data Acquisition System

Figure 2-23 (Ref. 20)

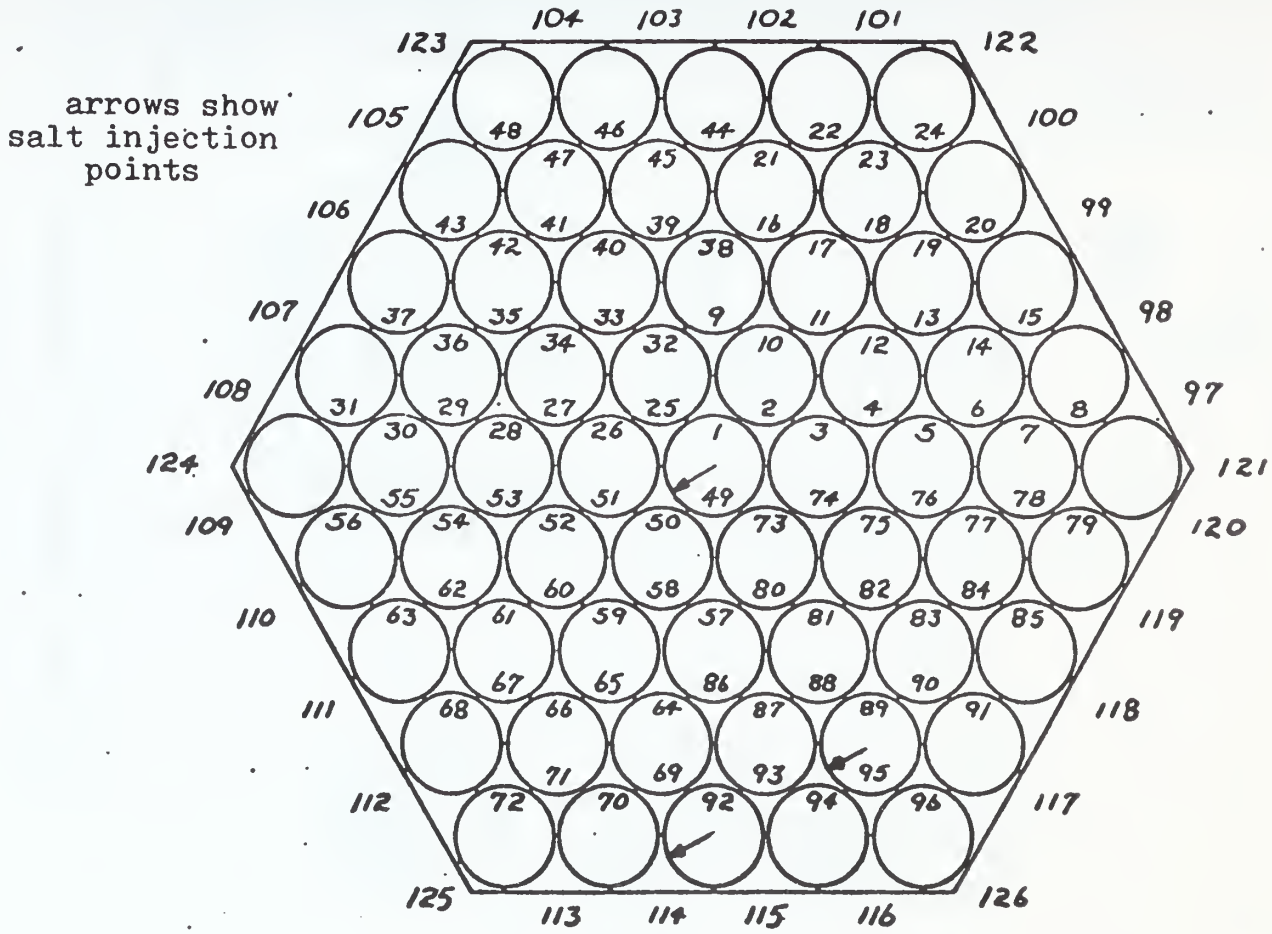

Probe Numbering Scheme

Figure 3-1

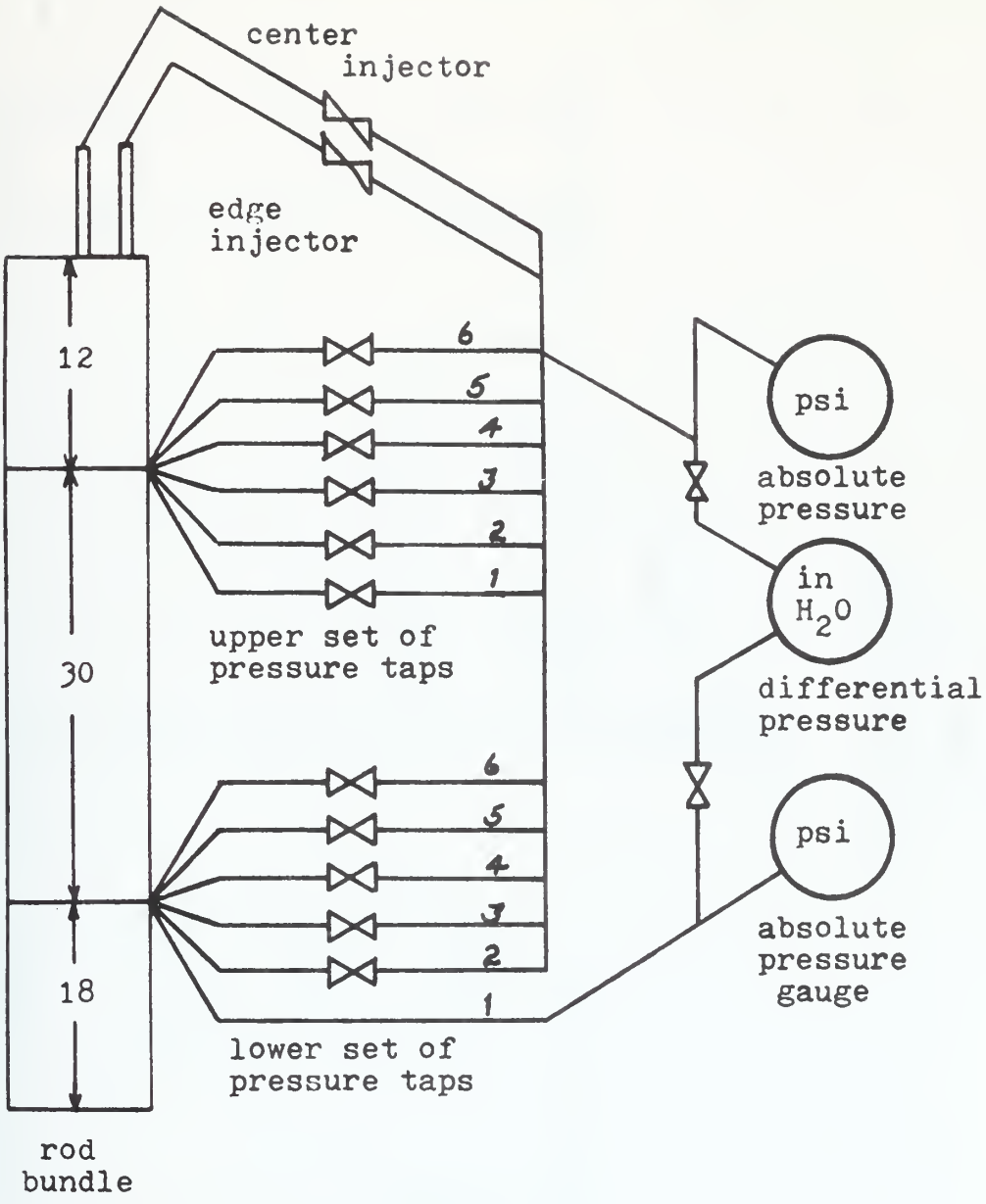

Manifold Arrangement For Pressure Readings

Figure 3-2

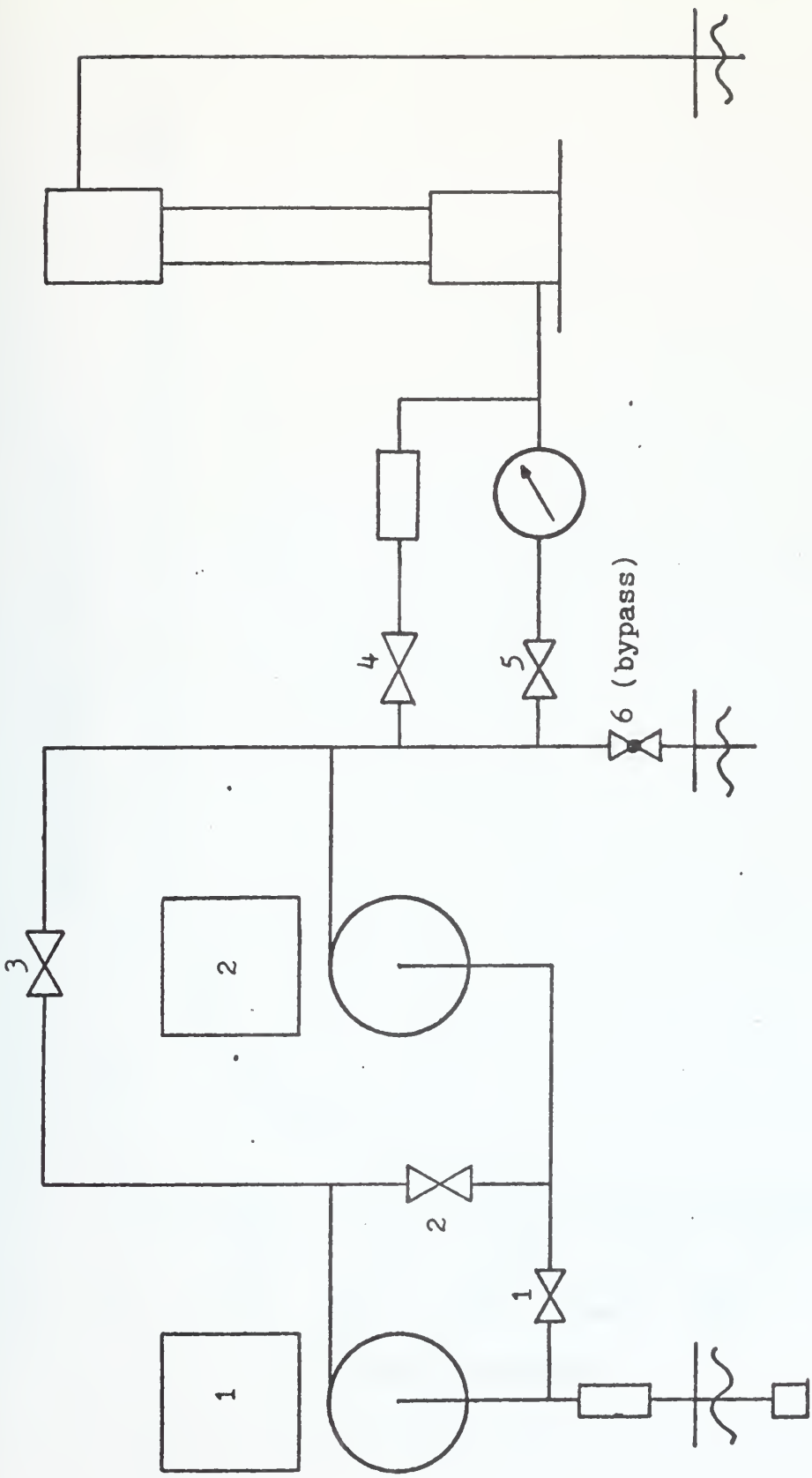

Flow Loop Diagram

Figure 3-3

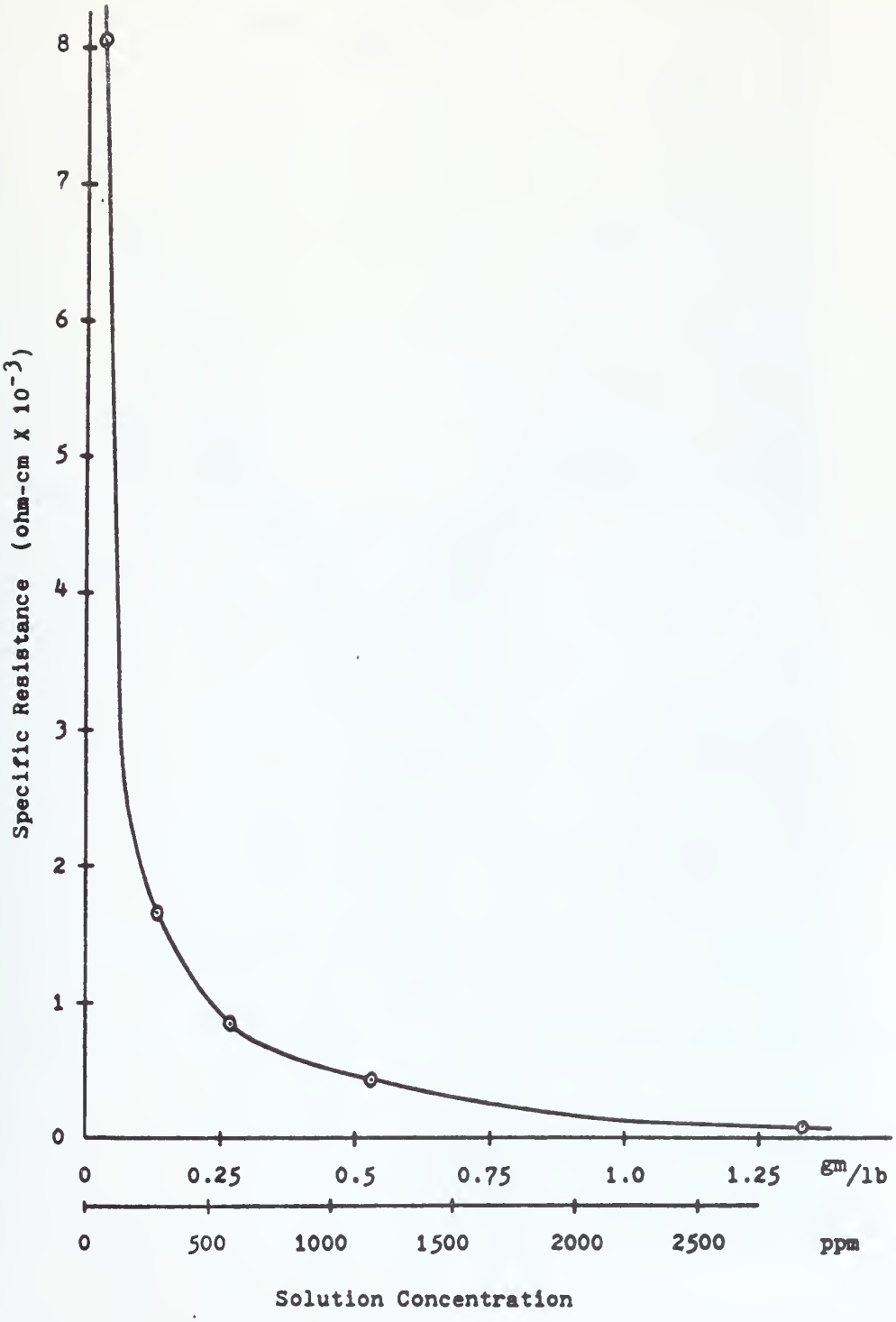
Specific Resistance (ohm-cm X 10^{-3})
8
7
6
5
4
3
2
1
0
0
0.25
0.5
0.75
1.0
1.25
gm/lb
0
500
1000
1500
2000
2500
ppm
Solution Concentration

Figure 3-4

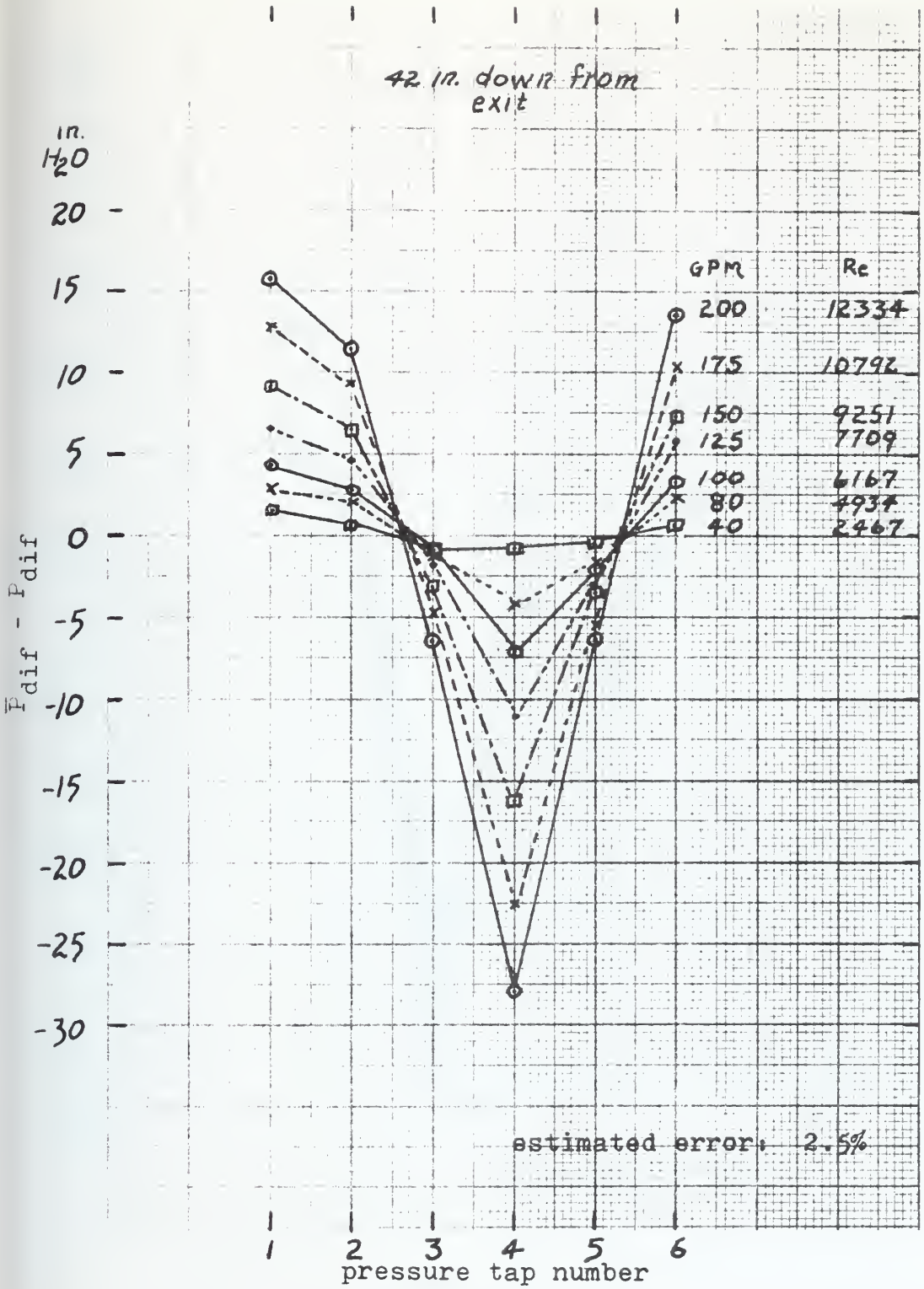
42 in. down from exit
in. H_2O
20
15
10
5
0
-5
-10
-15
-20
-25
-30
$\bar{P}_{dif} - P_{dif}$
GPM
Re
200
12334
175
10792
150
9251
125
7709
100
6167
80
4934
40
2467
estimated error: 2.5%
1
2
3
4
5
6
pressure tap number

Figure 4-1

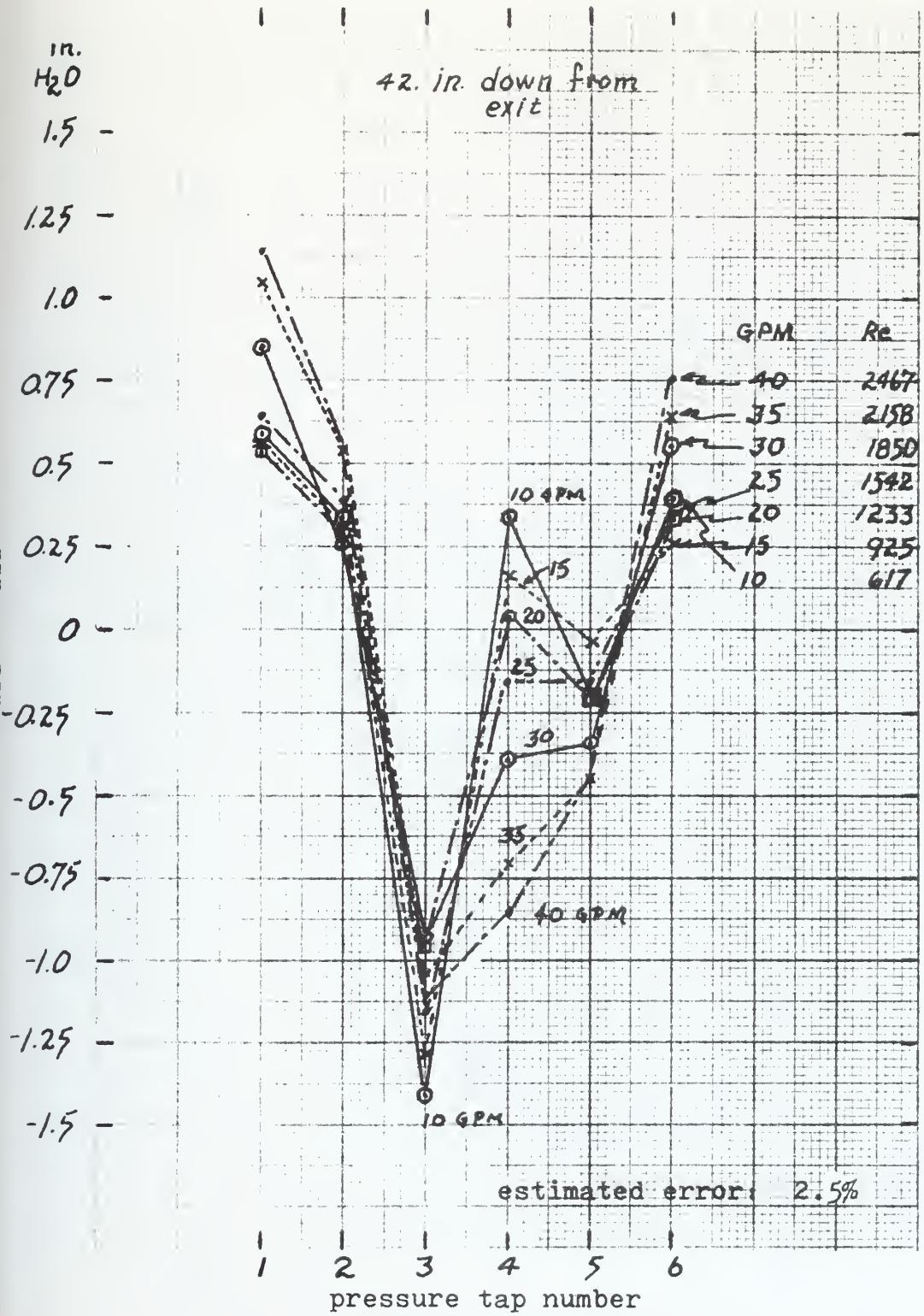
in. H_2O
42. in. down from exit
1.5
1.25
1.0
0.75
0.5
0.25
0
-0.25
-0.5
-0.75
-1.0
-1.25
-1.5
$P_{dif} - P_{dif}$
GPM
Re
40
2467
35
2158
30
1850
25
1542
20
1233
15
925
10
617
10 GPM
40 GPM
estimated error: 2.5%
1
2
3
4
5
6
pressure tap number

Figure 4-2

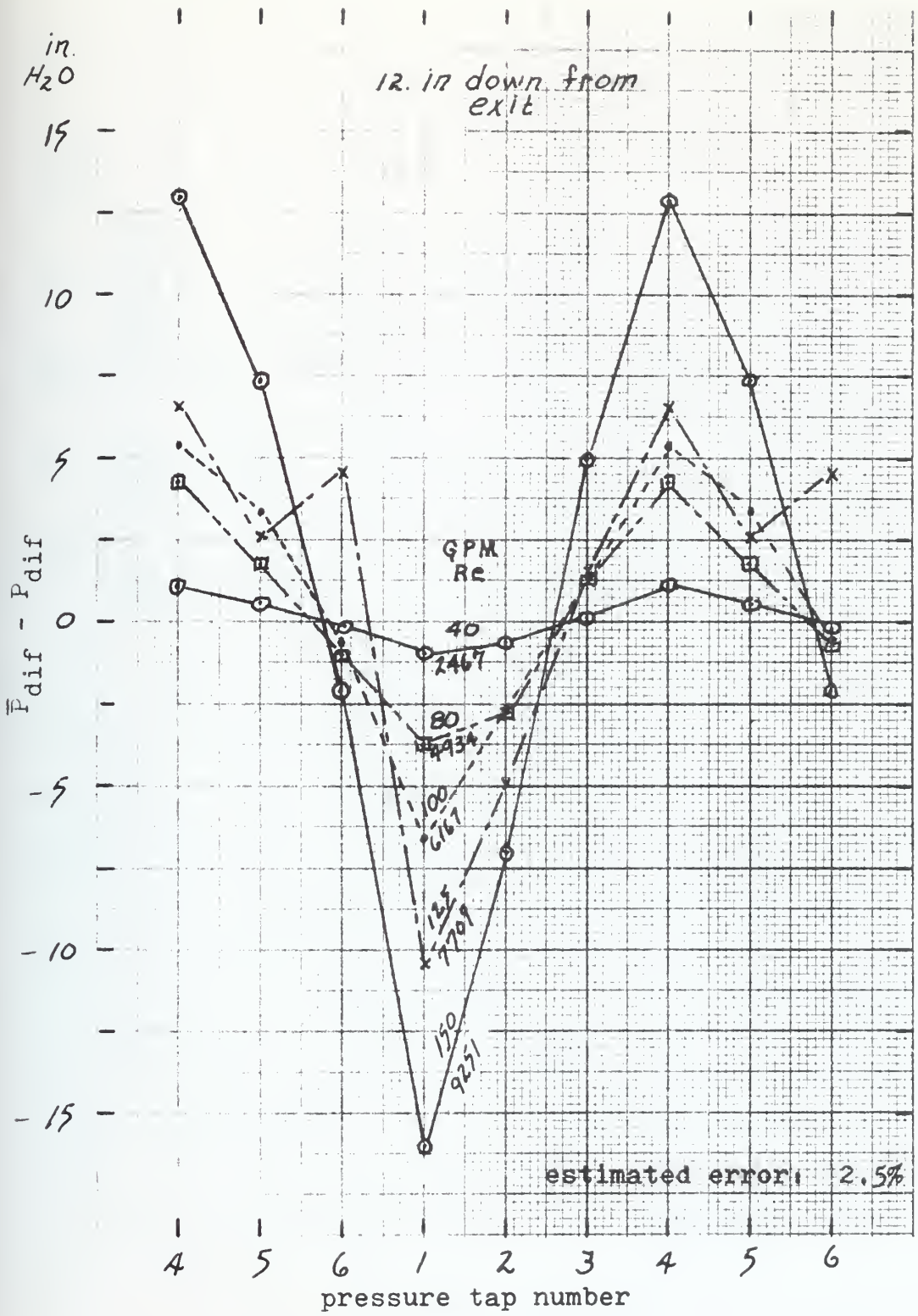
in. H_2O
12. in down from exit
15
10
5
0
-5
-10
-15
$\bar{P}_{dif} - P_{dif}$
GPM
Re
40
2467
80
4934
100
6167
125
7709
150
9251
estimated error: 2.5%
4
5
6
1
2
3
4
5
6
pressure tap number

Figure 4-3

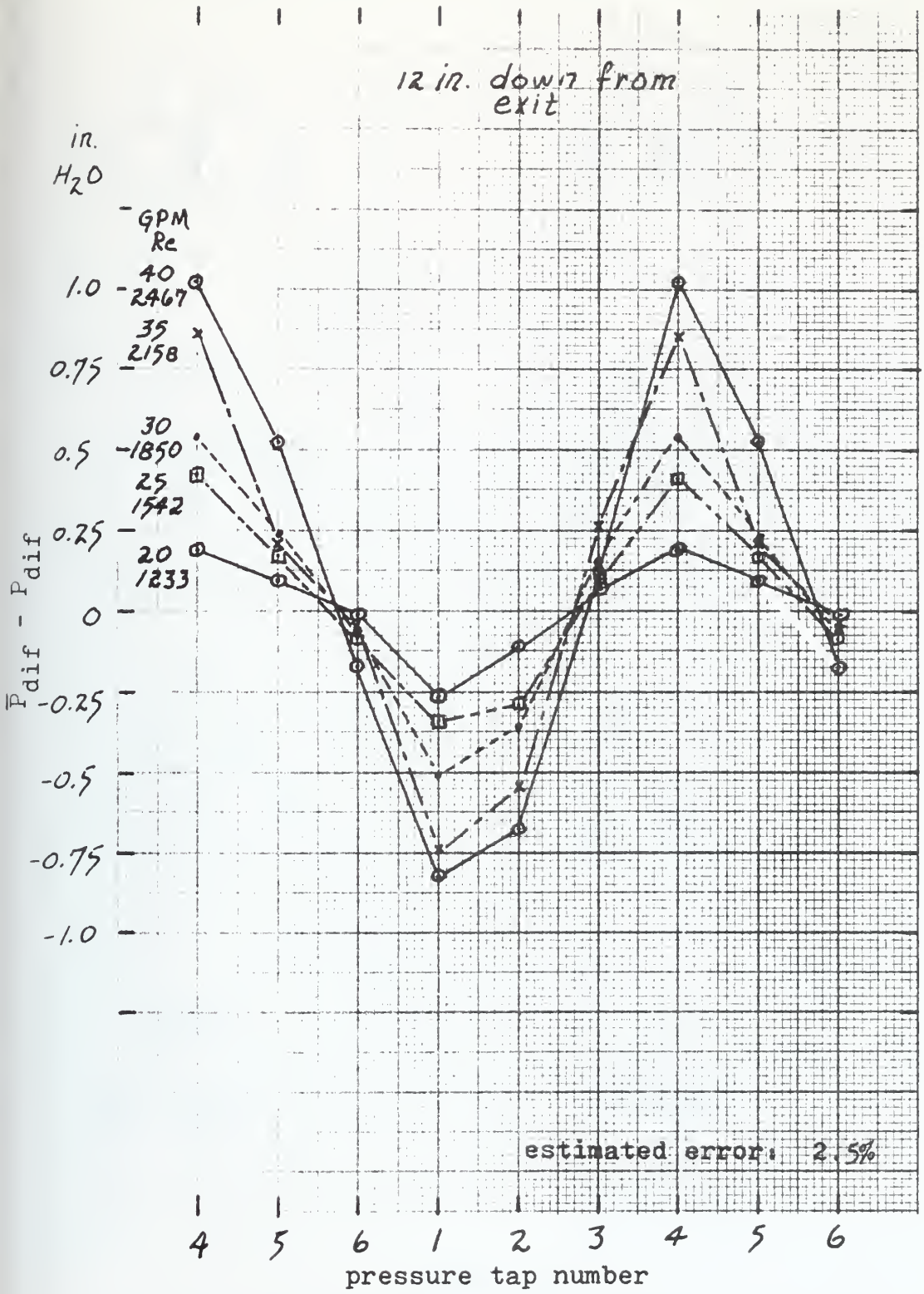
12 in. down from exit
in. H_2O
GPM
Re
40
2467
35
2158
30
1850
25
1542
20
1233
1.0
0.75
0.5
0.25
0
-0.25
-0.5
-0.75
-1.0
$\bar{P}_{dif} - P_{dif}$
estimated error: 2.5%
4
5
6
1
2
3
4
5
6
pressure tap number

Figure 4-4

The orientations shown are found every four inches for the ranges noted below each. The positions are the distances down from the bundle exit.

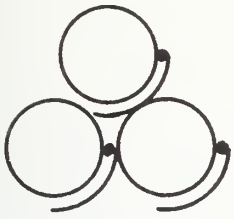

0 - 52

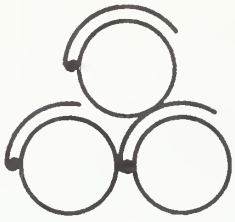

2 - 54

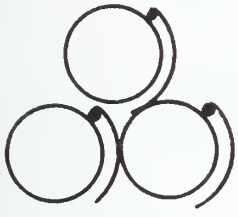

3.5 - 51.5

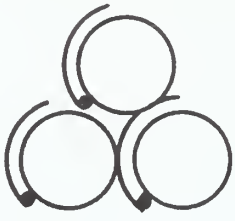

1.5 - 53.5

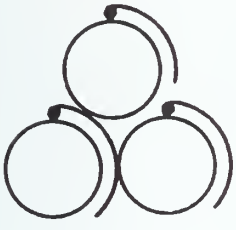

3 - 51

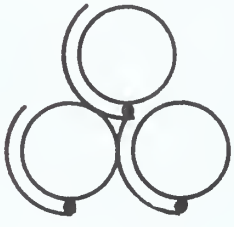

1 - 53

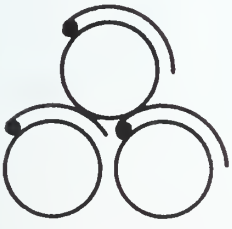

2.5 - 50.5

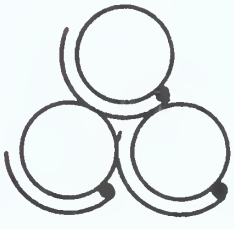

0.5 - 52.5

Figure 4-5

Wire Wrap Orientations At Various Axial Positions

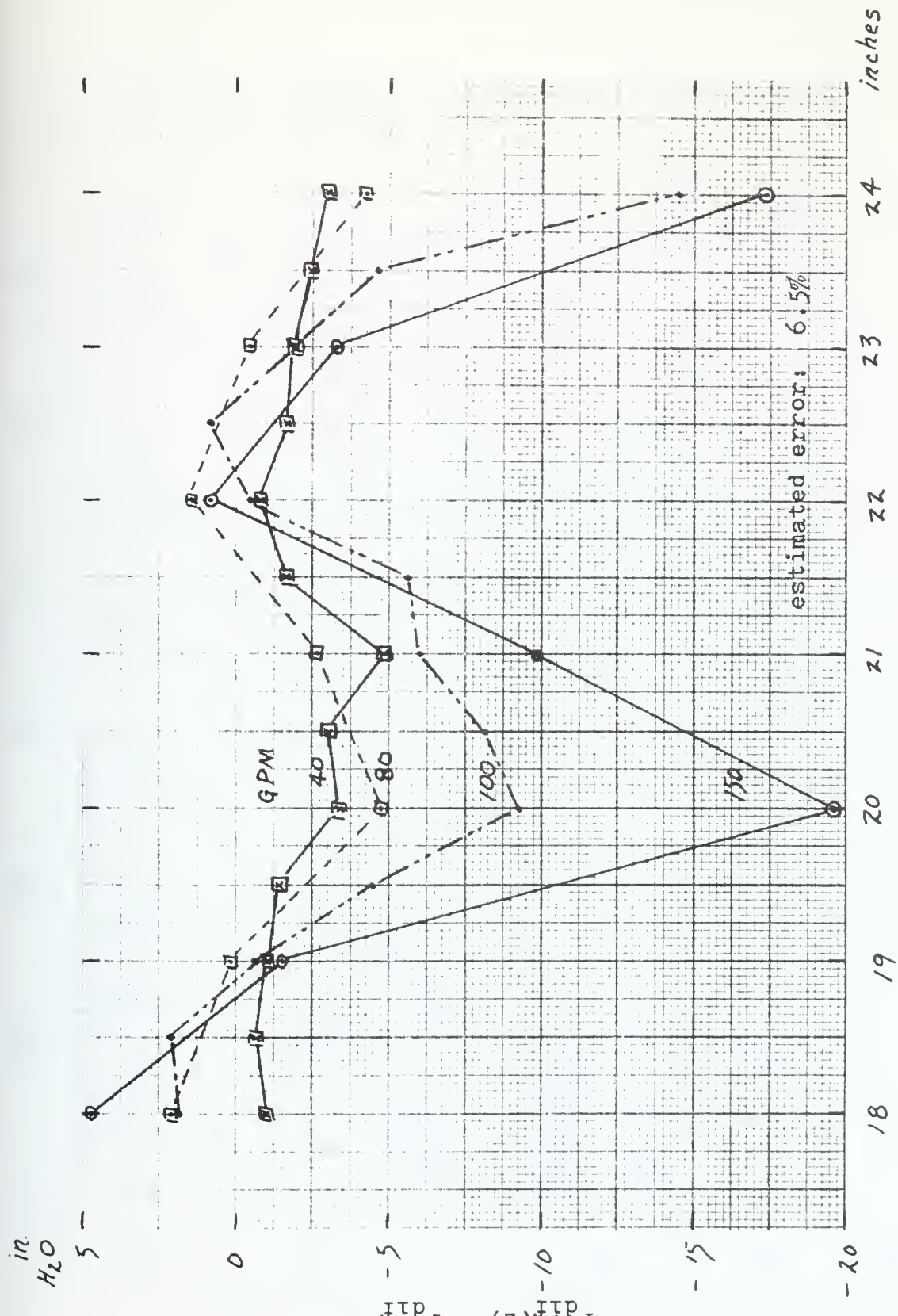

Axial Position Down From Exit

Figure 4-6

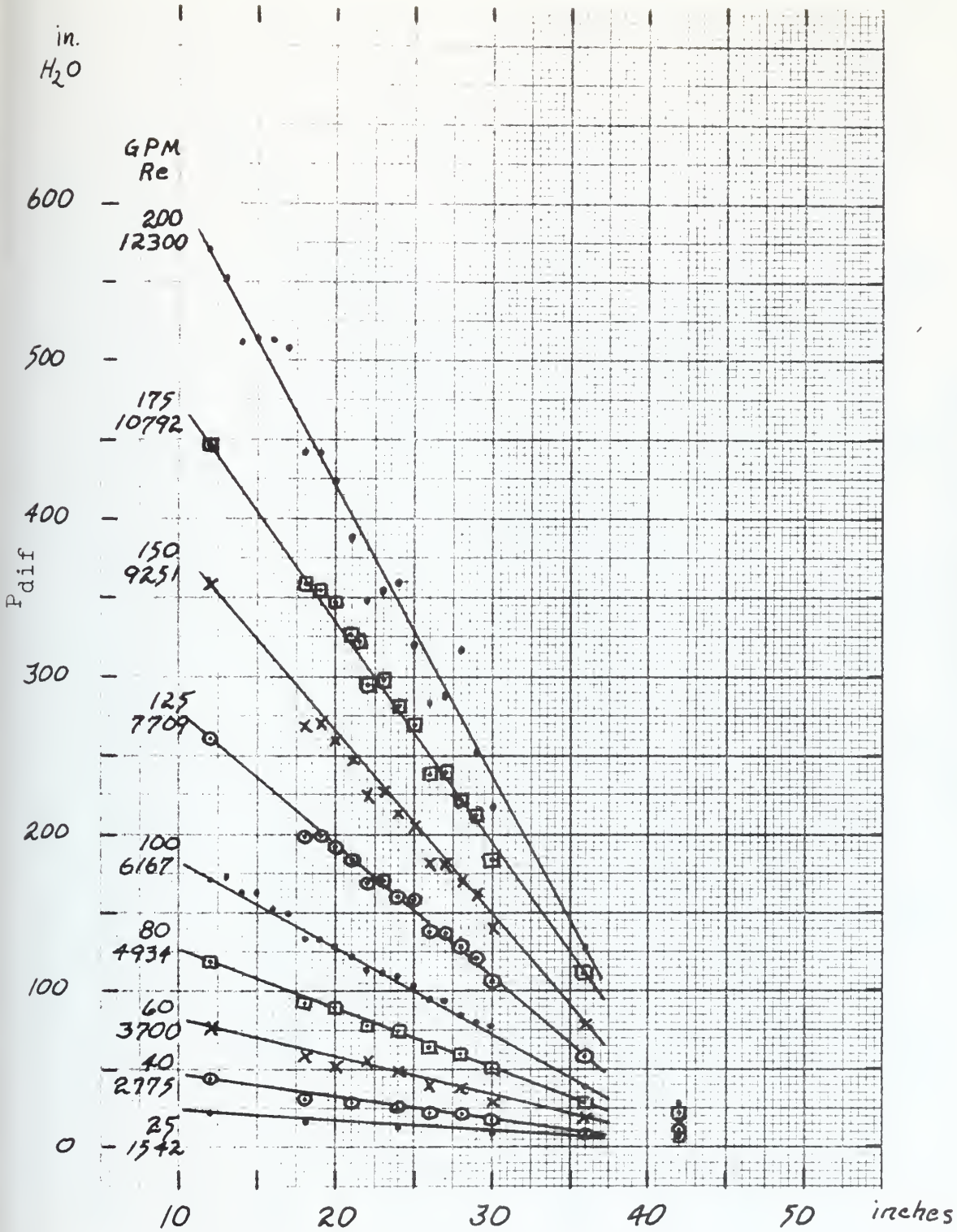
in.
H_2O
GPM
Re
600
200
12300
500
175
10792
400
150
9251
P_{dif}
300
125
7709
200
100
6167
80
4934
100
60
3700
40
2775
25
1542
0
10
20
30
40
50
inches
Axial Position Down From Exit

Figure 4-7

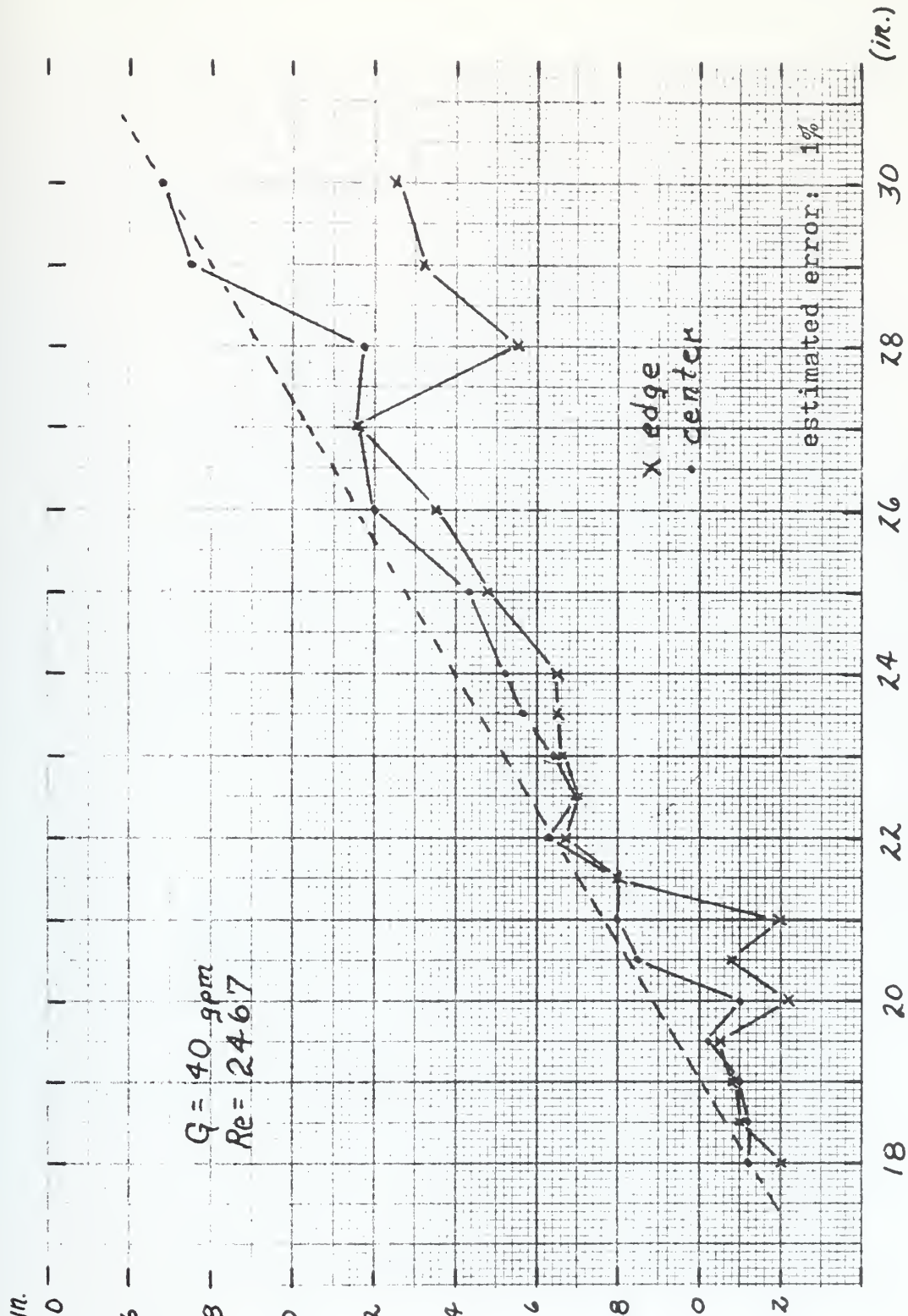
in. H2O
16
18
20
22
24
26
28
30
32
Pdif
G = 40 gpm
Re = 24617
x edge
• center
estimated error: 1%
18
20
22
24
26
28
30
(in.)
Axial Position Down From Exit

Figure 4-8

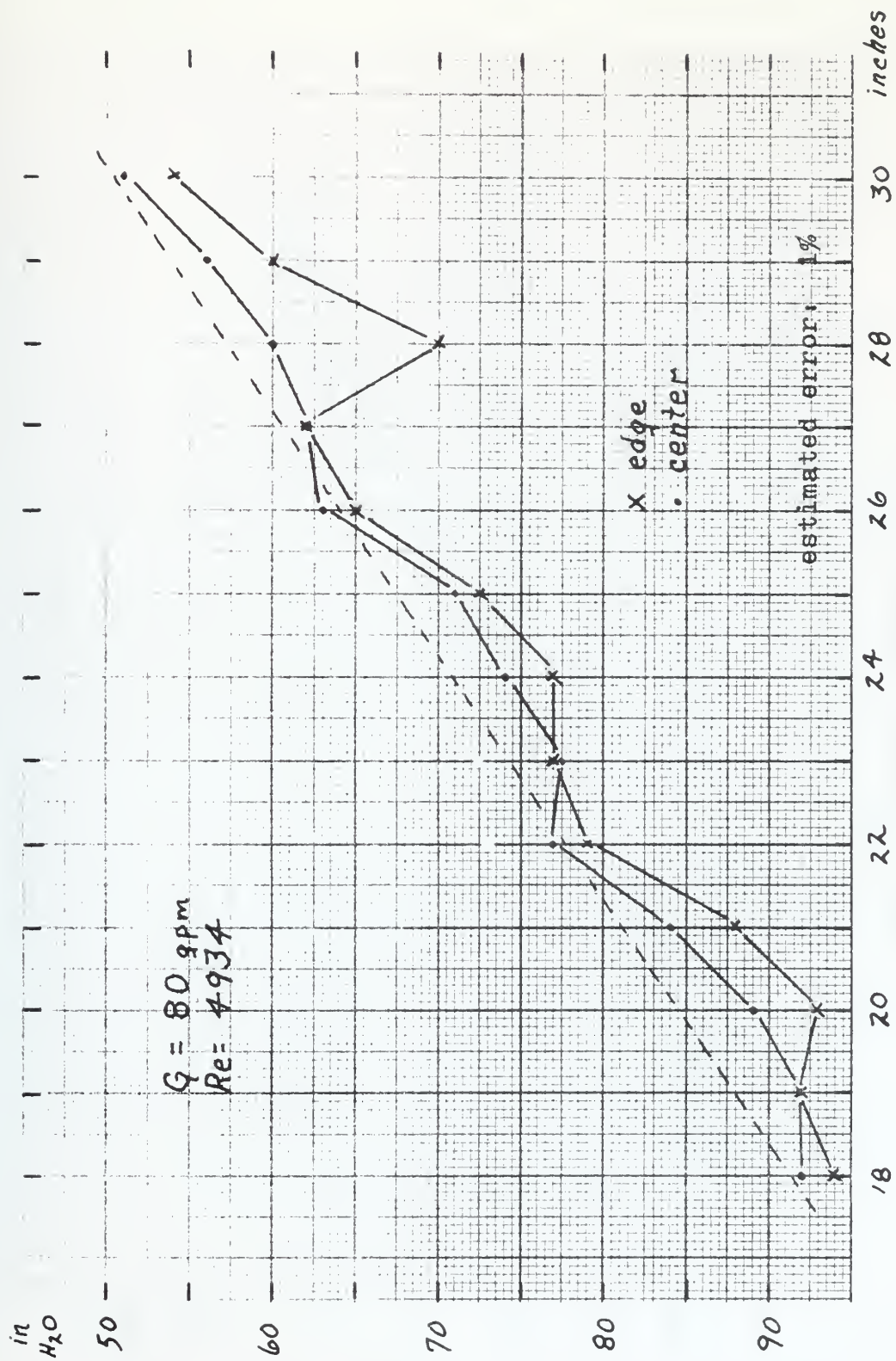

Axial Position Down From Exit

Figure 4-9

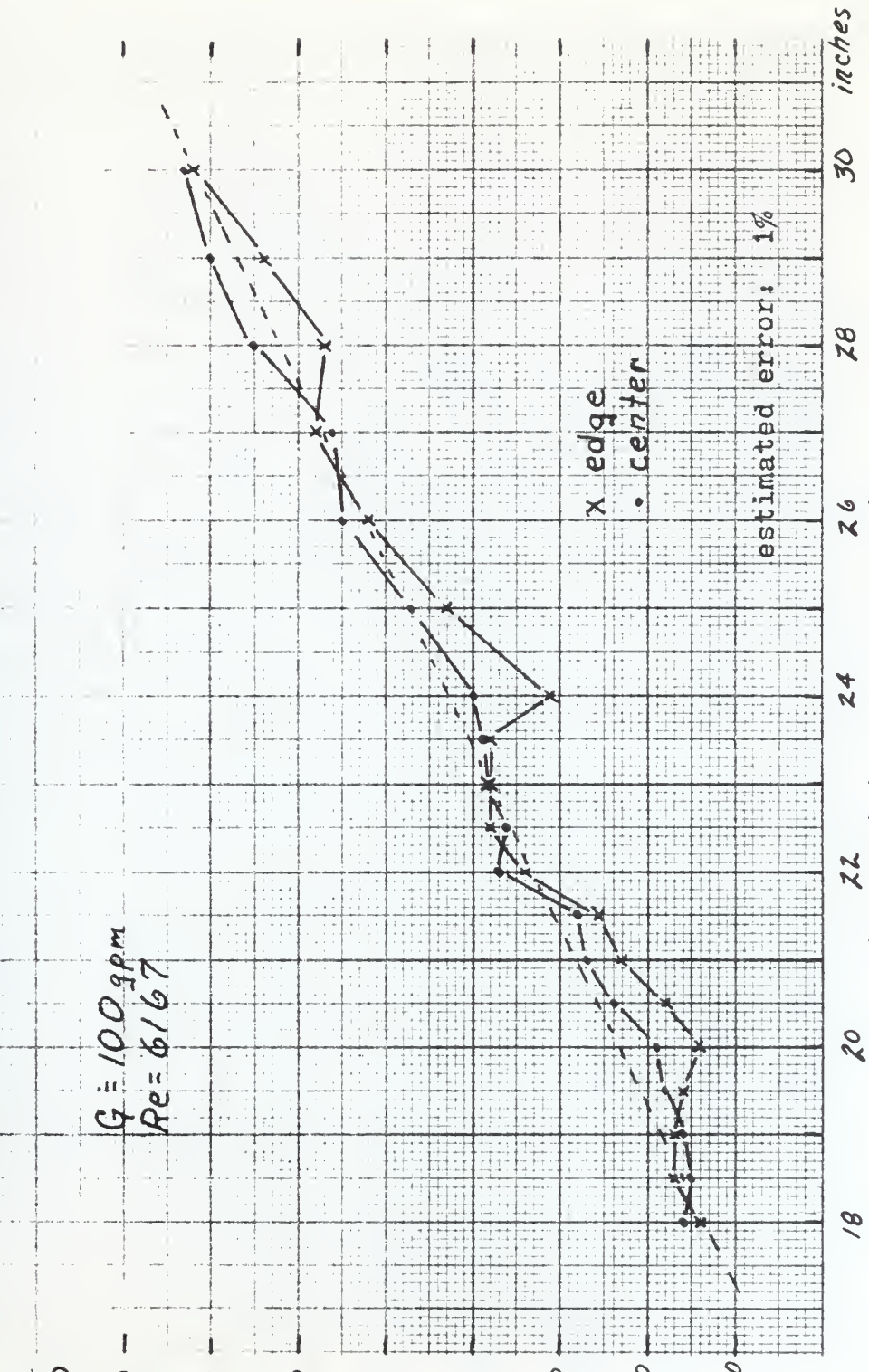
G = 100 gpm
Re = 6167
x edge
• center
estimated error: 1%
P_{dif}
in. H_2O
70
80
90
100
110
120
130
140
18
20
22
24
26
28
30
inches
Axial Position Down From Exit

Figure 4-10

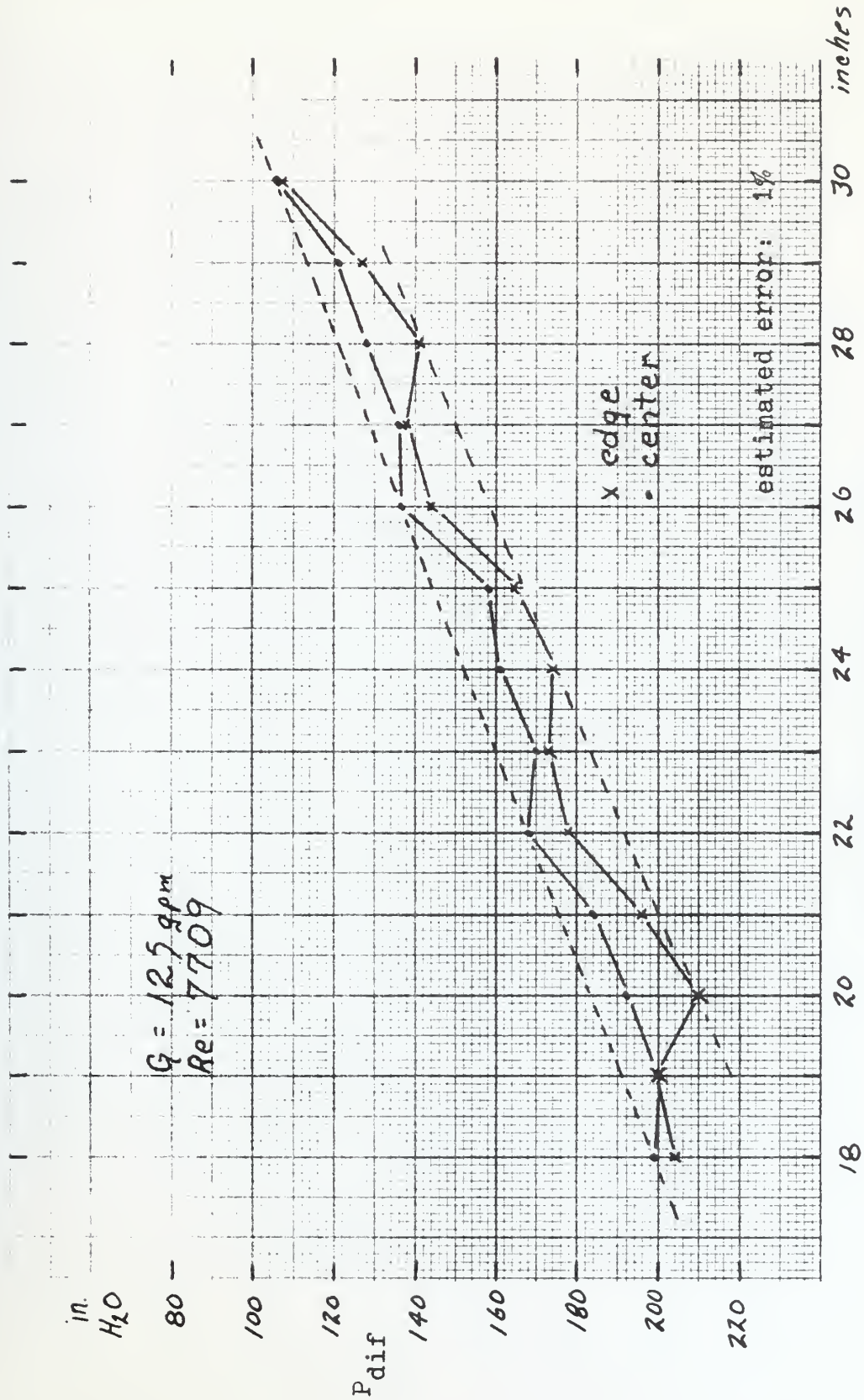

Axial Position Down From Exit

Figure 4-11

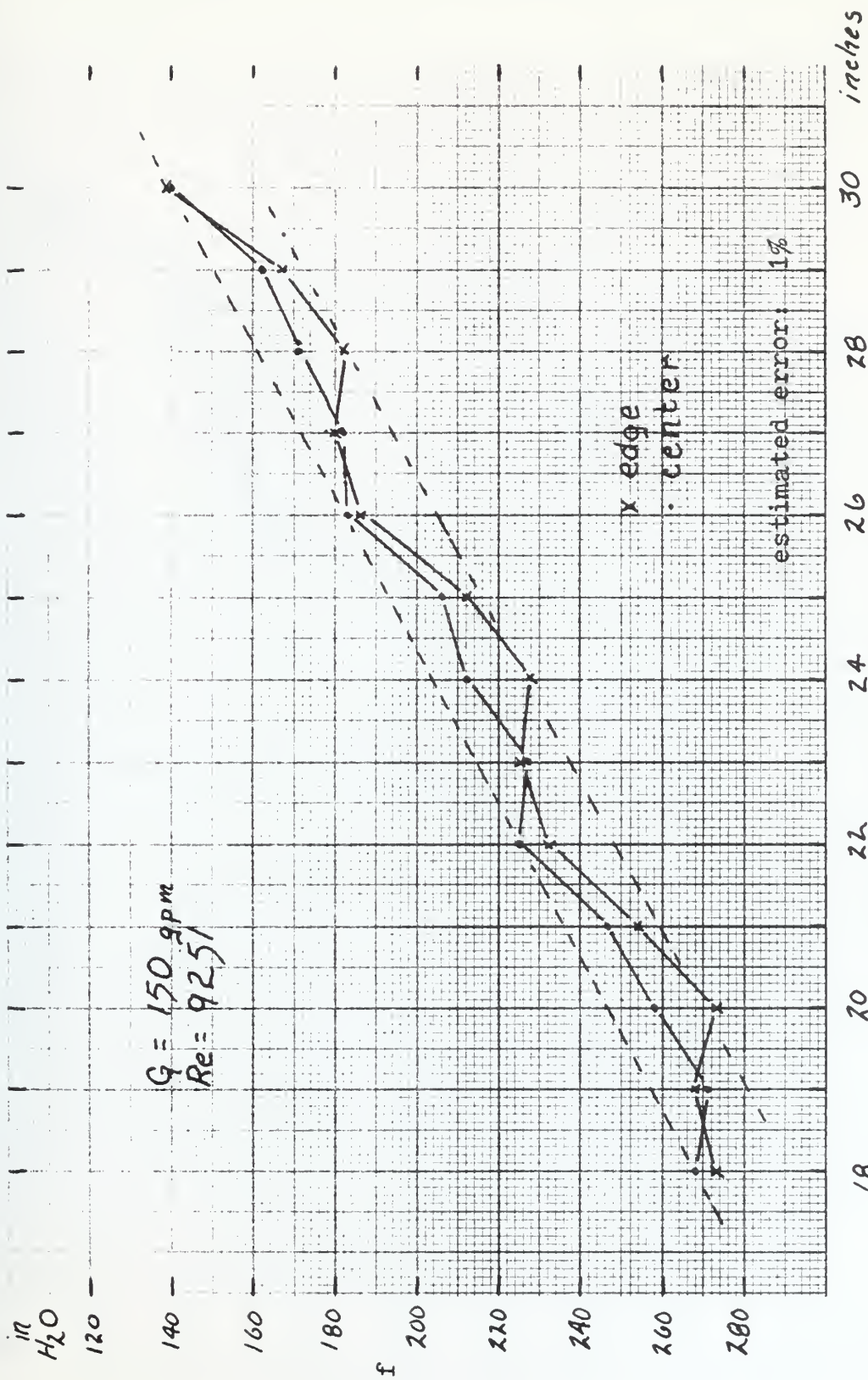

Axial Position Down From Exit

Figure 4-12

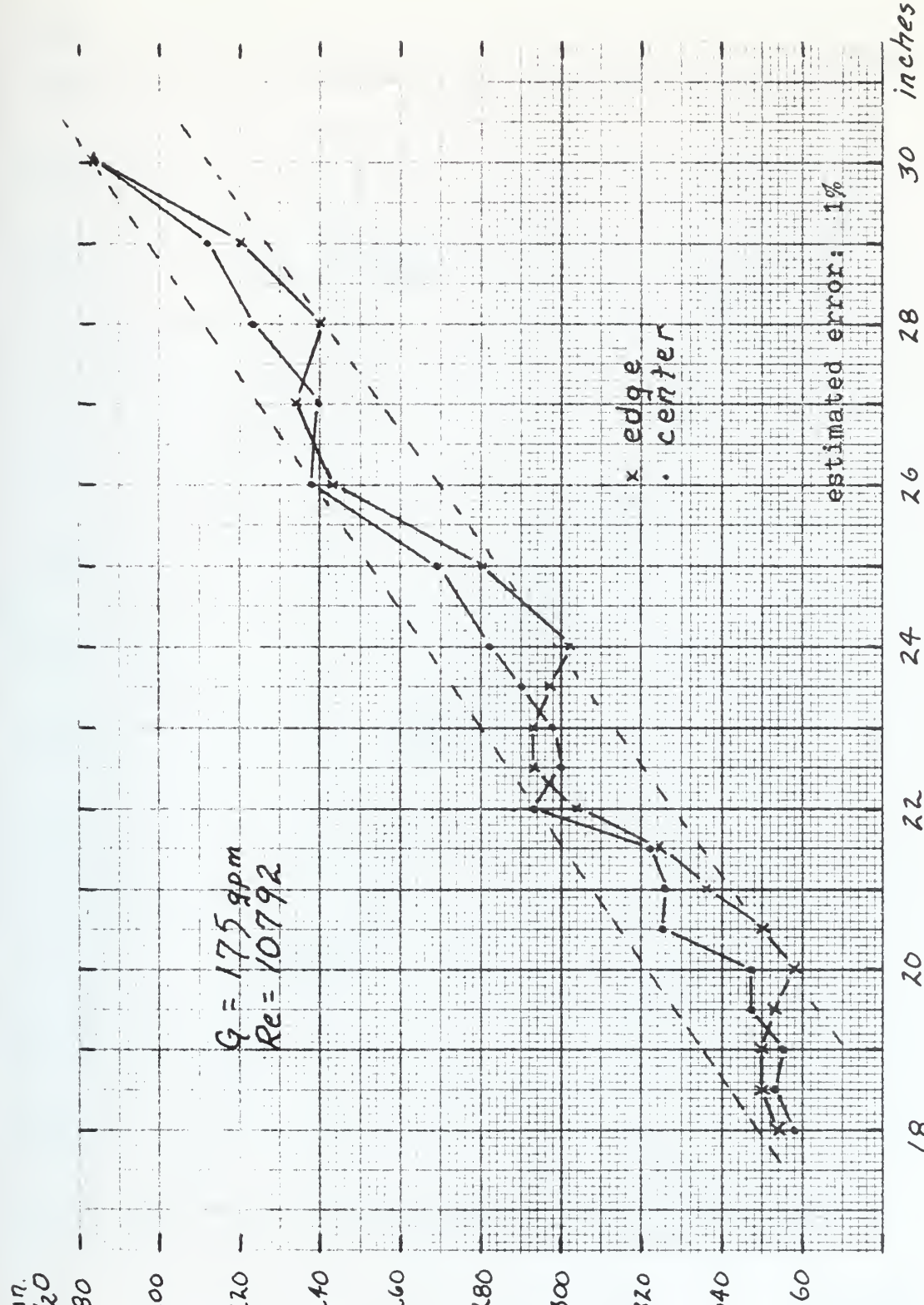

Axial Position Down From Exit

Figure 4-13

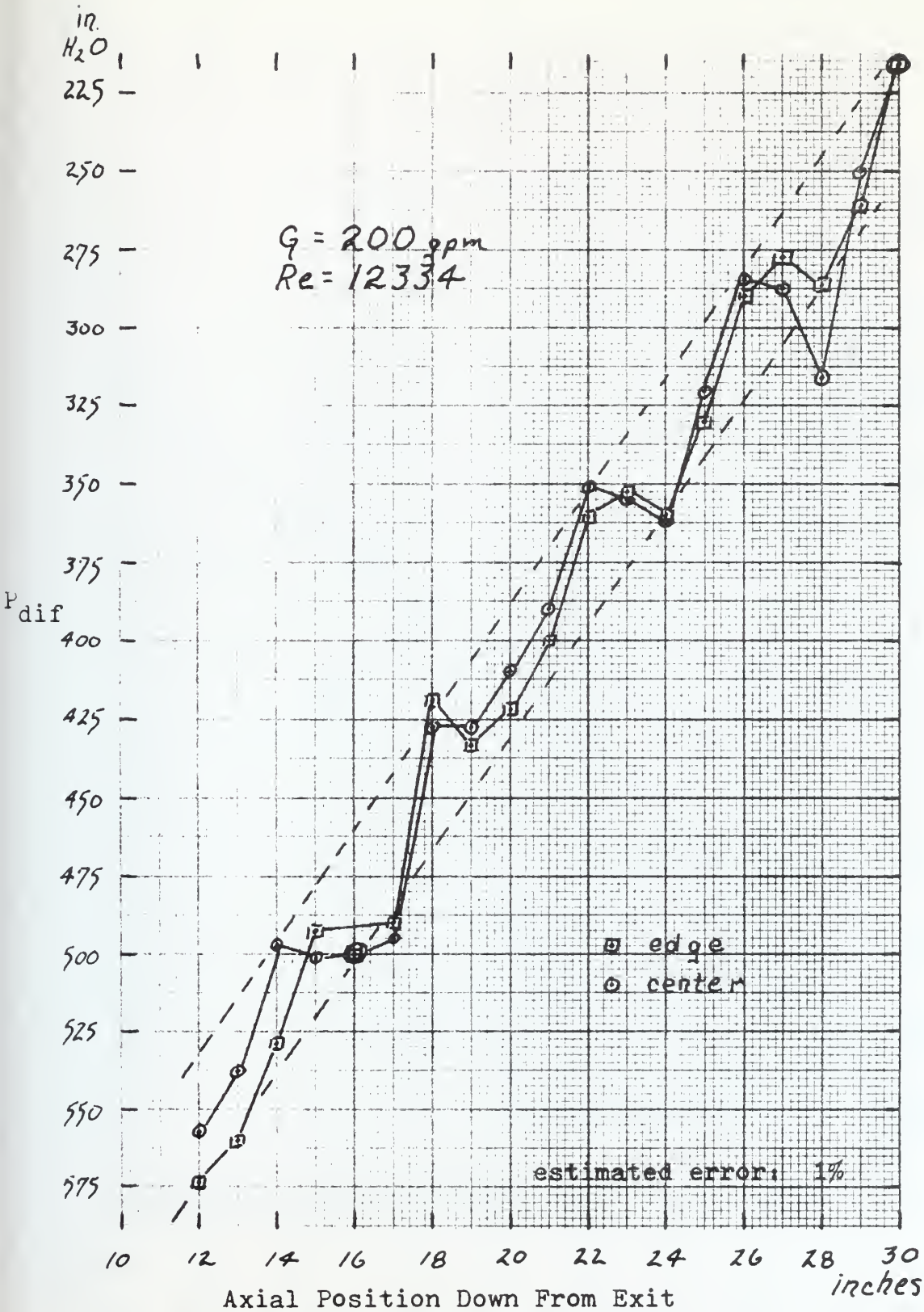
in. H_2O
225
250
275
300
325
350
375
400
425
450
475
500
525
550
575
P_{dif}
G = 200 gpm
Re = 12334
edge
center
estimated error: 1%
10
12
14
16
18
20
22
24
26
28
30
inches
Axial Position Down From Exit

Figure 4-14

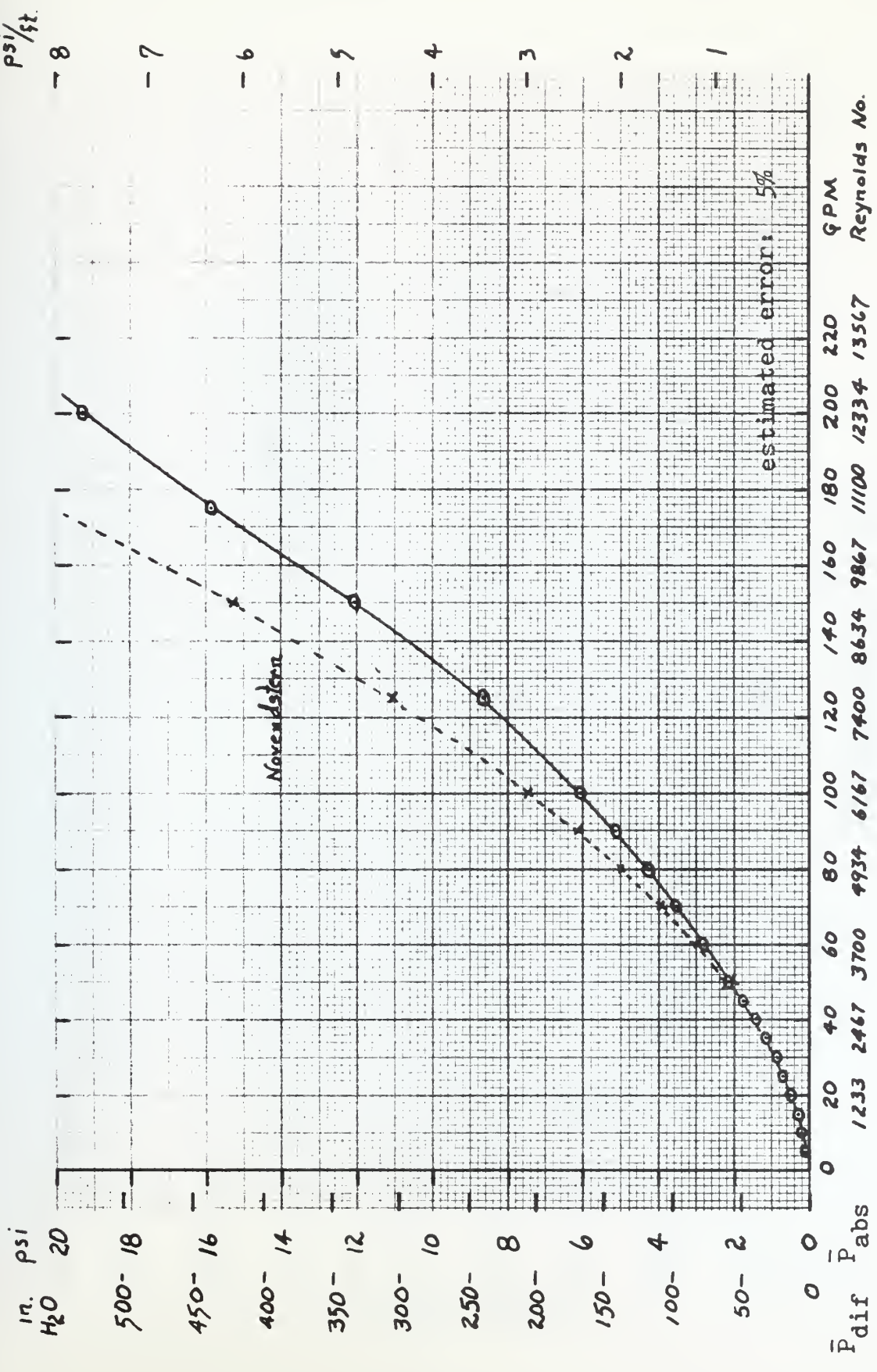

Flow Rate and Reynolds Number

Figure 4-15

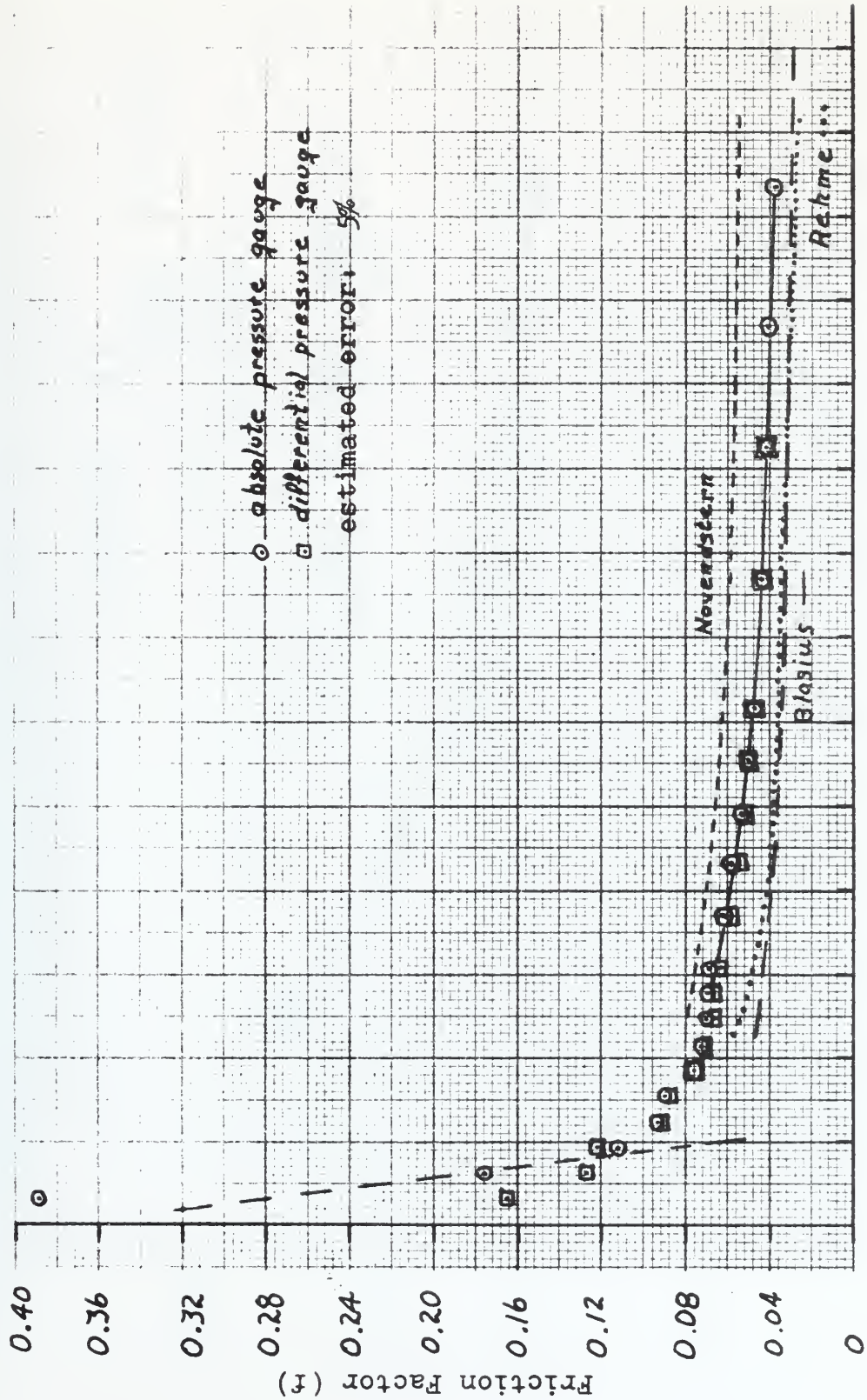
Friction Factor (f)
0.40
0.36
0.32
0.28
0.24
0.20
0.16
0.12
0.08
0.04
0
absolute pressure gauge
differential pressure gauge
estimated error 5%
Nevenstern
Blasius
Reichmeister
0 1 2 3 4 5 6 7 8 9 10 11 12 13 14
Reynolds Number x 10^{-3}

Figure 4-16

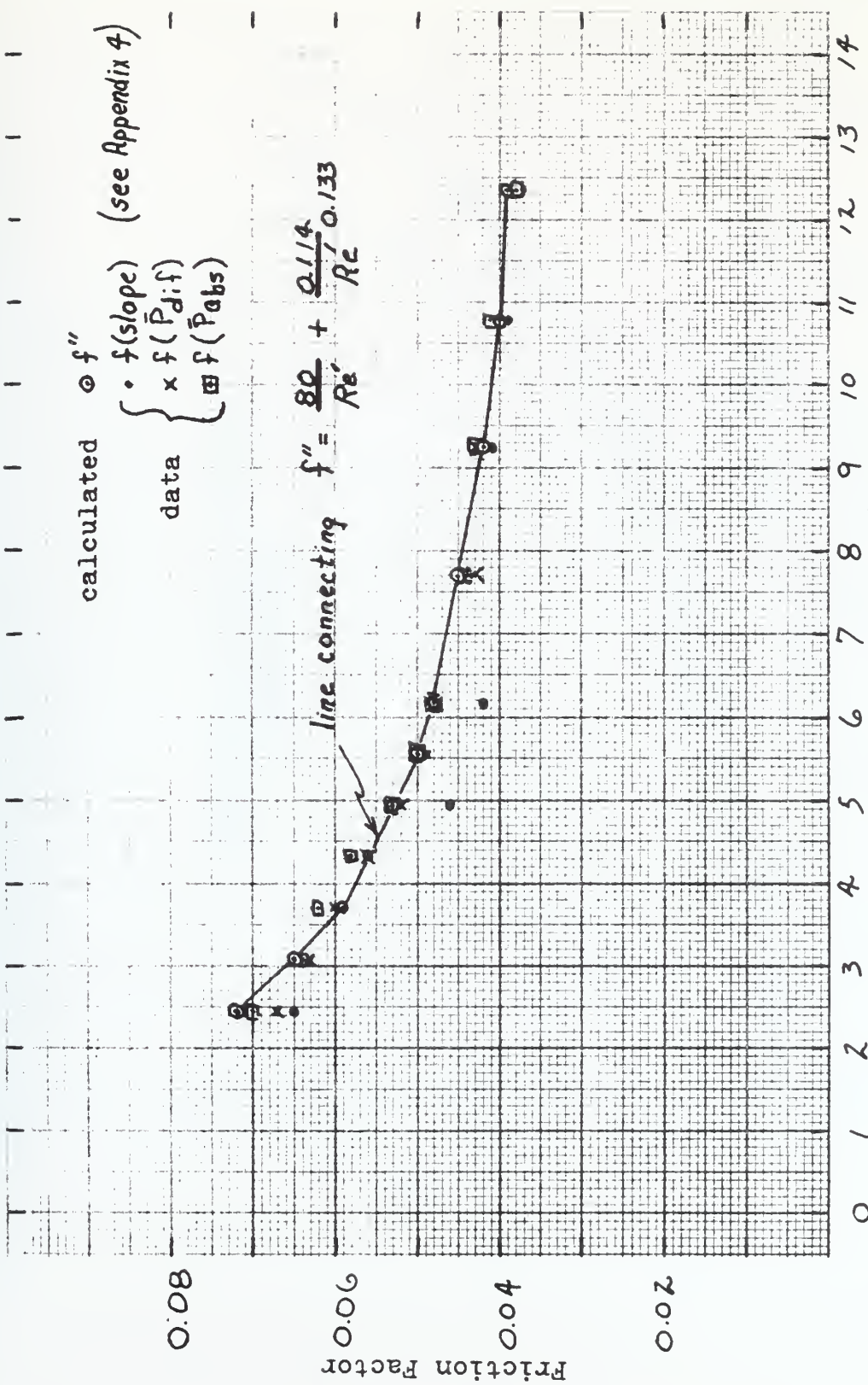
calculated ⊙ f″
• f(slope) (see Appendix 4)
data × f(P̄dif)
⊞ f(P̄abs)
line connecting
f″ = 80/Re′ + 0.114/Re′^0.133
Friction Factor
0.08
0.06
0.04
0.02
0 1 2 3 4 5 6 7 8 9 10 11 12 13 14
Reynolds Number x 10^-3

Figure 4-17

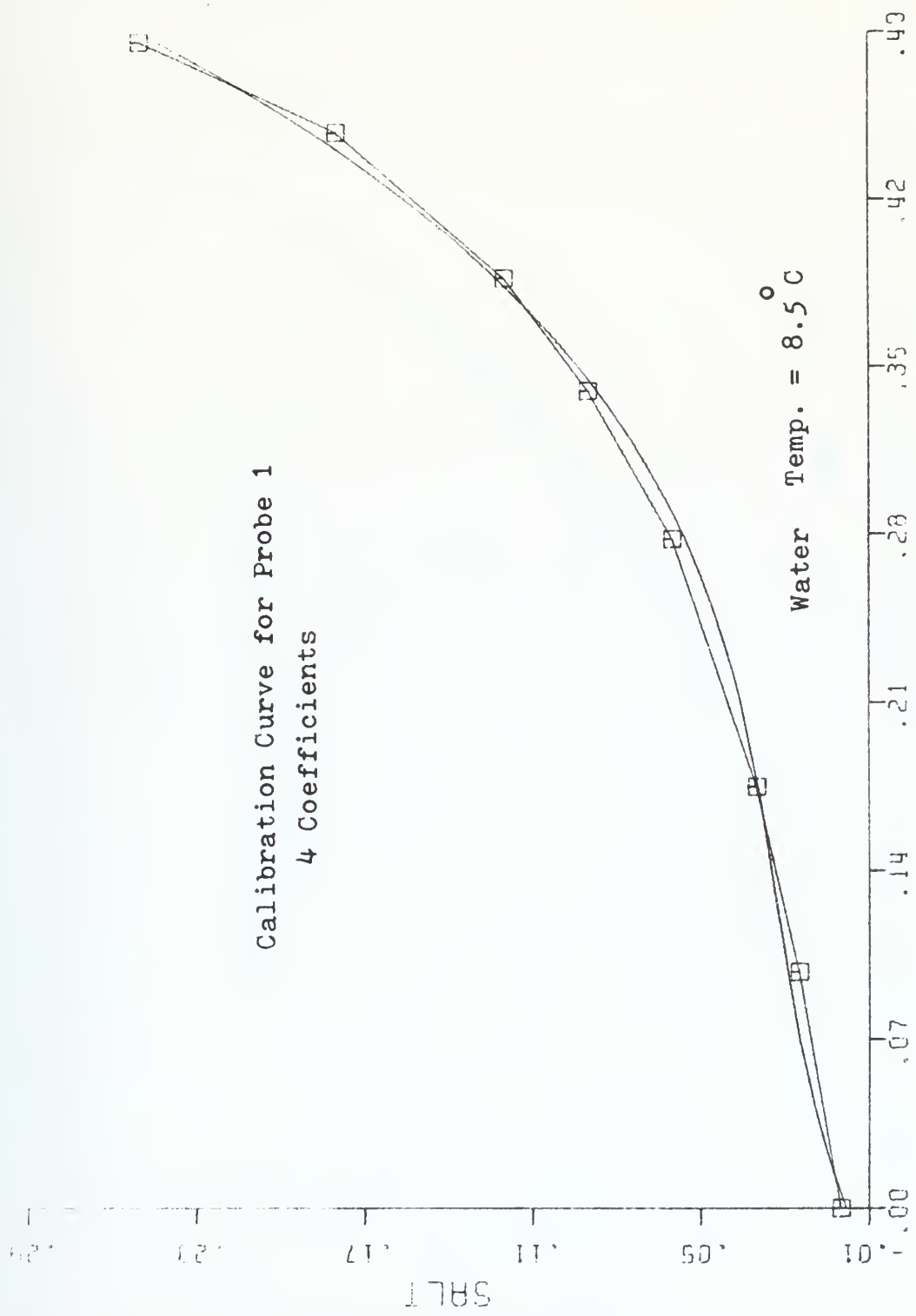
Calibration Curve for Probe 1
4 Coefficients
Water Temp. = 8.5 °C
SIGNAL
.00
.07
.14
.21
.28
.35
.42
.49
SALT
.01
.05
.11
.17
.23

Figure 4-18

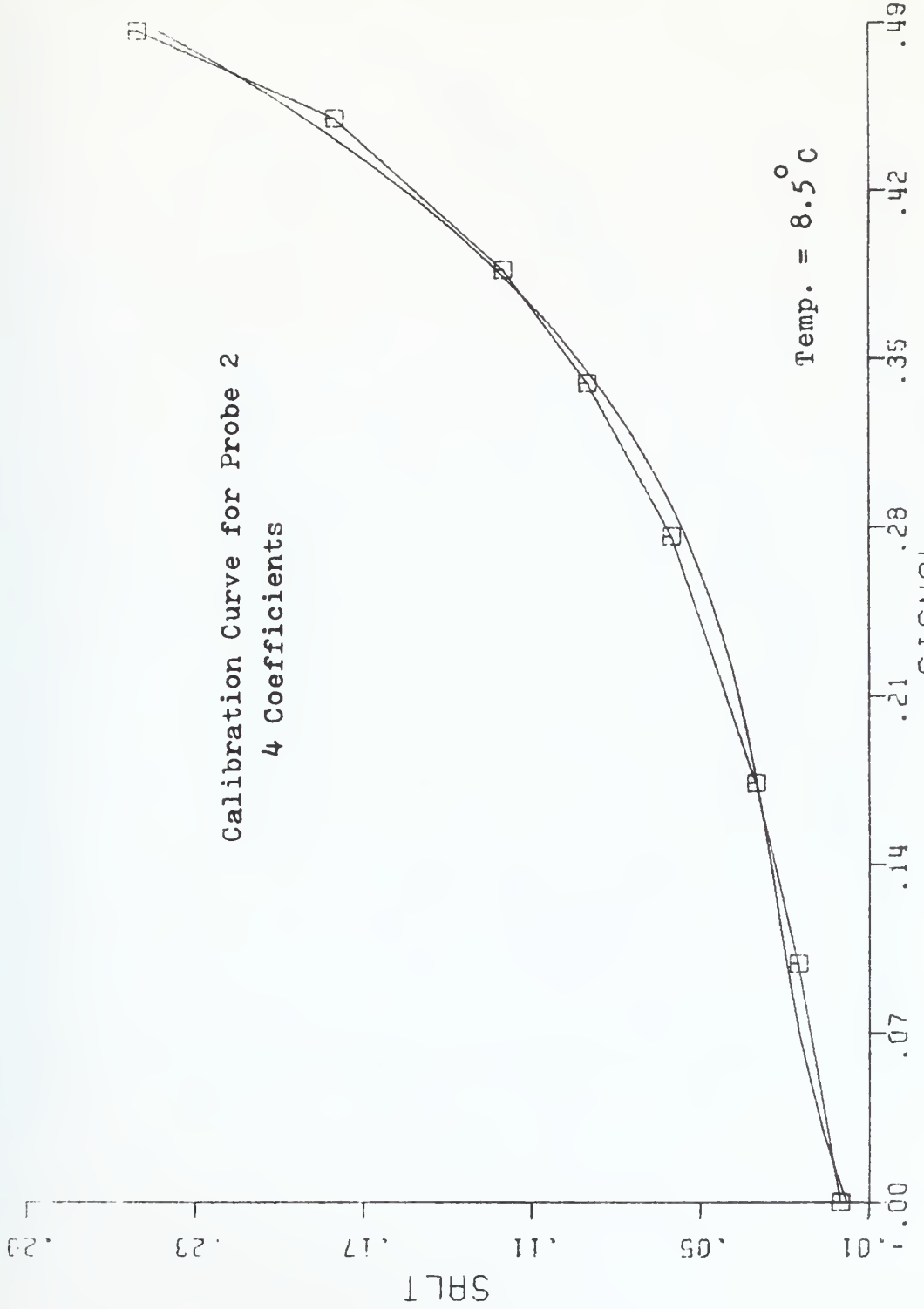
Calibration Curve for Probe 2
4 Coefficients
Temp. = 8.5° C
SALT
SIGNAL
.00
.07
.14
.21
.28
.35
.42
.49
.01
.05
.11
.17
.23
.29

Figure 4-19

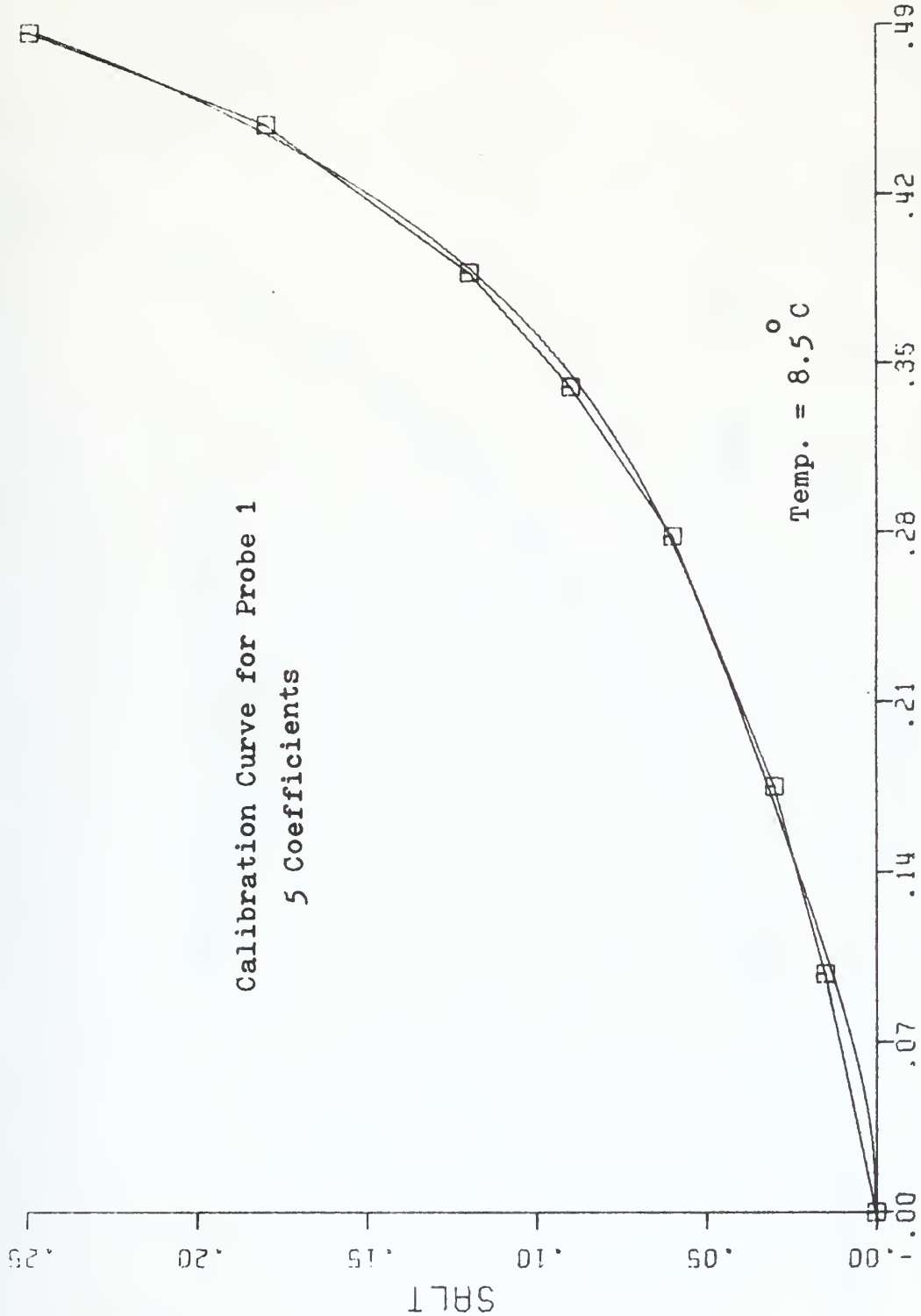
Calibration Curve for Probe 1
5 Coefficients
Temp. = 8.5 °C
SALT
SIGNAL
.00
.05
.10
.15
.20
.25
.00
.07
.14
.21
.28
.35
.42
.49

Figure 4-20

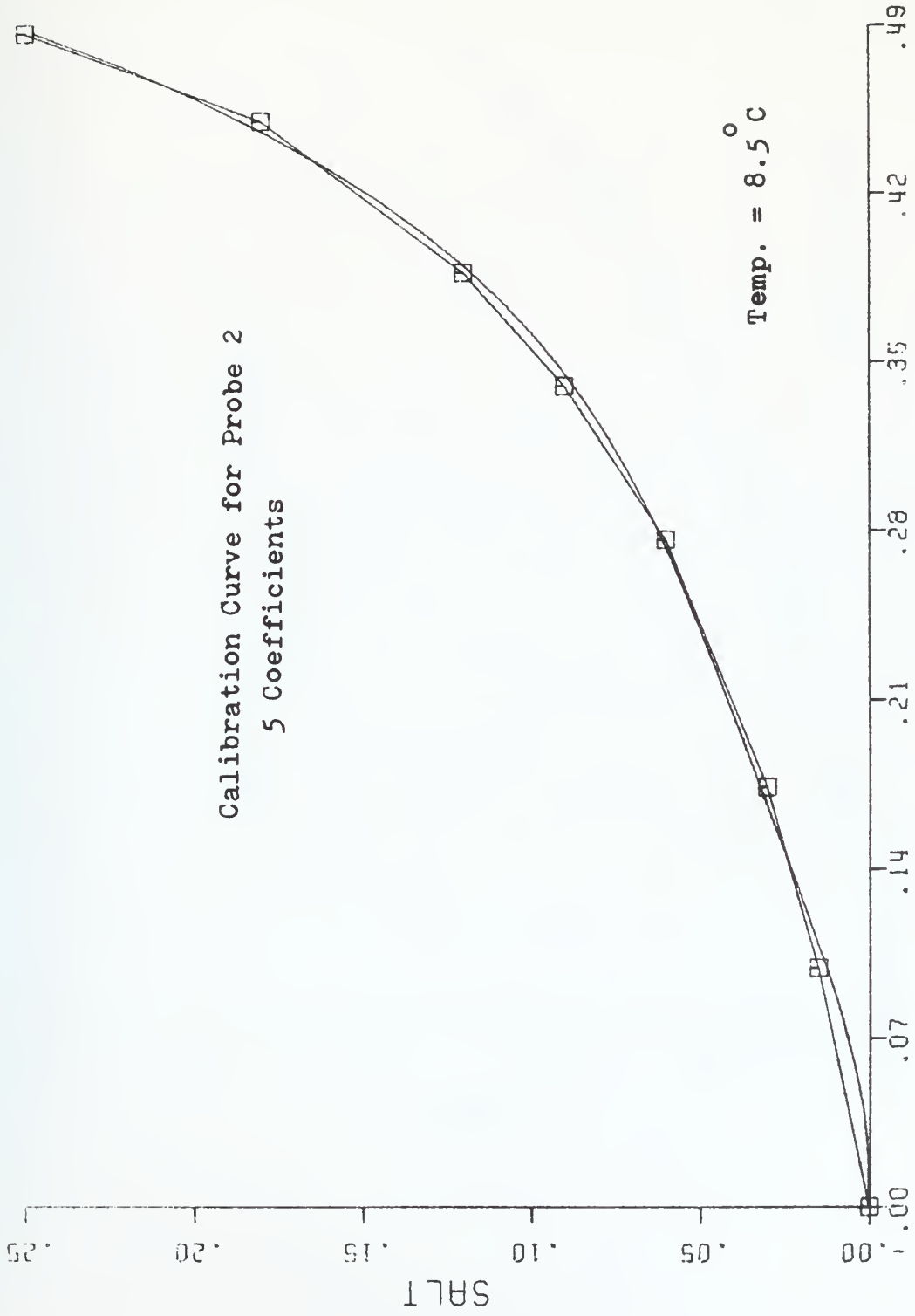
Calibration Curve for Probe 2
5 Coefficients
Temp. = 8.5 °C
SALT
SIGNAL
.00
.05
.10
.15
.20
.25
.00
.07
.14
.21
.28
.35
.42
.49

Figure 4-21

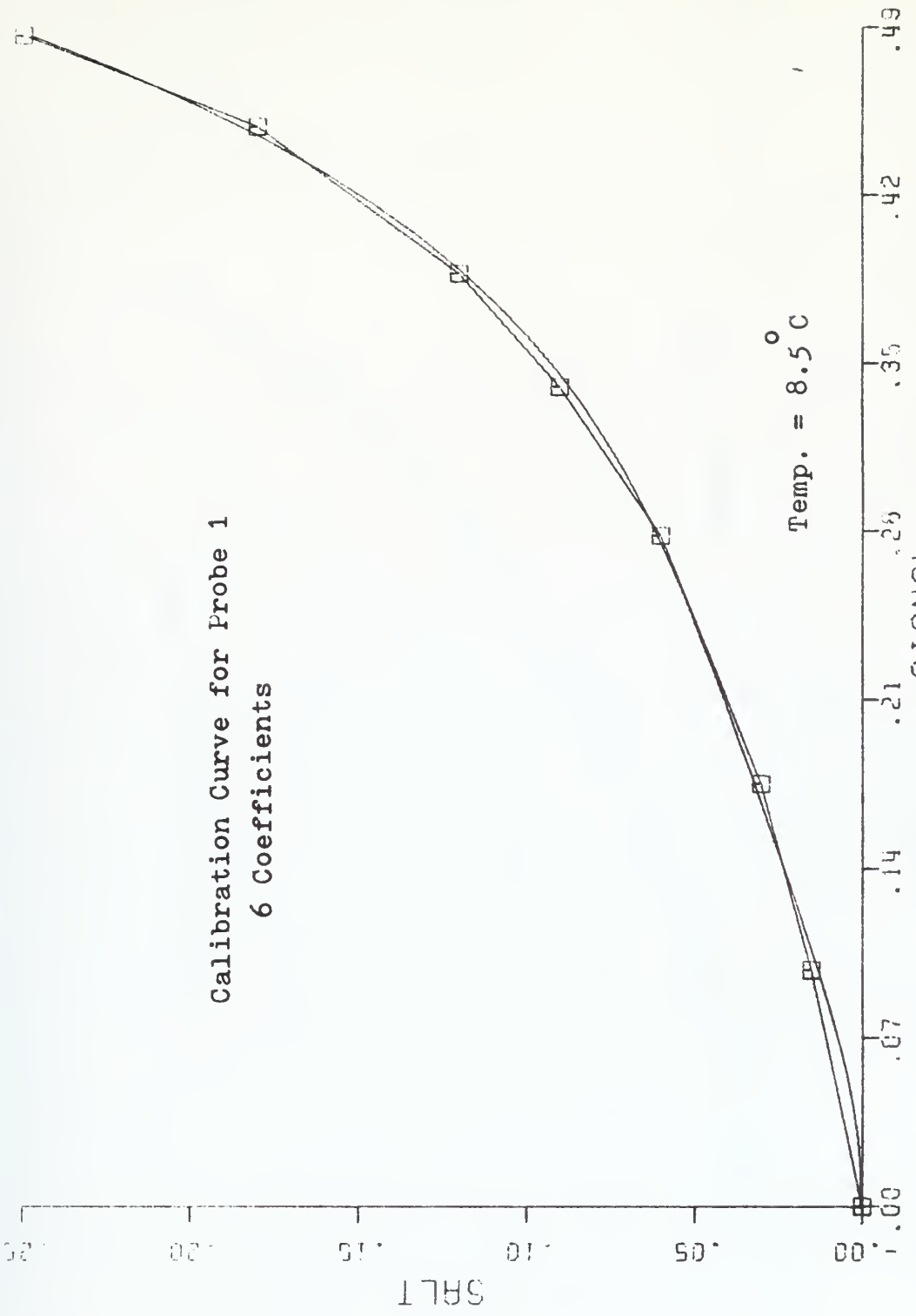
Calibration Curve for Probe 1
6 Coefficients
Temp. = 8.5 C
SALT
SIGNAL
.00
.07
.14
.21
.28
.35
.42
.49

Figure 4-22

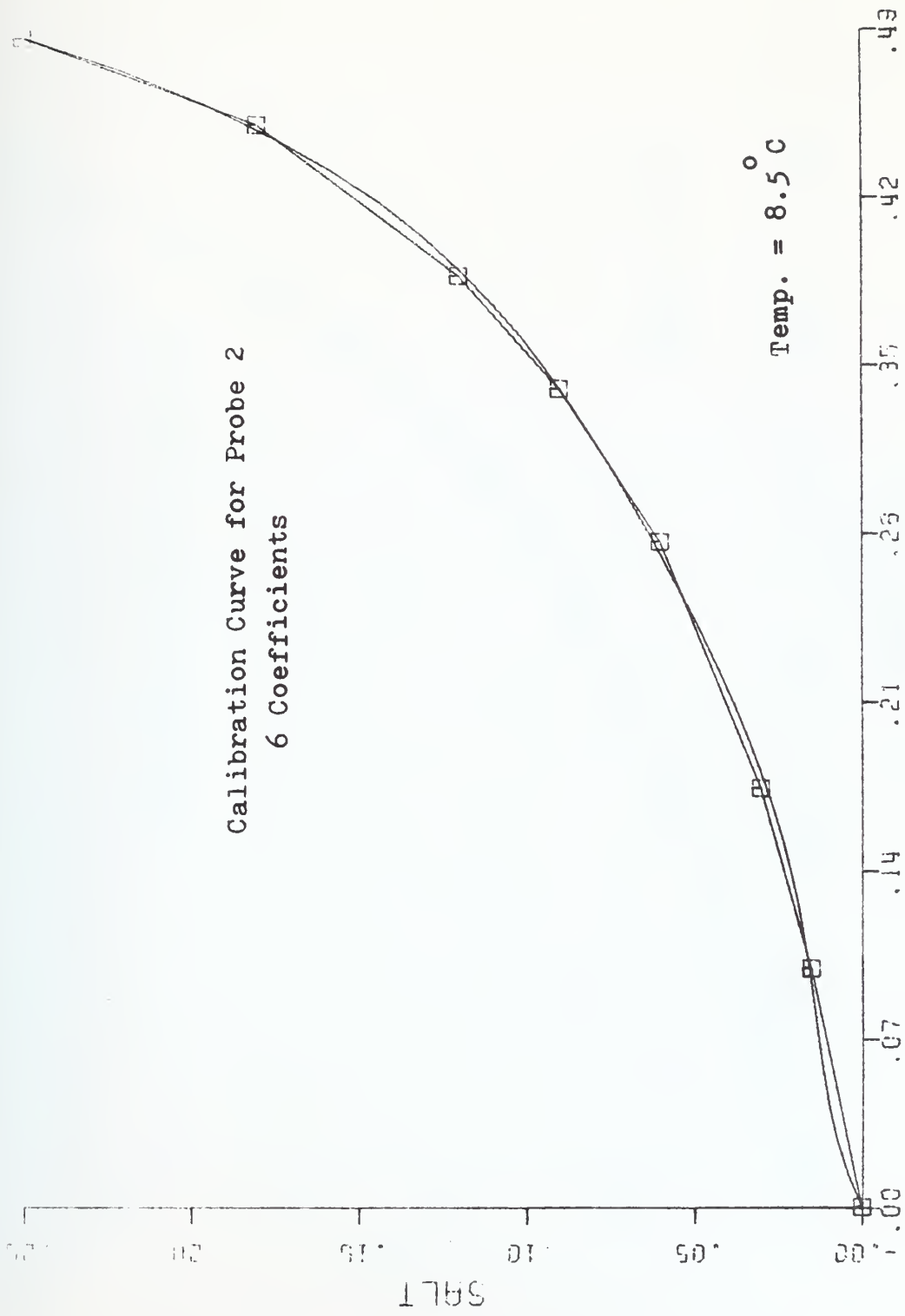
Calibration Curve for Probe 2
6 Coefficients
Temp. = 8.5 °C
SIGNAL
.00
.07
.14
.21
.28
.35
.42
.49
SALT
0.
10.
20.
30.
40.
50.

Figure 4-23

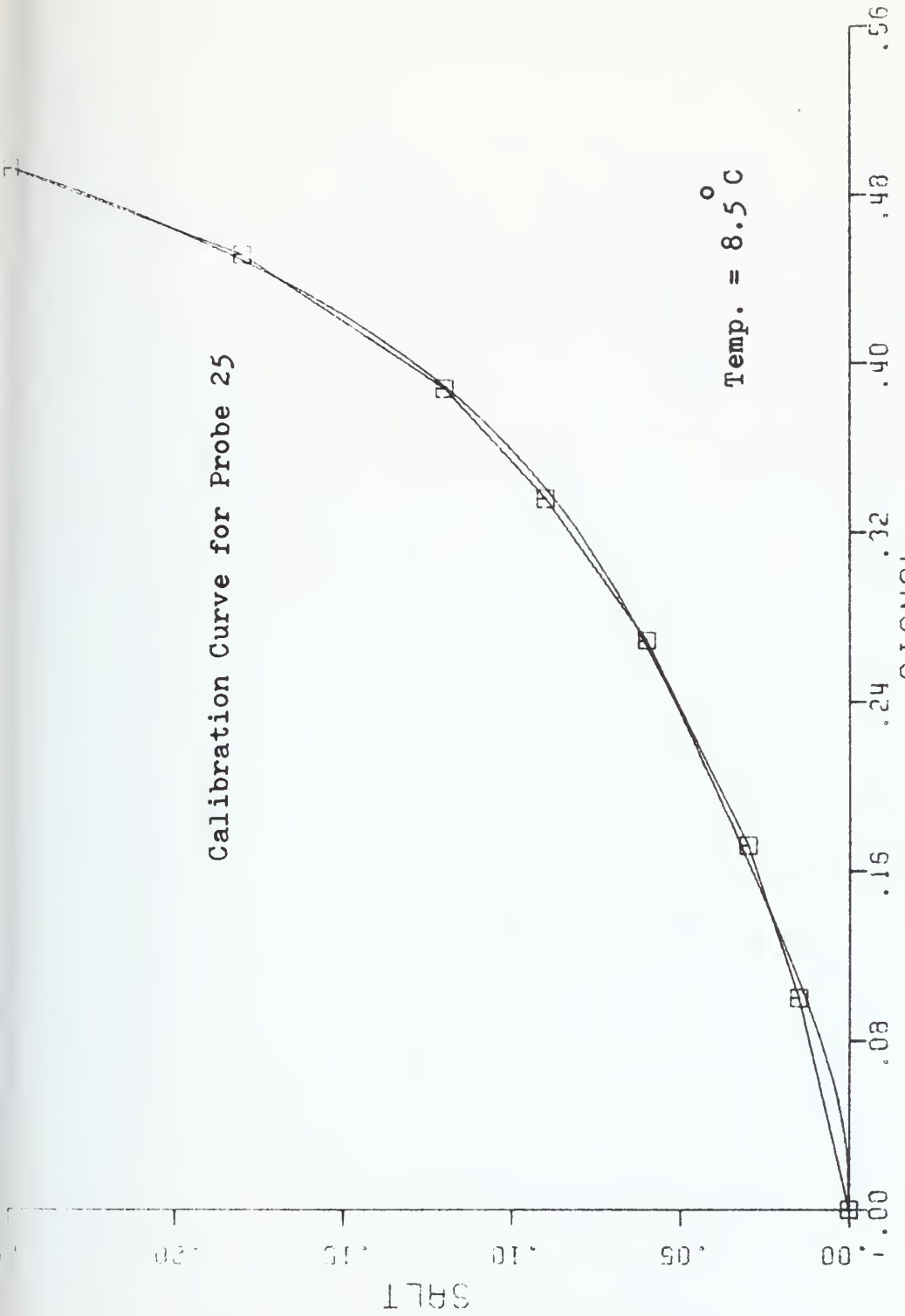
Calibration Curve for Probe 25
Temp. = 8.5 °C
SALT
SIGNAL
.00
.08
.15
.24
.32
.40
.48
.56

Figure 4-24

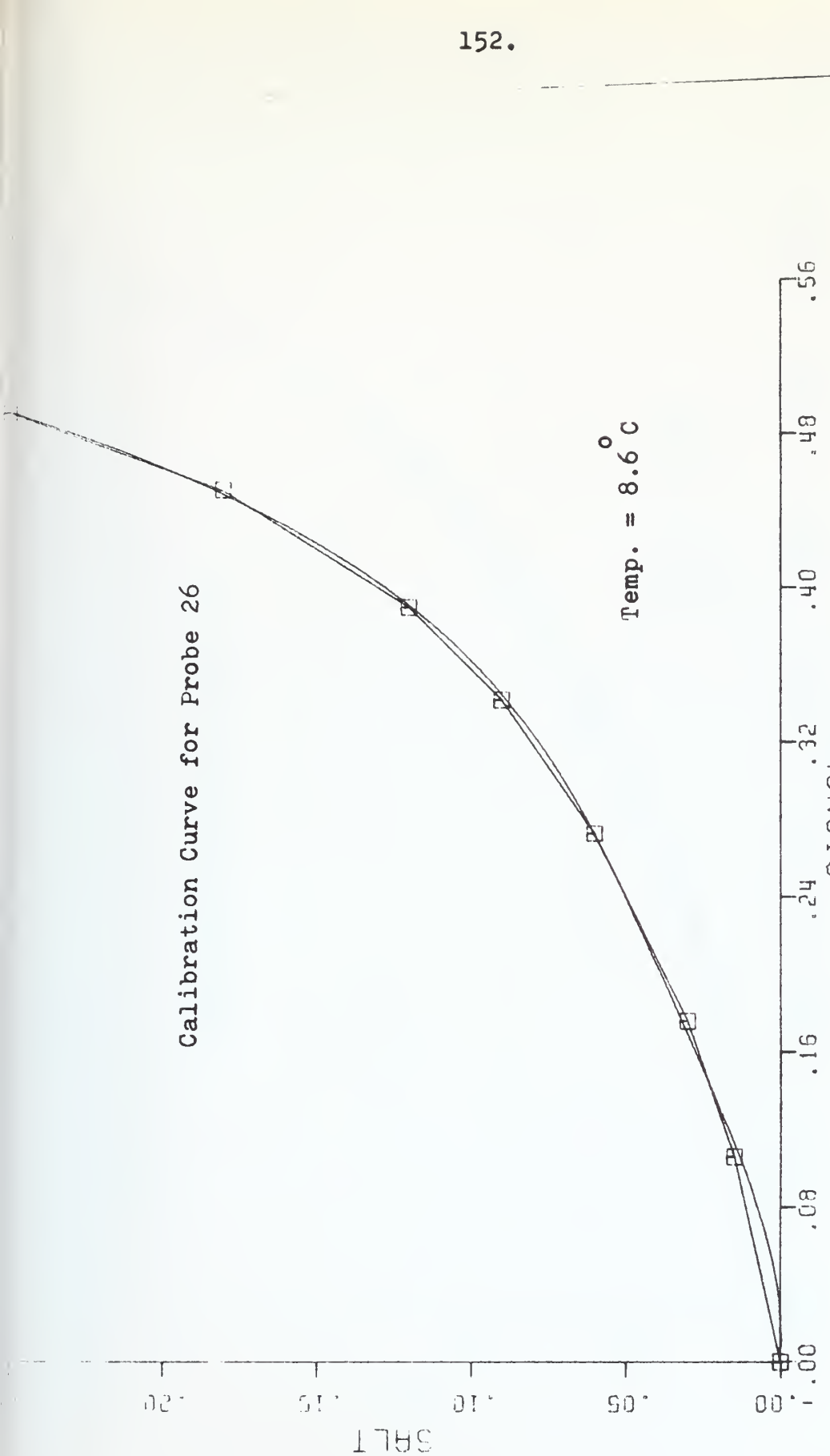
Calibration Curve for Probe 26
Temp. = 8.6°C
SALT
.00
.05
.10
.15
.20
SIGNAL
.00
.08
.16
.24
.32
.40
.48
.56

Figure 4-25

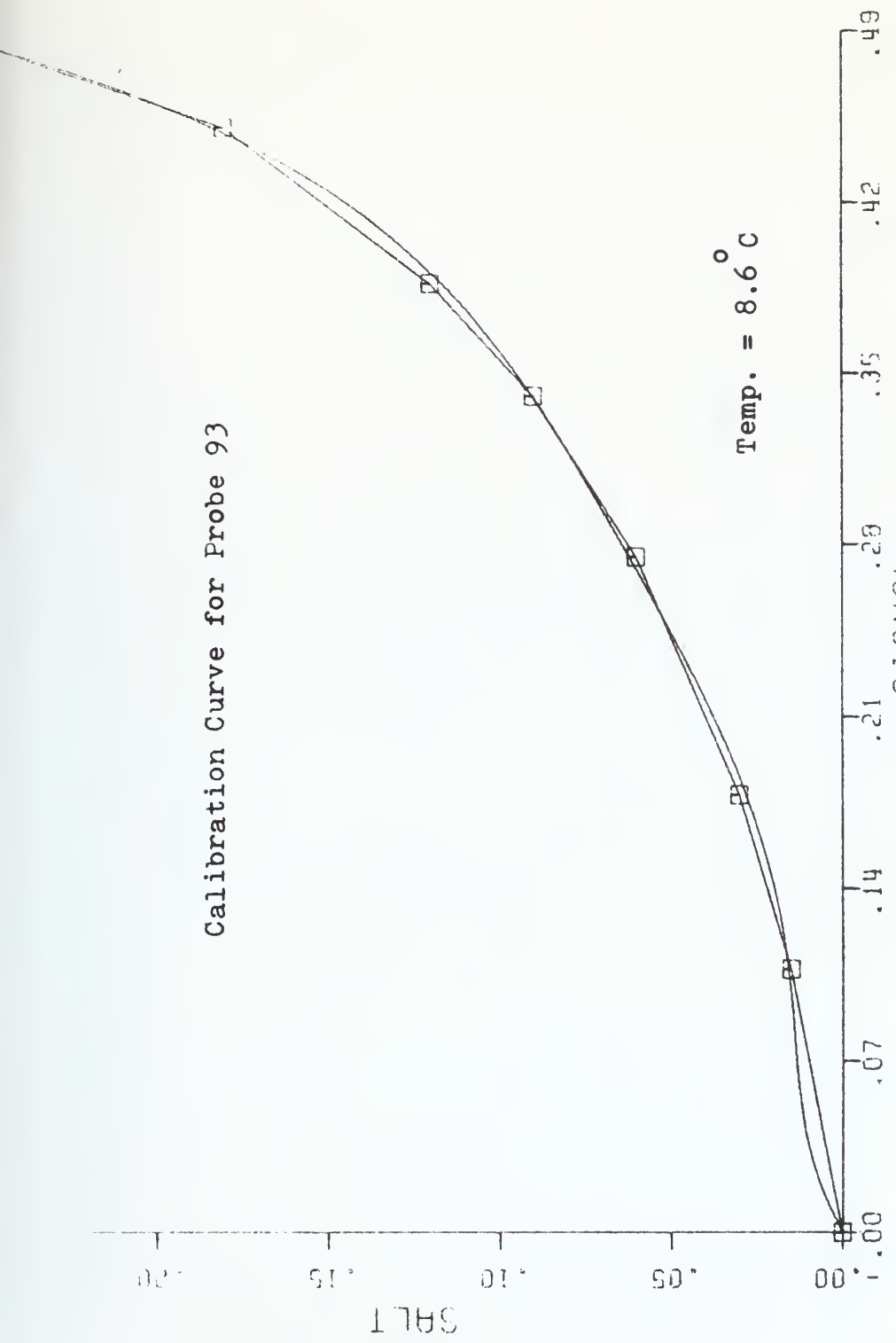
Calibration Curve for Probe 93
Temp. = 8.6 °C
SIGNAL
.00
.07
.14
.21
.28
.35
.42
.49
SALT
.00
.05
.10
.15

Figure 4-26

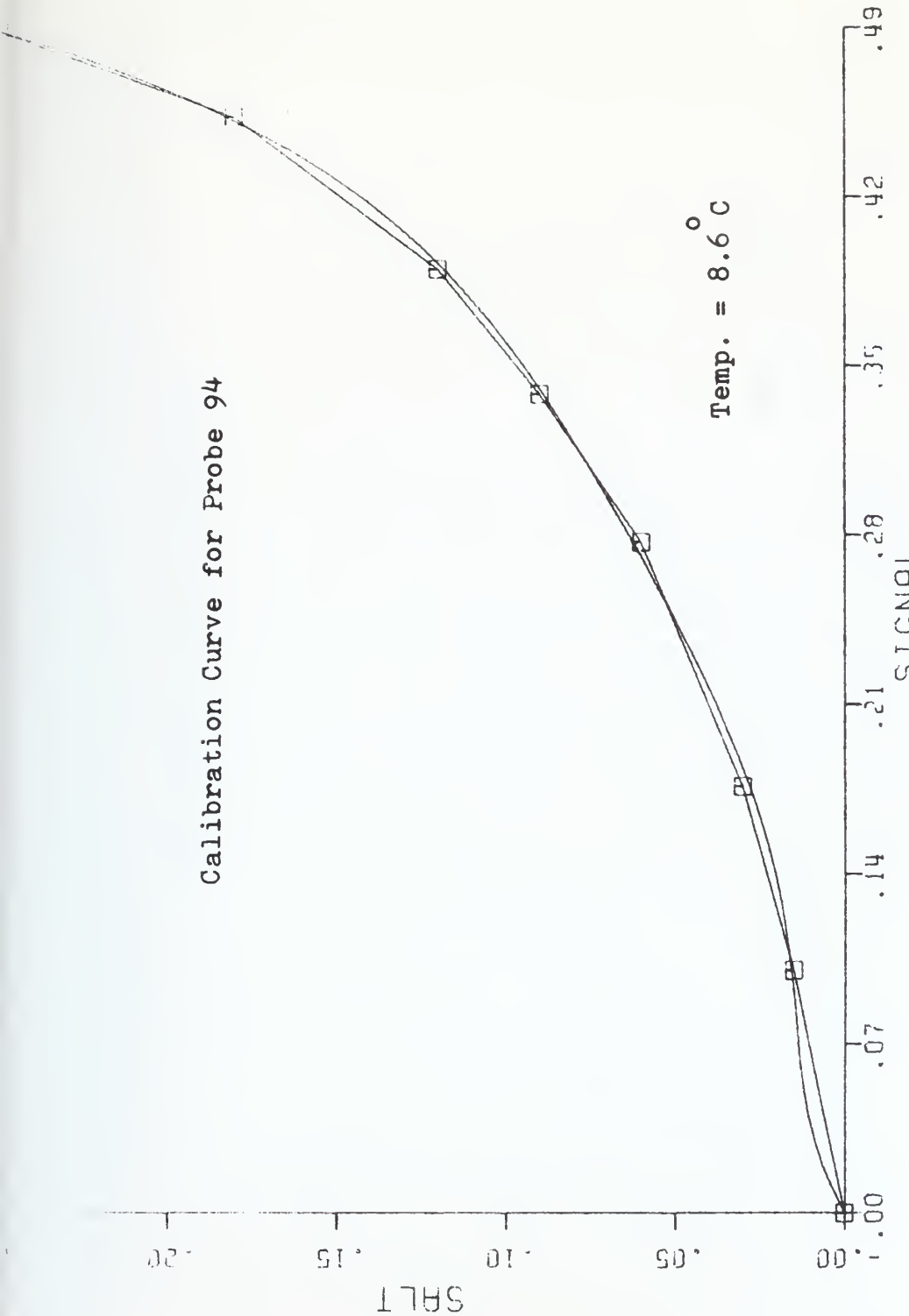
Calibration Curve for Probe 94
Temp. = 8.6 °C
SALT
SIGNAL
.00
.05
.10
.15
.20
.00
.07
.14
.21
.28
.35
.42
.49

Figure 4-27

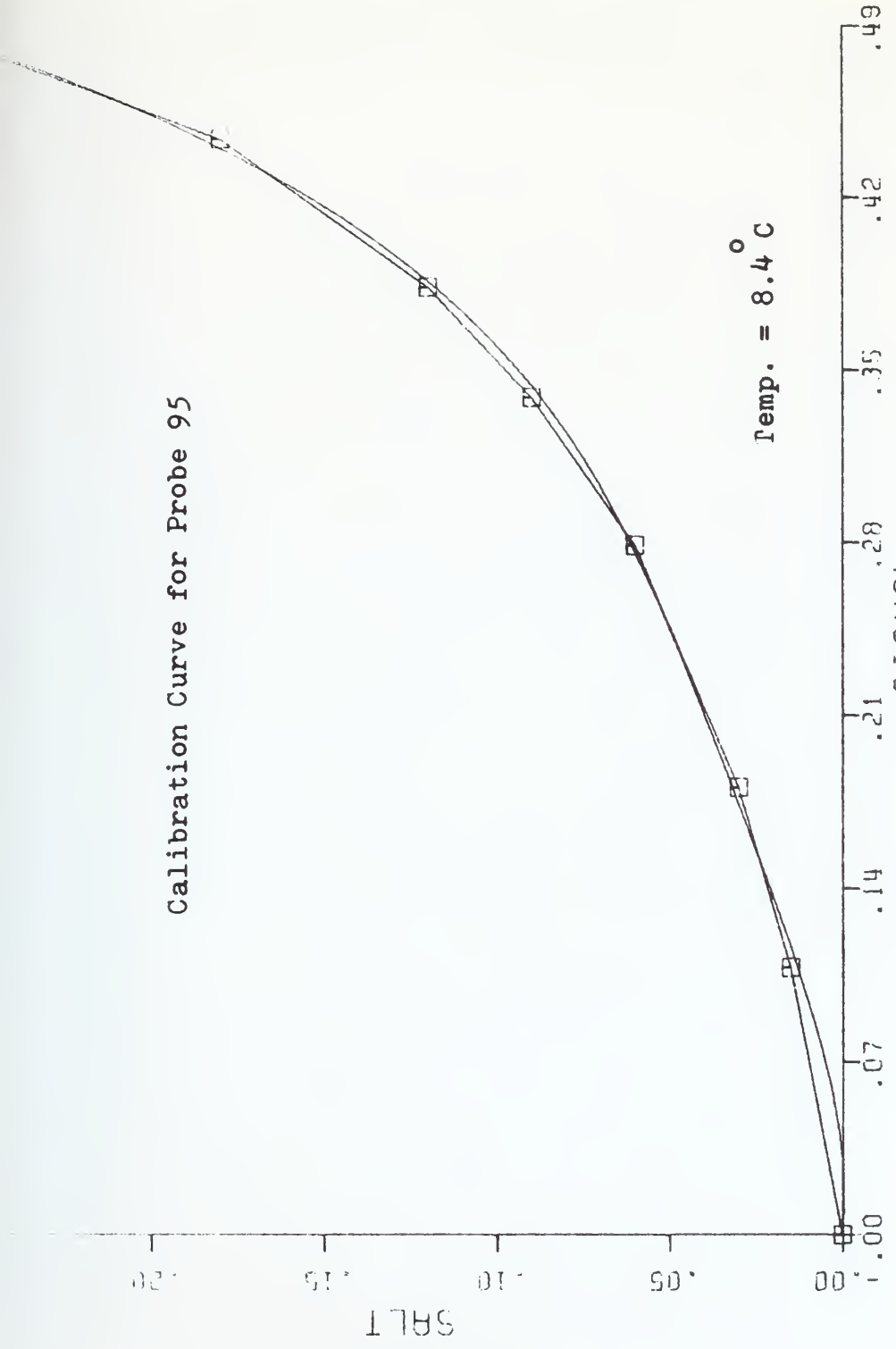
Calibration Curve for Probe 95
Temp. = 8.4 °C
SIGNAL
.00
.07
.14
.21
.28
.35
.42
.49
SALT
.00
.05
.10
.15
.20

Figure 4-28

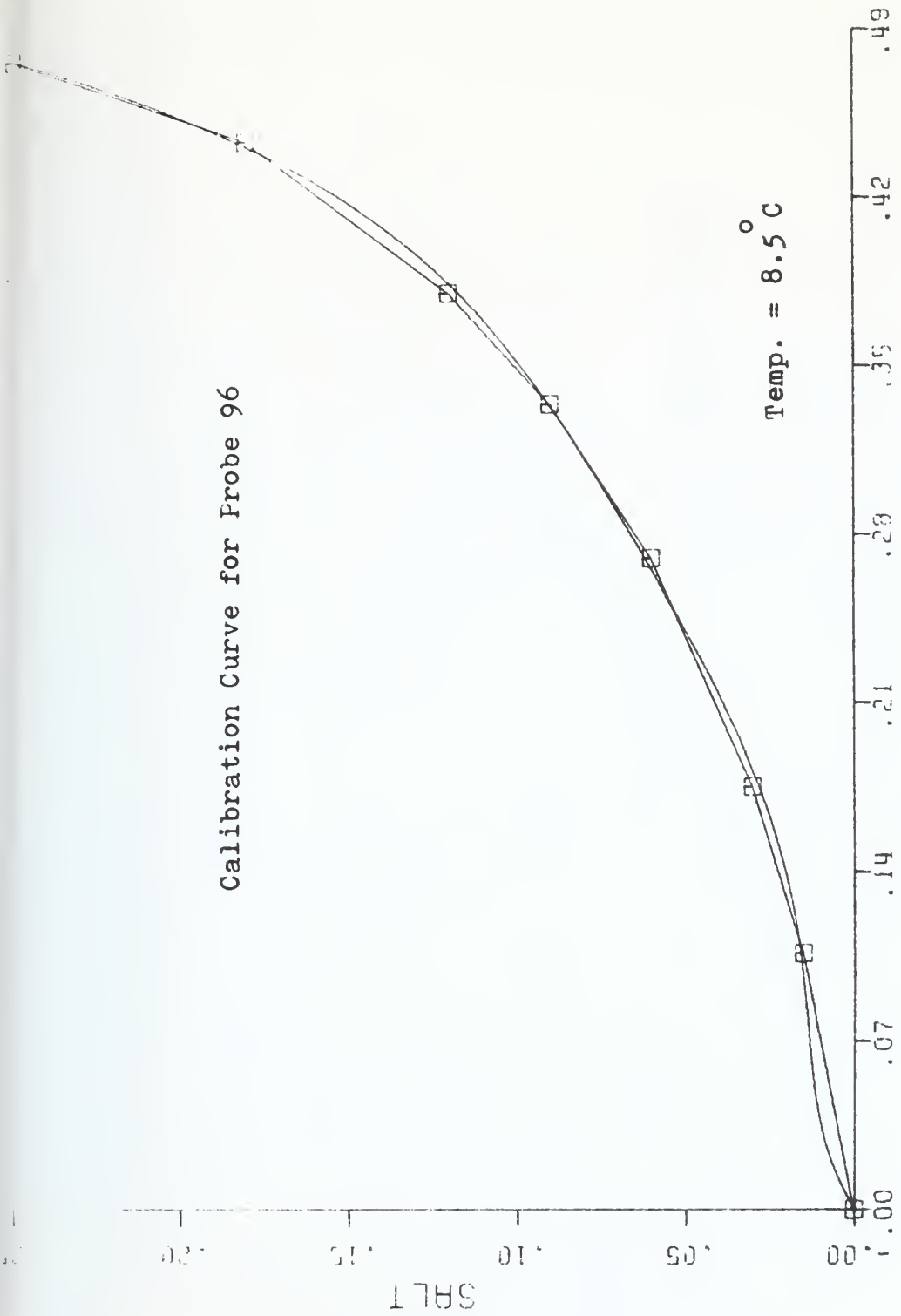
Calibration Curve for Probe 96
Temp. = 8.5 °C
SALT
SIGNAL
.00
.05
.10
.15
.20
.07
.14
.21
.28
.35
.42
.49

Figure 4-29

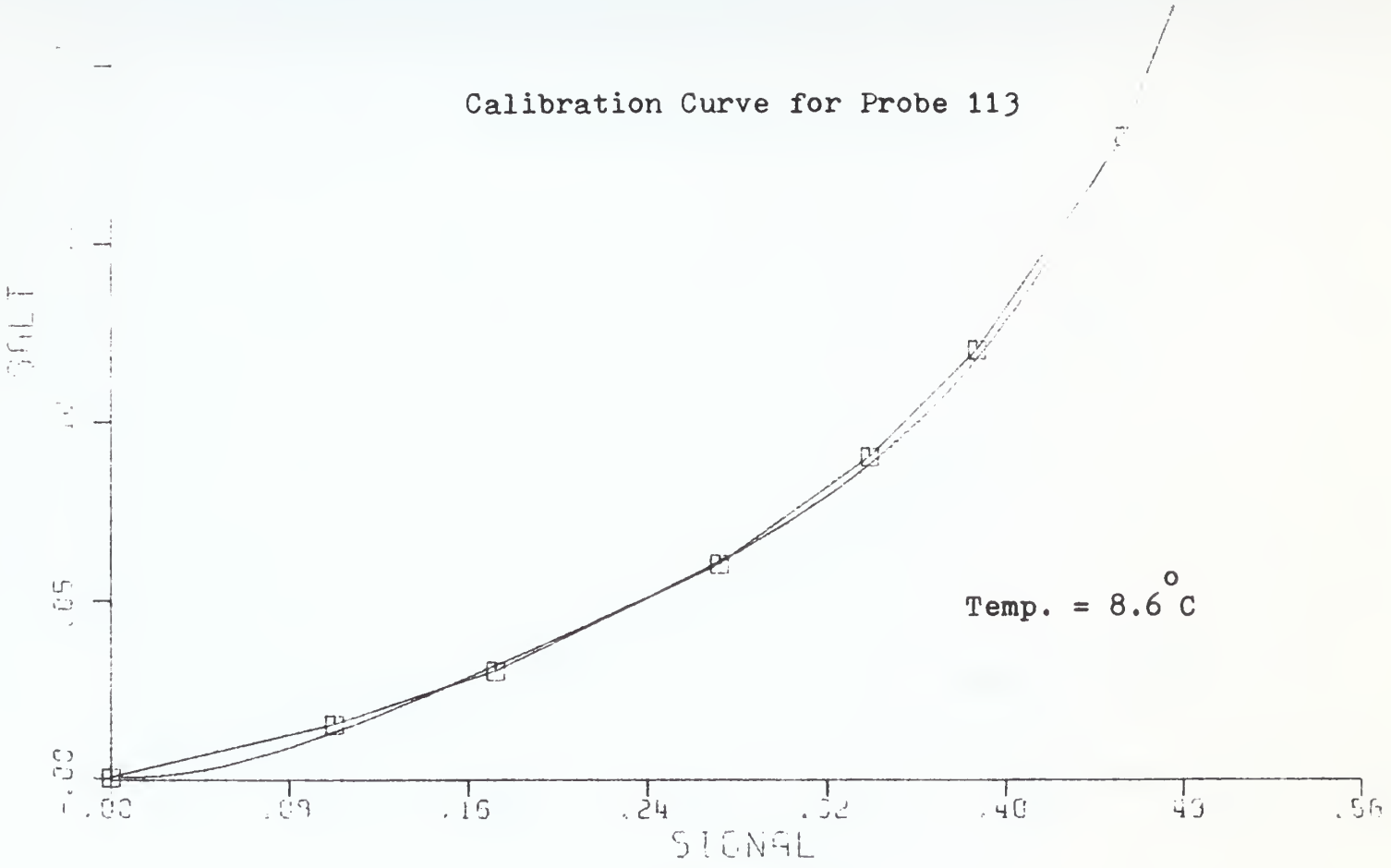
Calibration Curve for Probe 113
SALT
.65
.00
.08
.16
.24
.32
.40
.48
.56
SIGNAL
Temp. = 8.6 °C

Figure 4-30

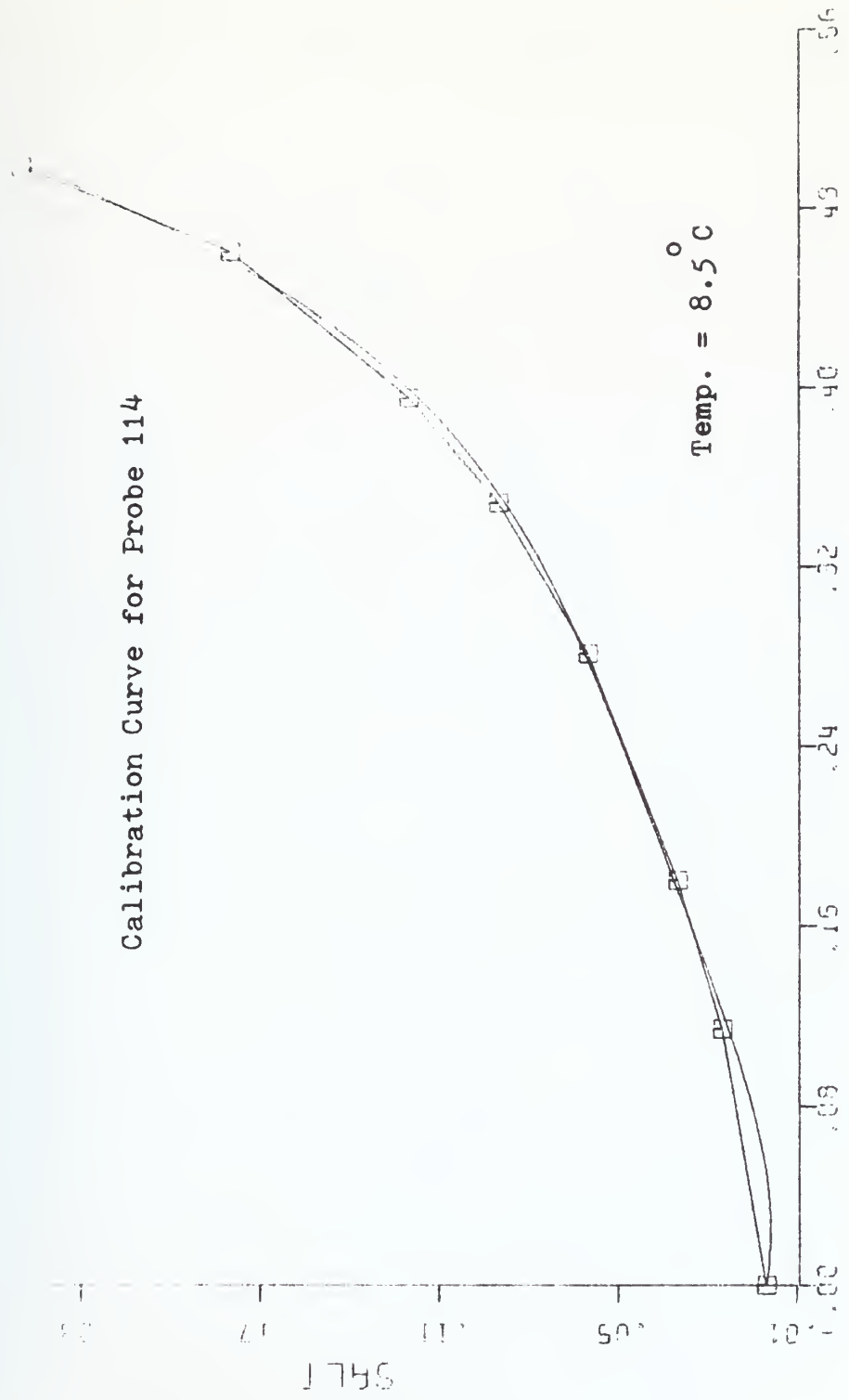
Calibration Curve for Probe 114
Temp. = 8.5 °C
SIGNAL
.24
.32
.40
.48
.56
.16
.08
.00

Figure 4-31

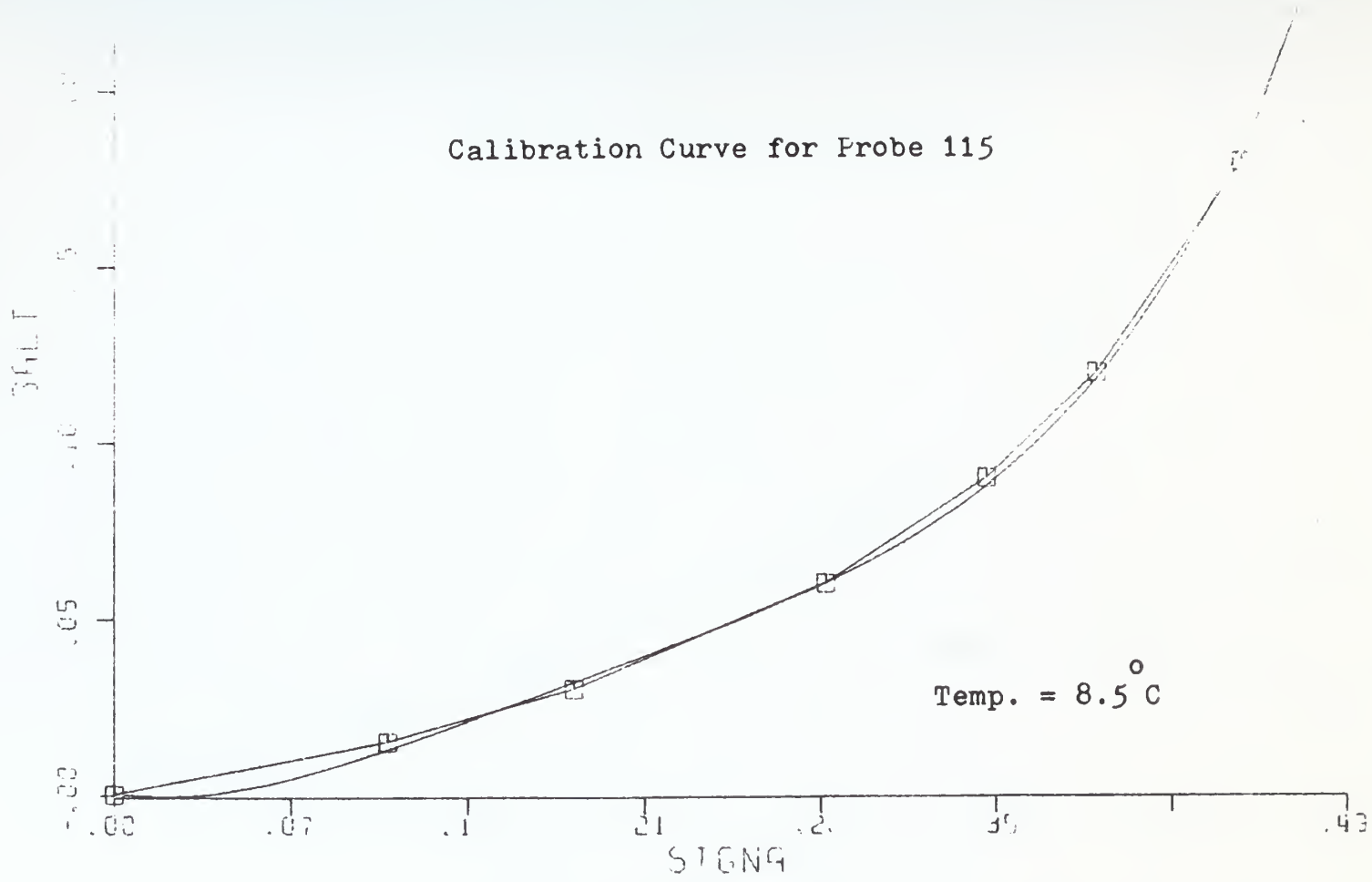

Figure 4-32

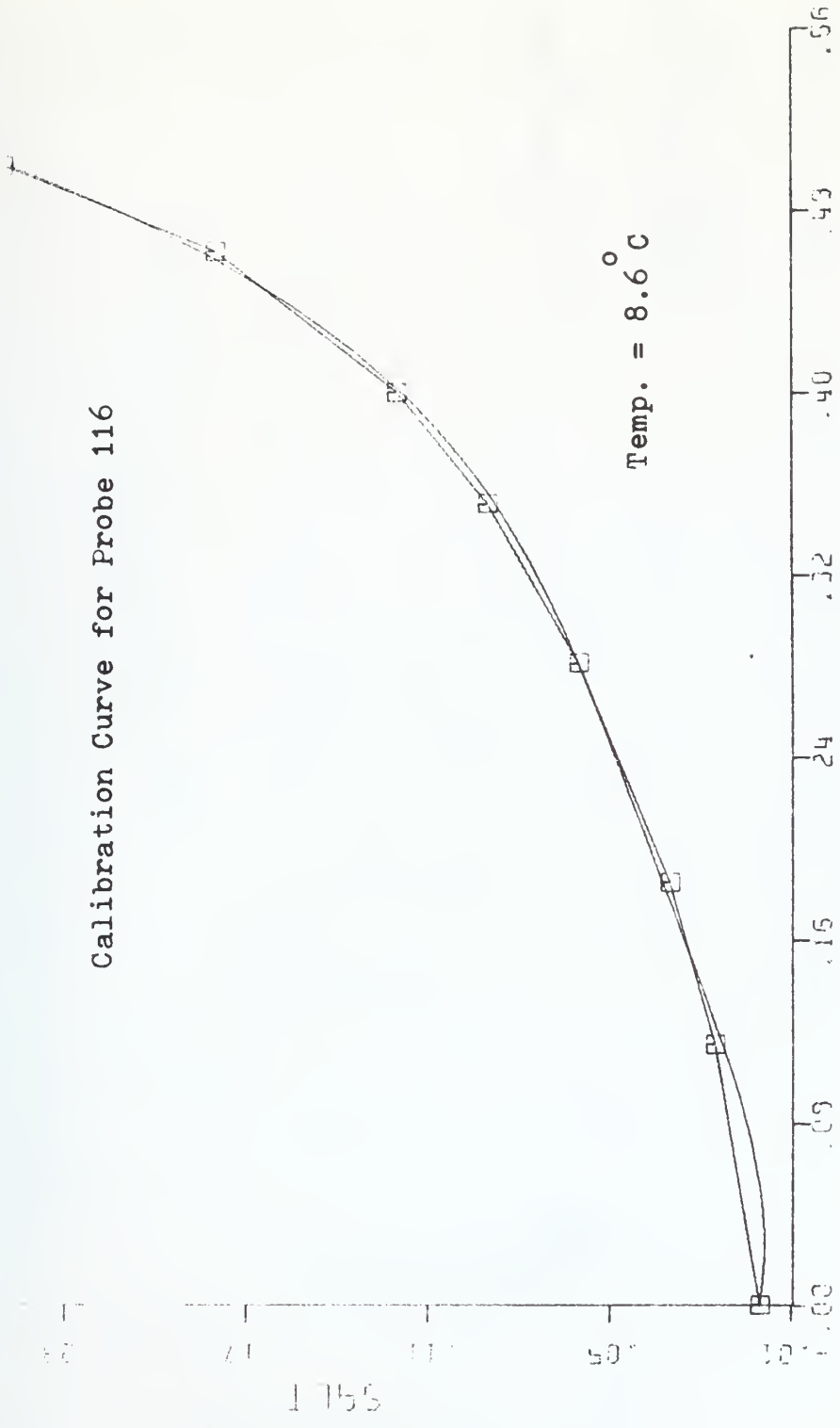
Calibration Curve for Probe 116
Temp. = 8.6 °C
SIGNAL
.56
.48
.40
.32
.24
.16
.08
.00

Figure 4-33

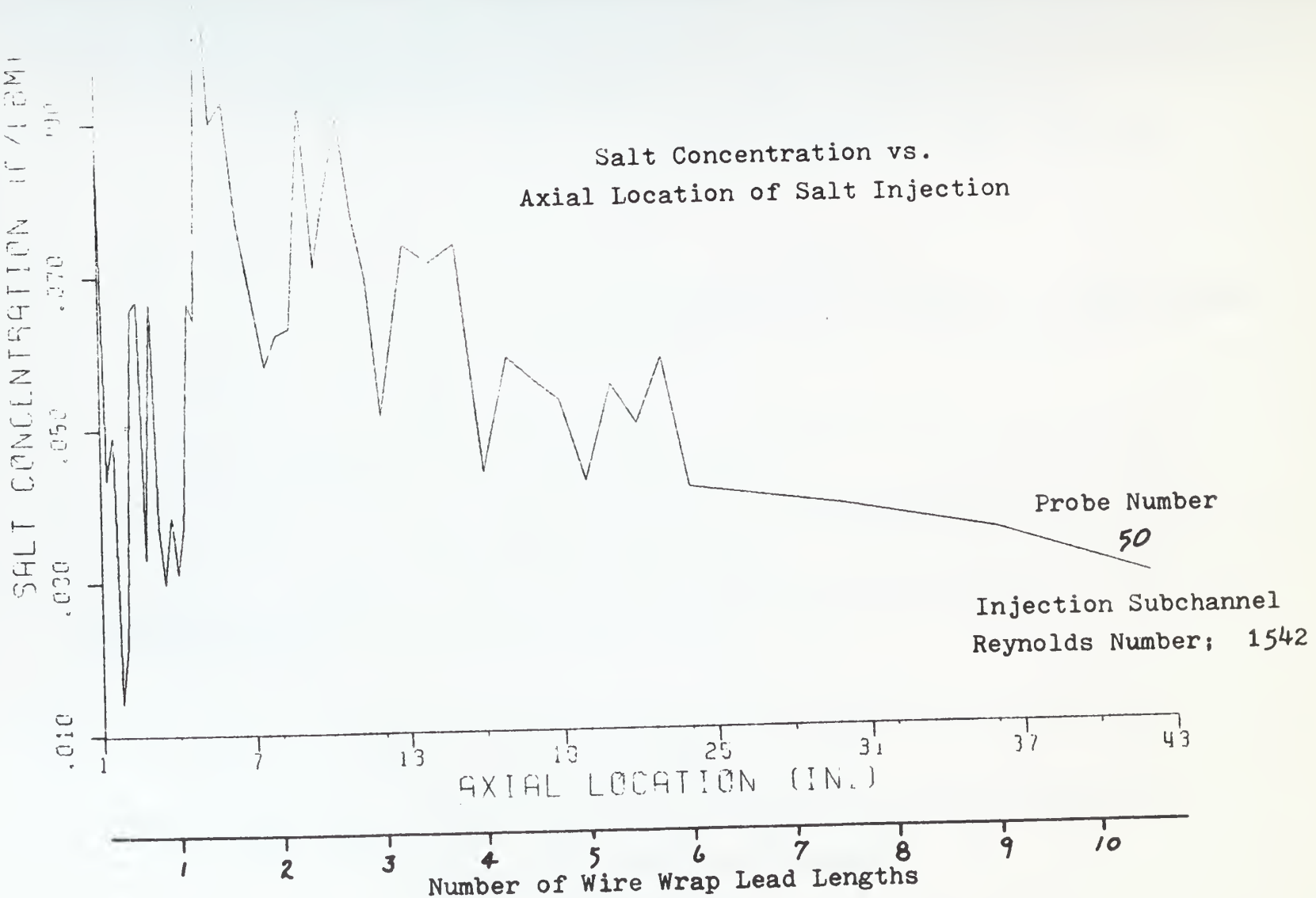
Salt Concentration vs.
Axial Location of Salt Injection
SALT CONCENTRATION
.010
.030
.050
.070
Probe Number
50
Injection Subchannel
Reynolds Number; 1542
1
7
13
19
25
31
37
43
AXIAL LOCATION (IN.)
1
2
3
4
5
6
7
8
9
10
Number of Wire Wrap Lead Lengths

Figure 4-34

Injection Subchannel: 50
Reynolds Number: 1542

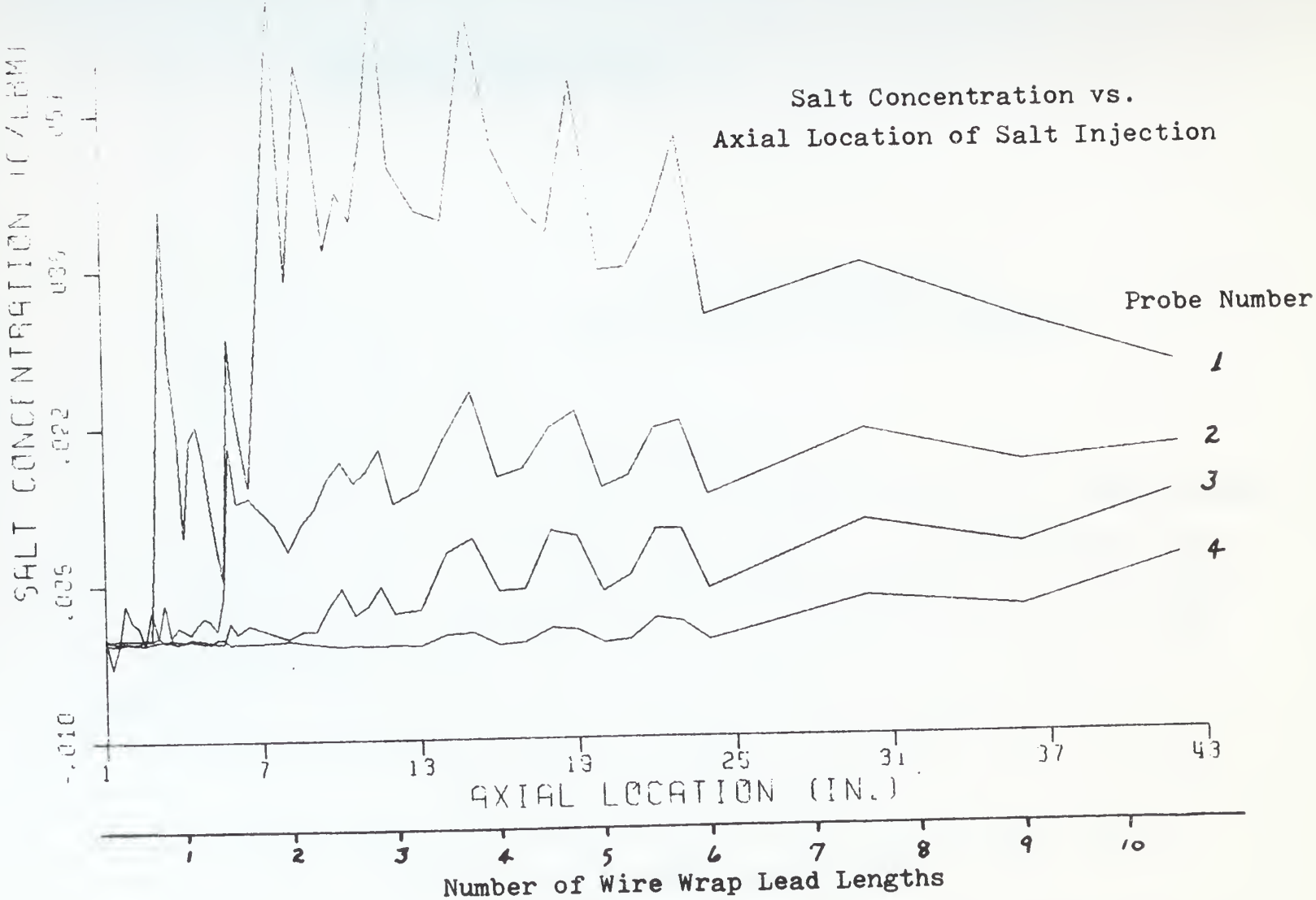

Figure 4-35

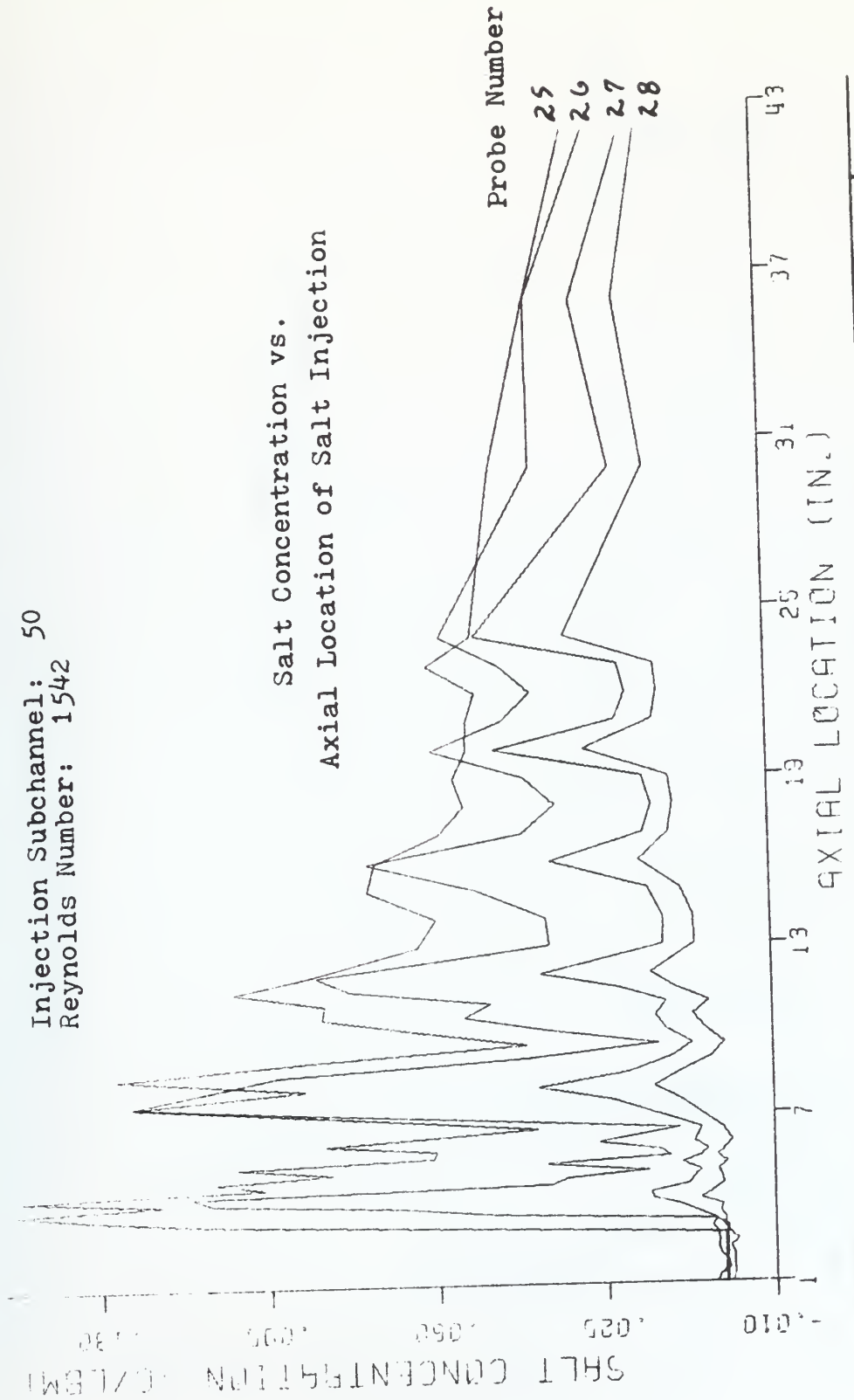
Injection Subchannel: 50
Reynolds Number: 1542
Salt Concentration vs.
Axial Location of Salt Injection
Probe Number
25
26
27
28
SALT CONCENTRATION G/LBM
.010
.025
.060
AXIAL LOCATION (IN.)
1
7
13
19
25
31
37
43
1
2
3
4
5
6
7
8
9
10
Number of Wire Wrap Lead Lengths

Figure 4-36

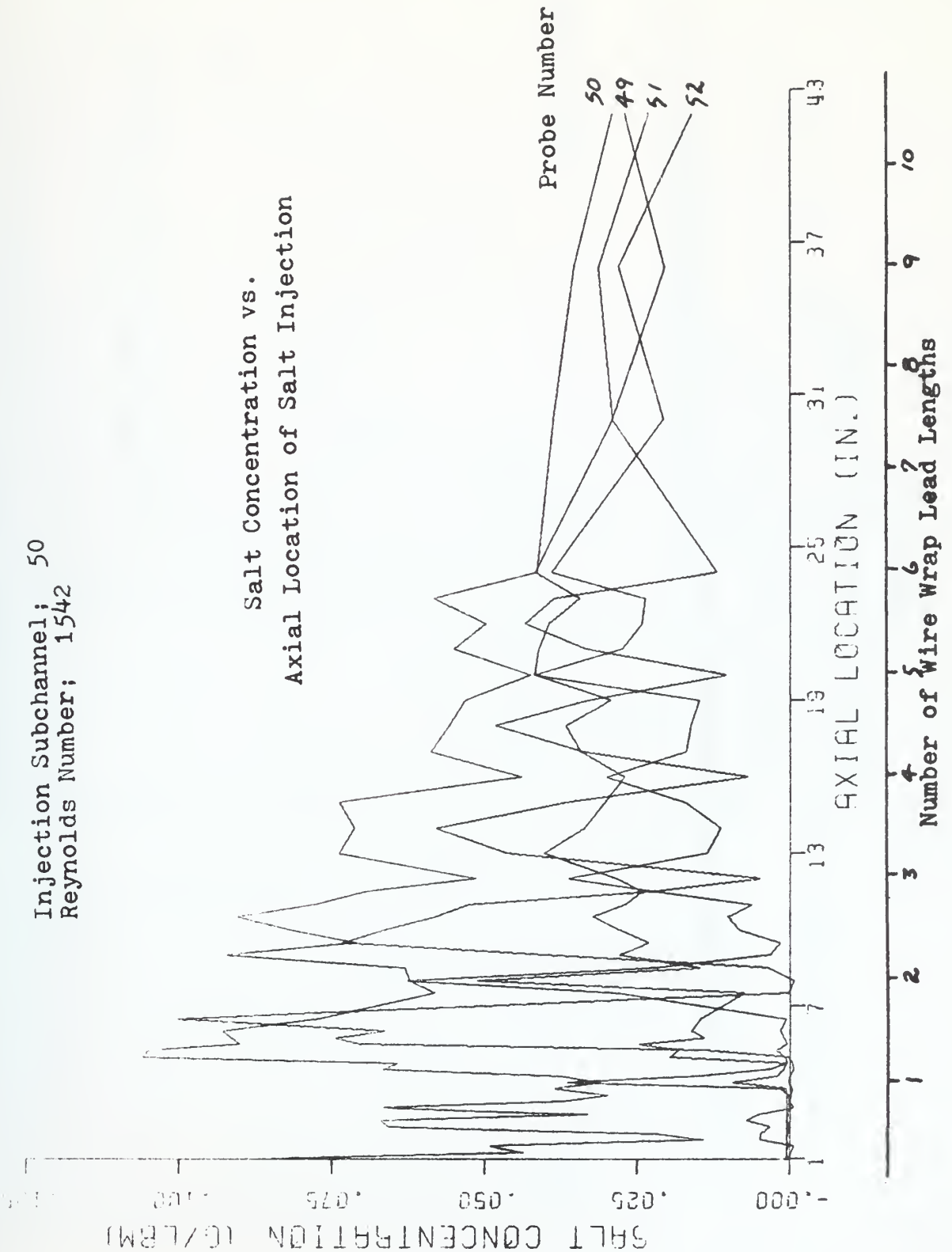
Injection Subchannel; 50
Reynolds Number; 1542
Salt Concentration vs.
Axial Location of Salt Injection
Probe Number
50
49
51
52
SALT CONCENTRATION (G/LBM)
.000
.025
.050
.075
AXIAL LOCATION (IN.)
1
7
13
19
25
31
37
43
1
2
3
4
5
6
7
8
9
10
Number of Wire Wrap Lead Lengths

Figure 4-37

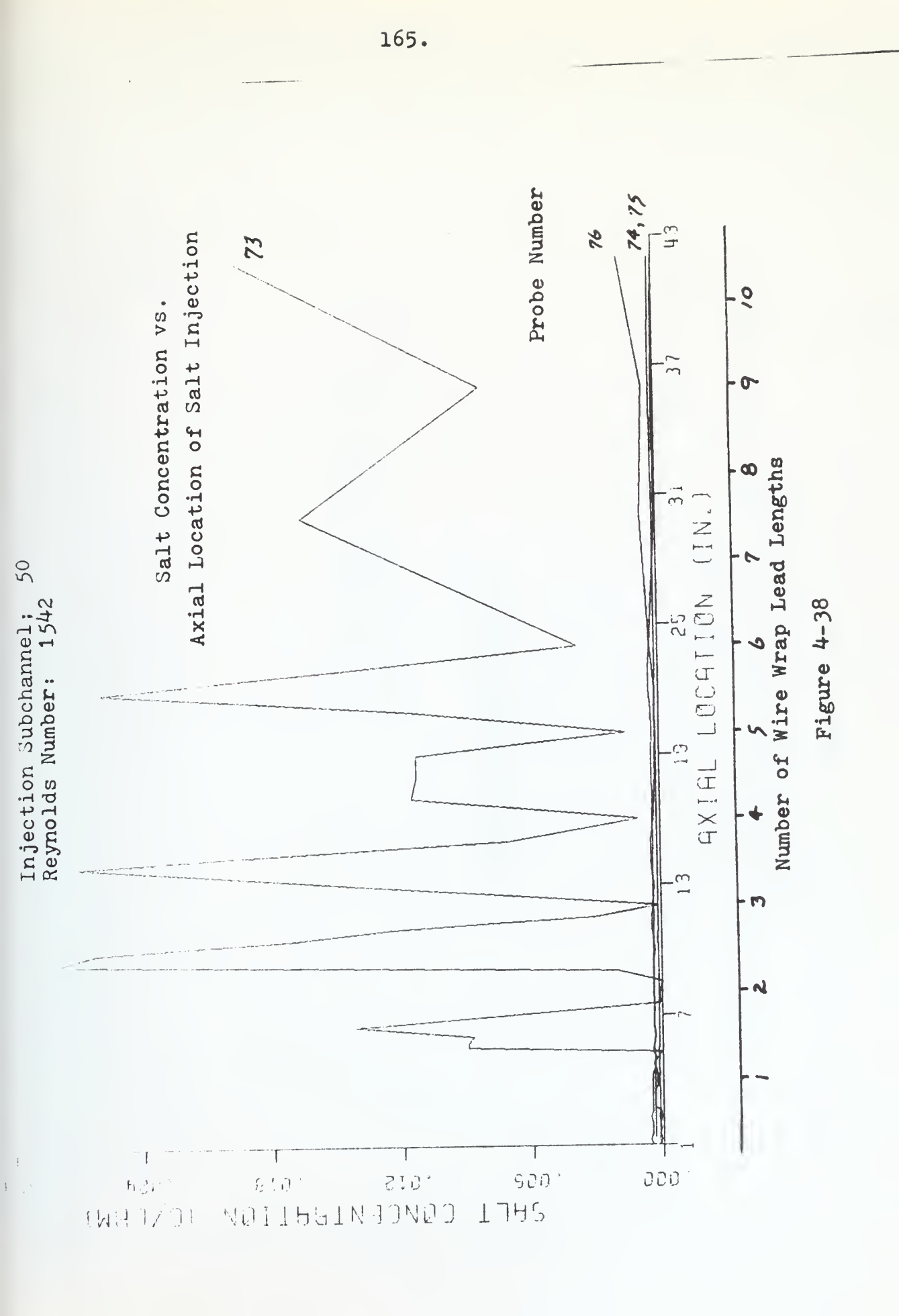
Injection Subchannel; 50
Reynolds Number: 1542
Salt Concentration vs.
Axial Location of Salt Injection
73
76
74, 75
Probe Number
SALT CONCENTRATION (G/LBM)
AXIAL LOCATION (IN.)
Number of Wire Wrap Lead Lengths

Figure 4-38

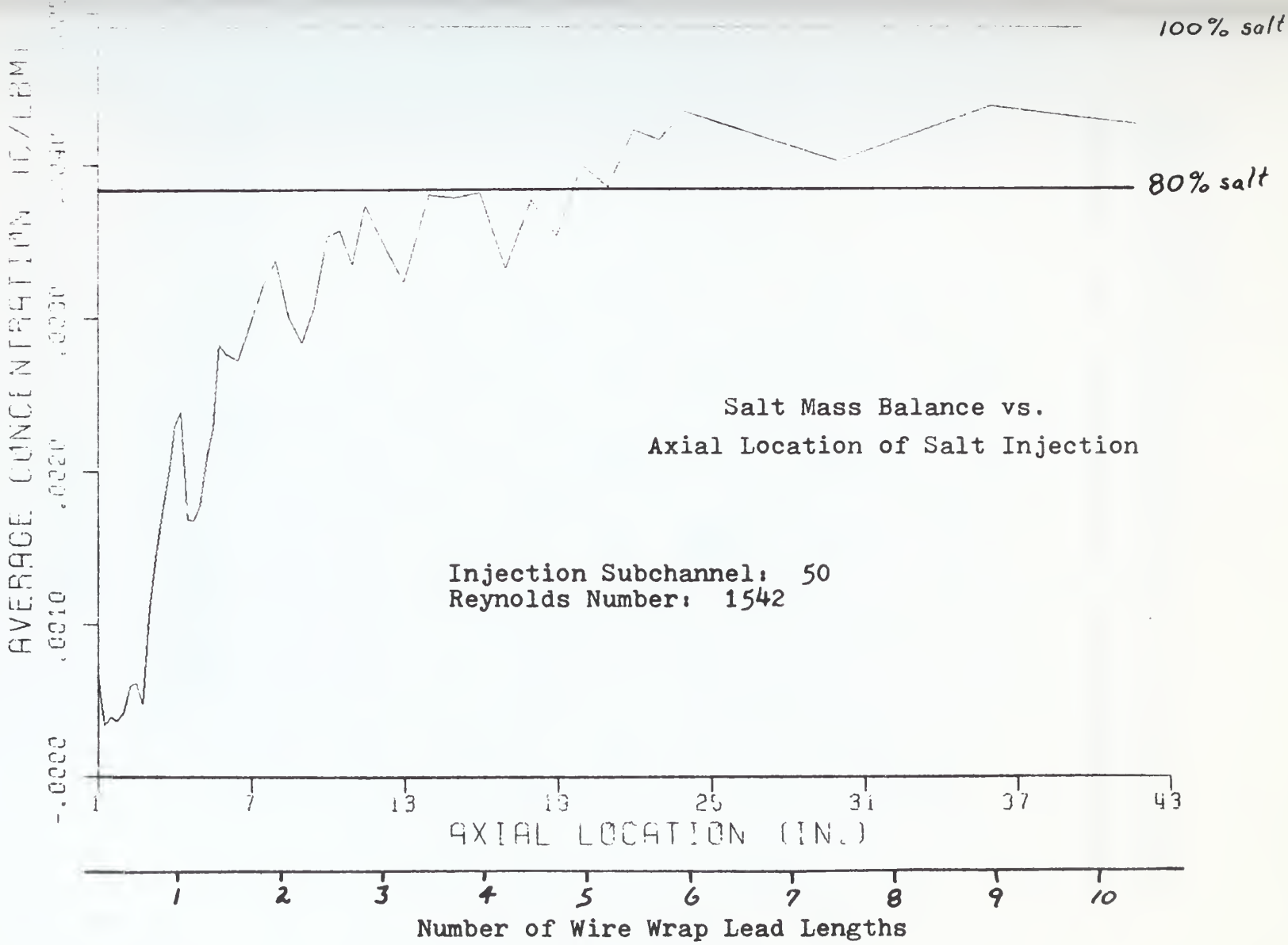

Salt Mass Balance vs.
Axial Location of Salt Injection

Injection Subchannel: 50
Reynolds Number: 1542

Figure 4-39

AXIAL POSITION # 4
AXIAL LOCATION = 24.00 INCHES
AVERAGE SALT CONCENTRATION =0.0043 G-SALT/LBM-WATER

SUBCHANNEL SALT CONCENTRATIONS IN MG-SALT/LBM-WATER:

							-1		0		0		0		0		-1							
						0		0		0		0		3		0								
							0		0		0		0		1									
					0		6		3		2		0		0		0							
						0		8		8		1		0		0								
				0		11		22		23		3		0		0		0						
					0		17		24		16		0		0		0							
			0		5		31		57		32		5		0		0		0					
				0		14		50		50		14		0		0		0						
		-1								+									-1					
				0		14		39		41		3		0		0		2						
			0		0		17		41		11		0		0		6		0					
				0		4		1		16		5		0		0		0						
					0		0		2		11		11		0		0		0					
						0		4		8		0		0		0								
					0		0		0		0		0		0		0							
							0		0		0		1		2									
						0		0		0		2		0		0								
							-1		0		0		0		0		-1							

Reynolds Number: 1542
Injection Subchannel: 50 (underlined)
See Figure 4-40a for injector orientation

Figure 4-40

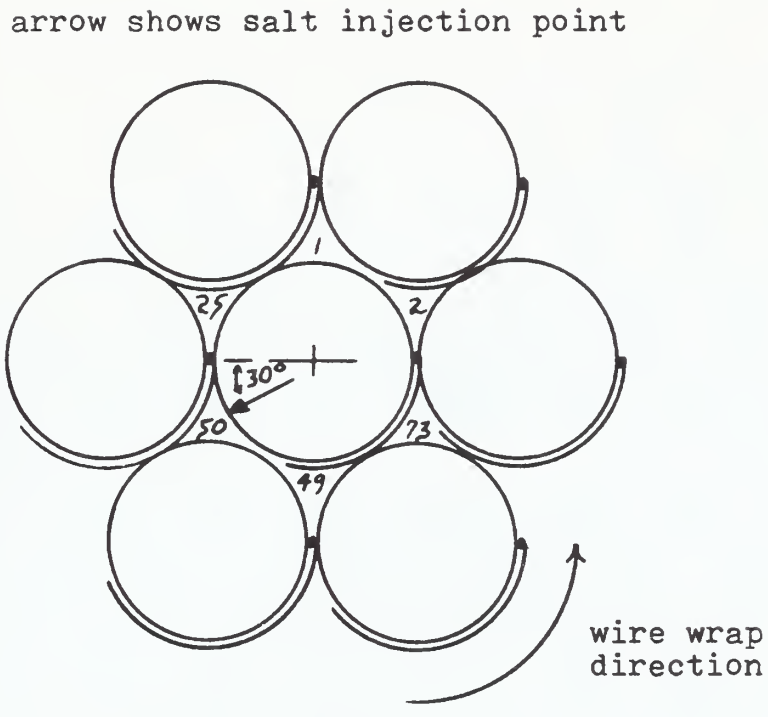

Wire Wrap Orientation for Central Injection At
36, 28, 24, 20, 16, 12, 8, and 4 Inches

Figure 4-40a

AXIAL POSITION # 20
AXIAL LOCATION = 10.00 INCHES
AVERAGE SALT CONCENTRATION =0.0035 G-SALT/LBM-WATER

SUBCHANNEL SALT CONCENTRATIONS IN MG-SALT/LBM-WATER:

							-1		0		0		0		0		-1							
					0		0		0		0		1		0									
						0		0		0		0		2										
				0		0		0		0		0		0		0								
					0		0		0		0		0		0									
			0		0		0		0		0		0		0		0							
				0		0		8		0		0		0		0								
		0		0		3		36		45		5		0		0		0						
			0		0		11		[62]		18		0		0		0							
	-1																	-1						
			0		0		8		81		26		0		0		16							
		0		0		2		27		66		0		0		8		0						
			0		0		7		43		3		1		0									
		0		0		0		10		32		0		1		0								
			0		-1		2		1		0		0											
		0		0		0		0		0		0		0										
			0		0		0		0		0		0											
				0		0		0		0		0												
					-1		0		0		0		0		-1									

Reynolds Number: 1542
Injection Subchannel: 50 (underlined)

Figure 4-41

AXIAL POSITION # 24
AXIAL LOCATION = 8.00 INCHES
AVERAGE SALT CONCENTRATION =0.0034 G-SALT/LBM-WATER

SUBCHANNEL SALT CONCENTRATIONS IN MG-SALT/LBM-WATER:

						-1		0		0		0		0		-1								
					0		0		0		0		0		0								
						0		0		0		0		1										
				0		0		0		0		0		0		0								
					0		0		0		0		0		0									
			0		-1		0		1		0		0		0		0							
				0		0		14		0		0		0		0								
		0		2		14		108		36		0		0		0		0						
			0		0		38		87		9		0		0		0							
	-1																	-1						
		0		1		62		62		0		0		0		0								
	0		0		8		51		0		0		0		0		0							
			2		0		2		0		0		0		0									
		0		0		0		0		0		0		0		0								
				0		-1		0		0		1		0										
			0		0		0		0		0		0		0									
					0		0		0		0		0											
						0		0		0		-1		0										
						-1		0		0		0		0		-1								

Reynolds Number: 1542
Injection Subchannel: 50 (underlined)

Figure 4-42

AXIAL POSITION # 27
AXIAL LOCATION = 6.00 INCHES
AVERAGE SALT CONCENTRATION =0.0028 G-SALT/LBM-WATER

SUBCHANNEL SALT CONCENTRATIONS IN MG-SALT/LBM-WATER:

						-1		0		0		0		0		-1								
				0		0		0		0		0		0										
					0		0		0		0		1											
			0		0		0		0		0		0		0									
				0		0		1		0		0		0										
		0		0		0		0		0		0		0		0								
			0		0		0		0		0		0		0									
	0		0		-1		26		23		0		0		0		0							
		0		0		6		83		14		0		0		0								
-1																		-1						
		0		-1		1		92		8		0		0		8								
	0		0		0		16		66		0		0		4		0							
			0		0		1		25		0		1		0									
		0		0		0		0		31		0		0		0								
			0		-1		0		0		0		0											
		0		0		0		0		0		0		0										
			0		0		0		0		0		0											
				0		0		0		0		0												
					-1		0		0		0		0		-1									

Reynolds Number: 1542
Injection Subchannel: 50 (underlined)

Figure 4-43